

THE DENSITY OF COSMIC-RAY NEUTRONS
IN THE ATMOSPHERE

Thesis by
Ralph Fraley Miles, Jr.

In Partial Fulfillment of the Requirements

For the Degree of
Doctor of Philosophy

California Institute of Technology

Pasadena, California

1963

ACKNOWLEDGEMENTS

The author wishes to thank Professor H. V. Neher, under whose supervision the work of this thesis was carried out. The Office of Naval Research supported the program, and their assistance is acknowledged.

The ionization chambers utilized in the experiment were designed by Professor Neher. The optimum geometry for the pulsing mechanism in the electrometer system was obtained in collaboration with Dr. H. R. Anderson, Jet Propulsion Laboratory of NASA. The all-metal purification system used for the BF_3 gas is essentially that described by H. V. Neher and S. Prakash (1).

I am indebted to Dr. R. C. Haymes for his assistance in the comparison of this work to the measurements of the Cosmic Ray Group, New York University. Dr. W. N. Hess (now at the Goddard Space Flight Center, NASA) and Dr. R. E. Lingenfelter (now at the Institute of Geophysics and Planetary Physics, UCLA) were helpful in the comparison of results with the Lawrence Radiation Laboratory, University of California. Messrs. H. W. Patterson and Al Smith of UCLRL performed the intercomparison of proportional counters in their calibration cavity.

My father, Col. R. F. Miles, USA (ret.), provided the food, camping equipment, and moral support for the balloon launching expeditions.

ABSTRACT

Neutrons are produced in the atmosphere by the interaction of cosmic-ray particles with the nuclei of nitrogen and oxygen. The density of these neutrons was determined experimentally by means of ionization chambers filled with $B^{10}F_3$, $B^{11}F_3$, and argon. The ionization current resulting from the $B^{10}(n,\alpha)Li^7$ reaction was obtained as a function of pressure altitude from 760 grams cm^{-2} (8,000 ft) to 6 grams cm^{-2} (115,000 ft) in a series of balloon flights at a geomagnetic latitude of $41^\circ N$. By comparing the current from the ionization chamber to the counting rate of a $B^{10}F_3$ proportional counter, when irradiating the instruments with a thermal neutron source, an absolute calibration of the ionization current in terms of thermal neutron density was made.

The large volume of the ionization chambers (9 liters) resulted in a significant reduction of statistical errors relative to earlier balloon flights. The small size of the flight units (3 kilograms) avoided the problems associated with local neutron production and moderation which are present in airplane measurements.

The data show a maximum in the neutron density of $4.8 \pm 1.2 \times 10^{-7}$ neutrons cm^{-3} at a pressure altitude of 100 g cm^{-2} (53,000 ft), a rapid decline above this altitude, and an exponential

decrease below 250 g cm^{-2} with an absorption length of $165 \pm 20 \text{ g cm}^{-2}$.

If the data are extrapolated to the top of the atmosphere by the use of neutron transport theory, a value of $1.6 \pm 0.8 \times 10^{-8}$ neutrons cm^{-3} is obtained. These results are in reasonable agreement with the work of the New York University Cosmic-Ray Group (2, 3).

TABLE OF CONTENTS

	Page
I. INTRODUCTION	1
II. THEORETICAL CONSIDERATIONS	4
III. THE EXPERIMENT	20
IV. THE INSTRUMENT	33
V. ANALYSIS AND COMPARISON OF THE DATA	42
VI. OTHER EXPERIMENTS	65
VII. CONCLUSIONS	78
References	82
Appendices	90
A. Symbols, Units, and Nomenclature .	90
B. Electrometer Unit	92
C. Preparation and Purification of BF_3	106
D. Ionization Chamber Self-Shielding Calculation	113
E. Balloon Flight Data	120
Figures	138

TABLE OF FIGURES

	Page
1. Pressure Altitude versus Standard Height . . .	139
2. Geometry for Absolute Calibration . . .	141
3. Balloon Flight Train at Launch	143
4. Quartz Electrometer Unit	145
5. Temperature Sensing Unit	147
6. Instrument Temperature on Flight No. 5 . . .	149
7. Ionization Current versus Collector Voltage .	151
8. Cosmic-Ray Ionization in the Atmosphere . .	153
9. Ionization Current of the B ¹⁰ F ₃ Chambers . .	155
10. Ionization Current of the B ¹¹ F ₃ Chambers . .	157
11. Ionization Current at Low Altitudes	159
12. Cosmic-Ray Neutron Density in the Atmosphere .	161
13. Ionization Due to Bomb Test Debris	163
14. Neutron Density as Determined by Hess, et al. and Lingenfelter	165
15. Neutron Density Measurements by the New York University Cosmic-Ray Group (Soberman) . .	167
16. Neutron Density Measurements by the New York University Cosmic-Ray Group (Haymes) . .	169
17. Neutron Density Measurements by L. C. L. Yuan	171
18. Equivalent Circuit of the Ionization Chamber .	173
19. Fiber Geometry for the Quartz Electrometer Unit	175
20. Boron Trifluoride Processing and Purification System	177

I. INTRODUCTION

The half life of the free neutron is 12 minutes. For this reason, excluding the possibility of solar production, the free neutrons existing in the atmosphere must be of local origin, i. e., either they represent part of the fragmentation products of the incident cosmic radiation, or they are the disintegration products of nuclei of the atmosphere which have experienced interaction with cosmic radiation.

Within a few years after the discovery of the neutron in 1932 by Chadwick (5, 6), cosmic-ray interactions were observed which were ascribed to this new particle (7, 8). Slow neutrons of cosmic-ray origin were first detected by Fünfer (9) in 1937 using boron lined counters. Balloon flights to measure the altitude dependence of slow cosmic-ray neutrons were made by Korff in 1939 (10), utilizing BF_3 filled proportional counters. Bethe, Korff, and Placzek (11) undertook the first theoretical treatment of the altitude dependence of cosmic-ray neutrons. The analysis predicted a maximum in the cosmic-ray neutron density at a depth greater than 100 grams cm^{-2} pressure altitude (53,000 ft), and a rapid decline at higher altitudes. The maximum was investigated by Yuan (12) in several balloon flights in 1948 and 1949. The geomagnetic latitude variation of the cosmic-ray neutron density was determined by Soberman (13) in a series of balloon flights made from 1952 to 1954 at $\lambda_m = 89^\circ\text{N}$, $\lambda_m = 55^\circ\text{N}$, and $\lambda_m = 10^\circ\text{N}$.

During the winter of 1957-58, Hess, Patterson, Wallace, and Chupp (14) measured the cosmic-ray neutron energy spectrum from thermal energies up to 1 BeV using several types of detectors in a B-36 aircraft operating at various altitudes up to 40,000 feet (200 g cm^{-2}). Using a multi-group diffusion theory approach, Hess, Canfield, and Lingenfelter (4) extended the neutron energy spectrum up to the top of the atmosphere and calculated the distribution of neutrons in space near the earth. It was first noted by S. F. Singer (15) and independently by P. J. Kellogg (16) that the decay of these neutrons furnishes a mechanism for injecting charged particles into the Van Allen Radiation Belts. Lingenfelter (17), in an article to be published in 1963, has surveyed the experimental results of all workers, and using the multi-group diffusion methods of reference 4, has calculated the production rate of C^{14} in the atmosphere by the $\text{N}^{14}(\text{n}, \text{p})\text{C}^{14}$ reaction.

A number of review articles on the subject of cosmic-ray neutrons have been written: Bethe, Korff, and Placzek (11) in 1940, Flügge (18) in 1943, Bagge and Fincke (19) in 1950, Freese and Meyer (20) in 1953, and Lingenfelter (17) in 1963.

The experimental results of this thesis constitute a measurement of the density of cosmic-ray neutrons throughout the atmosphere. It is actually a measurement of neutrons with energies less than 10 keV, since less than 1% of the counting rate of the detector is due to the

capture of neutrons with energies greater than this value. It is a measurement of neutron density, rather than neutron flux, due to the $1/v$ energy dependent character for the capture cross section of the detector.

II. THEORETICAL CONSIDERATIONS

A proper starting point for discussion of the production, slowing-down, and capture or decay of cosmic-ray neutrons in the atmosphere is the Neutron Transport Equation (21, 22). Let

$$N(\underline{r}, v, \underline{\Omega}, t) dV dv d\Omega \quad (\text{Eqn. 1})$$

represent the number of neutrons at time t in the volume element dV at the position \underline{r} , with a speed between v and $v + dv$ in a direction lying within a solid angle $d\Omega$ around the direction $\underline{\Omega}$.

The effects of gravity may be ignored for neutrons diffusing in the atmosphere, and for neutrons with energies greater than a few eV diffusing out of the top of the atmosphere. Thus the motion of a free neutron in the atmosphere, from creation to absorption or decay, can be described in terms of a series of well-defined, randomly occurring events. Between these events, the neutron proceeds with constant velocity along an essentially rectilinear trajectory. Neutron-neutron collisions may be ignored since the number of neutrons compared to the number of nuclei of air is insignificant ($\sim 10^{-25}$ at 50,000 ft, where the neutron density has its maximum value).

Therefore, for the neutrons in the atmosphere, an integro-differential equation may be written, expressing the time rate of change of neutrons at time t at the position \underline{r} .

$$\begin{aligned}
\frac{\partial N}{\partial t}(\underline{r}, v, \underline{\Omega}, t) &= -v\underline{\Omega} \cdot \underline{\nabla} N(\underline{r}, v, \underline{\Omega}, t) && \text{Neutron "leakage"} \\
&\quad -\frac{1}{\tau} N(\underline{r}, v, \underline{\Omega}, t) && \text{Neutron decay} \\
&\quad -\Sigma_t v N(\underline{r}, v, \underline{\Omega}, t) && \text{Scattering out plus absorption} \\
&\quad +S(\underline{r}, v, \underline{\Omega}, t) && \text{Neutron source function} \\
&\quad + \int_0^{\infty} dv' \int_0^{4\pi} d\Omega' \Sigma(v' \rightarrow v, \underline{\Omega}' \rightarrow \underline{\Omega}) v' N(\underline{r}, v', \underline{\Omega}', t) && \text{Scattering in}
\end{aligned}$$

(Eqn. 2)

where τ is the mean life of the neutron with respect to β -decay; Σ_t is the macroscopic total cross section (scattering out plus absorption), and $\Sigma(v' \rightarrow v, \underline{\Omega}' \rightarrow \underline{\Omega}) dv' d\Omega'$ is the macroscopic cross section for scattering a neutron from the velocity element $dv' d\Omega'$ into the velocity element $dv d\Omega$; $S(\underline{r}, v, \underline{\Omega}) dv d\Omega$ is the number of neutrons per sec per cm^3 produced in the velocity element $dv d\Omega$ at \underline{r} .

All of the processes of neutron migration, scattering, and absorption occur on a time scale short with respect to the time variations of the source function to be considered. Thus the equation reduces to one of a "steady-state" nature. Equating the removal processes to the creation processes, one obtains:

$$\begin{aligned}
v\underline{\Omega} \cdot \underline{\nabla} N(\underline{r}, v, \underline{\Omega}) + \frac{1}{\tau} N(\underline{r}, v, \underline{\Omega}) + \Sigma_t v N(\underline{r}, v, \underline{\Omega}) \\
= S(\underline{r}, v, \underline{\Omega}) + \int_0^{\infty} dv' \int_0^{4\pi} d\Omega' \Sigma(v' \rightarrow v, \underline{\Omega}' \rightarrow \underline{\Omega}) v' N(\underline{r}, v', \underline{\Omega}').
\end{aligned}$$

(Eqn. 3)

The half-life of the neutron is 11.7 ± 0.3 min (23). This time is quite long compared to the slowing down and capture time for neutrons at sea level where this time is 0.15 sec, and even for neutrons at 68,000 ft (50 g cm^{-2}) where the time is 3 sec. Above this altitude the neutrons may diffuse upward and escape into space, where decay becomes the only removal process. Thus for the analysis of neutrons in the atmosphere, the process of decay will be ignored.

It is necessary to define these quantities: neutron density, neutron flux, and the neutron current.

The neutron density at the position \underline{r} is obtained by integrating $N(\underline{r}, v, \Omega)$ over all velocities:

$$N(\underline{r}) \equiv \int_0^{\infty} dv \int_{4\pi} d\Omega N(\underline{r}, v, \Omega) . \quad (\text{Eqn. 4})$$

$N(\underline{r})$ is the number of neutrons cm^{-3} at \underline{r} .

The neutron flux is obtained by integrating $vN(\underline{r}, v, \Omega)$ over all directions:

$$\phi(\underline{r}, v) \equiv \int_{4\pi} d\Omega v N(\underline{r}, v, \Omega) . \quad (\text{Eqn. 5})$$

$\phi(\underline{r}, v)dv$ is the number of neutrons per sec with velocities between v and $v + dv$ that intercept a sphere of unit cross section area located at \underline{r} .

The neutron current is obtained by integrating $\Omega vN(\underline{r}, v, \Omega)$ over all directions:

$$\underline{J}(\underline{r}, v) = \int^{4\pi} d\Omega \underline{\Omega} v N(\underline{r}, v, \Omega) . \quad (\text{Eqn. 6})$$

$\underline{J}(\underline{r}, v) dv dA$ is the net number of neutrons per sec with speeds between v and $v + dv$ that cross a plane surface of area dA located at \underline{r} , and whose normal lies in the direction of \underline{J} .

Since the atmosphere forms only a thin layer on the surface of the earth, and as the slowing-down and diffusion distances for cosmic-ray neutrons are very small compared to distances over which geomagnetic variations of the neutron sources are significant, the density of neutrons depends only on the vertical position in the atmosphere. It is convenient to express this in units of $g \text{ cm}^{-2}$ mass of air overhead.

Integrating Equation 3 over all directions, making the transformation of variables from \underline{r} to $x \text{ g cm}^{-2}$, and noting that $v\Omega \cdot \nabla N(\underline{r}, v, \Omega) = \underline{\Omega} \cdot [\underline{\Omega} v N(\underline{r}, v, \Omega)]$, one obtains:

$$\underline{\nabla} \cdot \underline{J}(x, v) + \Sigma_t \varphi(x, v) = S(x, v) + \int_0^{\infty} dv' \Sigma(v' \rightarrow v) \varphi(x, v') . \quad (\text{Eqn. 7})$$

Given the source function $S(x, v)$ and the macroscopic cross sections Σ_t and $\Sigma(v' \rightarrow v)$, in principle $N(x, v)$, $\varphi(x, v)$, and $\underline{J}(x, v)$ can be obtained from Equation 7. For velocity dependent cross sections, a straightforward solution of this equation is not feasible. Various approximation techniques have been developed to render the equation more tractable.

If $\tilde{J}(\mathbf{x}, \nu)$ is a slowly varying function of \mathbf{x} , then the "diffusion" approximation,

$$\tilde{J}(\mathbf{x}, \nu) = -D \nabla \cdot \tilde{\varphi}(\mathbf{x}, \nu) ,$$

can be made. The necessary criterion is that $\nabla \cdot \tilde{\varphi}(\mathbf{x}, \nu) \ll \frac{\varphi(\mathbf{x}, \nu)}{\lambda_s}$,

where λ_s = scattering length. For neutrons in the atmosphere, this will be reasonably valid except near the boundary. The boundary condition is discussed in Chapter VI. Inserting the "diffusion" approximation in Equation 7, and noting that since \mathbf{x} is expressed in g cm^{-2} , the diffusion coefficient, D , will be independent of position,

$$-D \nabla^2 \varphi(\mathbf{x}, \nu) + \Sigma_t \varphi(\mathbf{x}, \nu) = S(\mathbf{x}, \nu) + \int_0^{\infty} d\nu' \Sigma(\nu' \rightarrow \nu) \varphi(\mathbf{x}, \nu') \quad (\text{Eqn. 8})$$

Hess, Canfield, and Lingenfelter (4) solve this equation numerically by dividing the velocity spectrum into a series of velocity intervals, or groups, and using constant cross sections obtained by averaging in the various velocity intervals, obtain a diffusion solution for each group. The source of neutrons for a particular group, below cosmic-ray production energies and above thermal energies, is essentially the neutrons scattered out of the next higher velocity interval. This "multi-group diffusion" approach is more satisfactory than any of the analytical approaches (11, 18, 19, 20), because it is easier to include such effects as the variation of the scattering and capture cross sections

between the different groups, and it is possible to account for the finite temperature of the scattering medium.

In order to obtain a solution to Equation 8, the source function, $S(x, v)$, must be explicitly inserted into the equation. All solutions to date have either restricted the range of applicability to those energies below production energies, or have introduced an experimentally determined function for $S(x, v)$. No attempt has been made to solve the problem from first principles, i. e., given the incident cosmic radiation and all applicable cross sections, calculate the distribution of neutrons throughout the atmosphere.

It is possible, in the energy range below the free neutron production energies ($E < 1 \text{ MeV}$), to make certain approximations and obtain reasonable estimates on most quantities of interest, such as characteristic energies and lengths, without resort to computer techniques. The methods and formulas used to calculate the following numbers are derived in S. Glasstone and M. C. Edlund, The Elements of Nuclear Reactor Theory (D. Van Nostrand, Princeton, 1952).

Quantities that are not too energy dependent can be estimated by solving the "one-velocity" problem, i. e., by assuming that monoenergetic neutrons are scattered or absorbed by nuclei of infinite mass. The scattering cross section for thermal neutrons ($E = 0.025 \text{ eV}$; $v = 2.2 \times 10^5 \text{ cm sec}^{-1}$) in air is 10.8 barns per nucleus and the absorption

cross section for nitrogen is 1.9 barns (24). The diffusion coefficient D in Equation 8 is equal to 0.9 g cm^{-2} for thermal neutrons. The mean free path for scattering is 2.4 g cm^{-2} and the mean free path for absorption is 16 g cm^{-2} . These quantities determine the distance a thermal neutron will diffuse before absorption. The vertical component of the average distance a thermal neutron will diffuse before absorption by the $\text{N}^{14}(\text{n}, \text{p})\text{C}^{14}$ reaction is 6 g cm^{-2} . This thermal diffusion and absorption will take place in a time of the order of 0.05 sec at sea level.

It is important to realize, however, that thermal capture lengths and capture times are not the significant quantities for cosmic-ray neutrons in the atmosphere. This is so because the $\text{N}^{14}(\text{n}, \text{p})\text{C}^{14}$ capture reaction removes the neutrons during the slowing-down process before thermal energies are reached. Most of the neutrons are knock-on and evaporation products of nuclei disrupted by cosmic-ray interactions. Typically, the initial energies of these neutrons range from a few hundred thousand electron volts up to many million electron volts, and even as high as the energy of the incident cosmic-ray particles. Below about 500 keV the neutrons are slowed down principally by elastic collisions with the nuclei of air. The $\text{N}^{14}(\text{n}, \text{p})\text{C}^{14}$ capture reaction raises the maximum in the differential energy flux spectrum from thermal energies (0.025 eV) to about 0.1 eV.

For s-wave (isotropic in the center of mass system) elastic scattering of neutrons by nuclei, the average logarithmic energy decrement,

$$\xi = \ln \frac{E_1}{E_2} ,$$

is independent of the kinetic energy of the collision. For air, $\xi = 0.136$. This implies that 134 elastic collisions are necessary for a 2 MeV neutron to thermalize. If these neutrons slow down in an infinite nonabsorbing medium, they will have an energy spectrum of the form:

$$\varphi(E) \propto \frac{1}{E} .$$

If absorption occurs in the medium, this $1/E$ spectrum must be multiplied by an exponential term, referred to as the "resonance escape probability" (Σ_a = absorption cross-section; Σ_s = scattering cross-section):

$$\varphi(E) = \frac{Q_0}{[\xi \Sigma_s + \gamma \Sigma_a] E} \exp \left\{ - \int_E^{E_0} \frac{\Sigma_a}{\xi \Sigma_s + \gamma \Sigma_a} \cdot \frac{dE'}{E'} \right\} ,$$

(Eqn. 9)

where $Q_0 =$ neutrons $\text{cm}^{-3} \text{sec}^{-1}$ slowing down past the energy E_0 , and where ξ and γ have numerical values somewhat dependent upon the assumptions made in the derivation as to the exact manner in which the slowing-down process takes place. For air, $\xi \approx 0.136$ and $\gamma \approx 0.09$.

If the macroscopic cross sections for air are substituted in Equation 9 and the integration carried out, a maximum at about 0.1 eV is obtained for $\varphi(E)$, the neutron flux. The multi-group diffusion calculation of Hess, et al. yielded a $1/E^{0.9}$ neutron flux spectrum in the range of 1 MeV down to 0.2 eV, with a maximum at 0.1 eV. It appears that the thermal motions of the medium and the binding energies of the molecules of air do not exert a major influence on the shape of the energy spectrum; the shape of the spectrum is determined mainly by the $N^{14}(n,p)C^{14}$ absorption (25).

The vertical component of the average distance a 2 MeV neutron will diffuse before it is slowed down to 0.1 eV is of the order of 50 g cm^{-2} . This occurs in a time of about 0.15 sec at sea level. Even at an altitude of 100,000 ft (10 g cm^{-2} pressure altitude), the slowing down time is short compared to the mean life of the neutron with respect to beta decay--15 seconds compared to a beta decay mean life of 1013 seconds. Of course, at 100,000 ft there is a large probability that the neutron will diffuse out into space, where beta decay will be the only removal process. Lingenfelter (17) estimates that the neutron source function should have a maximum at about 50,000 ft (100 g cm^{-2} pressure altitude), with an exponential absorption length of 170 g cm^{-2} below this altitude. Thus, because of the short slowing down distance, it follows that the density of cosmic-ray neutrons should exhibit a maximum at an atmospheric depth of 100 g cm^{-2} with an

exponential absorption length below this altitude of 170 g cm^{-2} . Above a pressure altitude of 100 g cm^{-2} , the neutron density should drop rapidly toward small values because of the outward diffusion, as is discussed in Chapter VI.

The free neutrons present in the atmosphere arise from several sources: products of knock-on collisions of cosmic-ray nucleons with the nuclei of the air, evaporation products from nuclei excited by cosmic ray interactions, neutrons that arrive as bound nucleons in cosmic radiation, neutrons produced by solar high energy particles interacting with the uppermost portion of the atmosphere (principally at high latitudes during solar flares), and neutrons that are produced by charge exchange reactions in the chromosphere and corona of the sun.

Hess, Canfield, and Lingenfelter (4) have estimated that the maximum in the knock-on source spectrum occurs at 10 MeV, and that the maximum in the evaporation source spectrum occurs at 1 MeV. Fitting these spectra to the experimental data of Hess, et al. (4, 14), Hess obtains the following integrated source values for $\lambda_m = 45^\circ$:

$$\begin{aligned} S(\text{knock-on}) &= 1.2 \text{ neutrons cm}^{-2} \text{ sec}^{-1} \\ S(\text{evaporation}) &= 5.0 \text{ neutrons cm}^{-2} \text{ sec}^{-1} . \end{aligned}$$

The number of neutrons that arrive as bound nucleons in cosmic radiation and are subsequently released in nuclear interactions can be

estimated from the data of Anderson (26). The vertical cut-off for $\lambda_m = 41^\circ$ is about 5 BV in magnetic rigidity units. Anderson obtains for the integral flux in 1958, using the charge composition of Waddington (27):

$$\text{Cosmic-Ray Flux (> 5 BV)} = 0.058 \text{ particles cm}^{-2} \text{ sr}^{-1} \text{ sec}^{-1}.$$

A summation of the bound neutrons in cosmic-rays is carried out in Table I. In order to obtain the bound neutron current incident at the top of the atmosphere (bound neutrons $\text{cm}^{-2} \text{ sec}^{-1}$), these values must be multiplied by a number of the order of π (π results for the assumption of isotropy of the incident radiation over the upper hemisphere).

$$\left[\begin{array}{l} \text{Bound Neutron Current Incident} \\ \text{at the Top of the Atmosphere} \end{array} \right] = 0.07 \text{ neutrons cm}^{-2} \text{ sec}^{-1}.$$

This number is small with respect to the total number of neutrons produced by cosmic-ray interactions per cm^2 column of air in the atmosphere, and can therefore be neglected.

Simpson (28) has made an estimate of the triton production due to the nuclear interactions of solar high energy particles in the atmosphere. A similar calculation can be carried out for the production of free neutrons in the atmosphere by the solar high energy particles. The number of neutrons produced per second averaged over a solar cycle can be determined as:

TABLE I

BOUND NEUTRON FLUX INCIDENT AT THE TOP OF THE
ATMOSPHERE AS DETERMINED FROM THE ELEMENTAL
ABUNDANCES IN COSMIC RADIATION

Element	Z	Flux > 5 BV particles $\text{cm}^{-2} \text{sr}^{-1} \text{sec}^{-1}$	Average number of neutrons	Bound Neutron Flux neutrons cm^{-2} $\text{sr}^{-1} \text{sec}^{-1}$
Hydrogen	1	500×10^{-4}	0	0
Helium	2	74×10^{-4}	2	148×10^{-4}
Light	3-5	1.7×10^{-4}	5.5	9×10^{-4}
Medium	6-9	4.7×10^{-4}	6.5	31×10^{-4}
Heavy	10-19	1.6×10^{-4}	9.5	15×10^{-4}
Very Heavy	20-28	0.6×10^{-4}	25	15×10^{-4}

Total number of neutrons $\text{cm}^{-2} \text{sr}^{-1} \text{sec}^{-1} = 218 \times 10^{-4}$

$$S = \frac{1}{T} \int dE G_o \psi(E) \eta(E) \delta(E) ,$$

- where S = neutrons $\text{cm}^{-2} \text{sec}^{-1}$ produced in the atmosphere averaged over the earth and over the time interval T ,
- $G_o = \frac{1}{4}$ = conversion factor from omnidirectional intensity in space to particle current incident at the top of the atmosphere,
- $\psi(E)$ = the differential energy flux spectrum of the solar high energy particles integrated over the time interval T ,
- $\eta(E)$ = the number of free neutrons produced in nuclear interactions due to an incident particle of energy E ,
- $\delta(E)$ = the fraction of the earth geomagnetically allowed for a solar high energy particle of energy E .

Interpretation and correlation of the data obtained by riometers and neutron monitors installed in a number of ground stations, and by particle detectors flown on balloons, sounding rockets, and satellites permit reasonably valid estimates (within a factor of two) to be made for the flux of solar high energy particles since 1956. H. H. Malitson and W. R. Weber (29) estimate that the time integrated omnidirectional intensity of solar high energy particles (mostly protons) from 1956 through 1961 is 2.1×10^{10} protons cm^{-2} with energies greater than 30 MeV. Most of the solar flares generated protons with differential energy spectra of the form $1/E^4$ for energies greater than 100 MeV. The time averaged spectra can be fit to $1/E^{2.6}$ for solar protons between 30 MeV and 100 MeV.

The number of neutrons produced per incident proton can be estimated from cosmic-ray data (30,31) and from a Monte Carlo calculation performed by the Oak Ridge National Laboratory (32). In the energy range of 50 MeV to 400 MeV for the incident protons, the average number of neutrons produced per nuclear inelastic collision is observed to vary from 0.86 to 1.9. For protons in this energy range, the mean free path for inelastic collisions in air is approximately 90 g cm^{-2} (33).

The fraction of the earth that is geomagnetically allowed to solar protons of energy E can be determined from the cutoff rigidities calculated by J. J. Quenby and W. R. Weber (34). The values obtained in this manner actually form only a lower limit as abrupt decreases in the geomagnetic cutoff have been observed coincident with the start of the main phase of some geomagnetic storms. This breakdown of the geomagnetic cutoff has been observed at Minnesota on several occasions (35), but its relation to flare importance and heliographic position, and the state of the interplanetary medium is complex. For solar protons of energies of 30 MeV to 400 MeV, the allowed fraction of the earth varies between 7% and 15%. The breakdown of the geomagnetic cutoff at high latitudes probably does not increase the allowed fraction by much more than a factor of 2, and then only occasionally.

If it is assumed that the solar proton fluxes observed between 1956 and 1961 are representative of those to be expected over an eleven

year solar cycle, then a time-and-global average of 0.05 neutrons per second produced per cm^{-2} column of air is obtained. This number is roughly two orders of magnitude lower than the number of free neutrons produced by galactic cosmic-rays.

The measurements of Meyer and Vogt (36, 37) indicate that a proton flux with a differential energy spectrum of $1/E^2$ in the energy range of 80 MeV to 350 MeV is continually present in the primary radiation in the years of high solar sunspot activity. This flux is observed to decrease in intensity with the declining level of sunspot activity, concurrent with the increase of galactic cosmic radiation. Meyer and Vogt interpret these measurements to mean that this low energy $1/E^2$ proton flux is of solar origin. If protons are accelerated to such energies in the chromosphere or corona of the sun, then most certainly neutrons in this energy range are also produced there by charge exchange reactions. The question as to whether they would be detected at the top of the atmosphere is only one of intensity. The beta decay process does not prevent these neutrons from arriving in the vicinity of the earth: 34% of 100 MeV neutrons should not decay during the sun-earth transit. It must be noted, however, that the integrated intensity of these $1/E^2$ solar protons is relatively low. Only about 0.01 protons $\text{cm}^{-2} \text{sr}^{-1} \text{sec}^{-1}$ were observed. This $1/E^2$ flux, averaged over a sunspot cycle, is at least one order of magnitude smaller than the flux of solar flare particles in the same energy range.

On two balloon flights flown at constant altitude through sunset, Haymes (38) observed no high altitude neutron intensity diurnal variation. No experimental evidence exists that indicates that the solar neutron flux constitutes a significant source of free neutrons in the atmosphere.

The free neutrons measured in the work of this thesis are principally products of knock-on collisions of cosmic-ray nucleons with the nuclei of the air and evaporation products from nuclei excited by cosmic-ray interactions. The geomagnetic latitude of 41° has a vertical cutoff of about 5 BV in magnetic rigidity units; only particles from a few of the largest solar flares would be able to penetrate the magnetic field and interact with the atmosphere. It appears that all other sources of free neutrons may be neglected at this latitude.

Hess, et al. (4) have estimated that of the total number of cosmic-ray neutrons that are produced in the atmosphere, 76% initially have energies below 1 MeV, 17% have initial energies between 1 MeV and 10 MeV, and 7% have initial energies greater than 10 MeV. These neutrons are removed by several processes: 66% are captured in the $N^{14}(n,p)C^{14}$ reaction, 16% are captured by other reactions, 17% diffuse upward out of the atmosphere, and less than 1% strike the earth and are captured.

III. THE EXPERIMENT

The density of cosmic-ray neutrons was derived from measurements using ionization chambers filled with $B^{10}F_3$, $B^{11}F_3$, and argon gases. The ionization current resulting from the $B^{10}(n,\alpha)Li^7$ reaction in the $B^{10}F_3$ chambers was utilized to detect the neutrons. The $B^{11}F_3$ and argon chambers monitored the background current due to the ionizing component of cosmic radiation.

The $B^{10}(n,\alpha)Li^7$ reaction has a cross section of $3,813 \pm 50$ barns for thermal neutrons (for a neutron velocity of 2.2×10^5 cm sec⁻¹, which is the most probable velocity of neutrons in thermal equilibrium at 20°C). The uncertainty estimated for the cross section results partially from variations in the B^{10} isotopic concentration in natural boron. Variations as large as 3% in the B^{11}/B^{10} ratio of natural boron have been observed in samples obtained from different locations around the world (39). Thode, et al. (39) have observed a variation of 0.5% in the B^{11}/B^{10} ratio of California boron. It is unfortunate, from the point of view of accurate neutron measurements, that boron should have such an appreciable variation in its isotopic concentration. Furthermore, there exists the possibility of an unknown chemical or physical separation of the isotopes during the process of the determination of the isotopic ratio (40). The value of 3,813 barns quoted here corresponds to a capture cross section of 755 ± 2 barns obtained for a sample of boron containing 19.8% B^{10} (24). The error of ± 50 barns

assigned to the $B^{10}(n,\alpha)Li^7$ reaction corresponds to the standard deviation of the recent values determined for natural boron as listed by F. Ajzenberg-Selove and T. Lauritsen (41). Undoubtedly, part of this variation is due to different isotopic ratios.

For incident neutrons of thermal energies, 94% of the $B^{10}(n,\alpha)Li^7$ reactions proceed via an excited state of Li^7 , a percentage which does not change significantly in the energy range up to 10 keV (42,43). The subsequent decay to the ground state of Li^7 releases a 0.47 MeV γ -ray. The ionization chamber is transparent to γ -rays of this energy, and this amount of energy is lost. The remaining 6% of the $B^{10}(n,\alpha)Li^7$ reactions proceed directly to the ground state of Li^7 . For this channel the entire Q-value of 2.79 MeV is available for ionization.

TABLE II

Reaction	%	Q-value
$B^{10}(n,\alpha)Li^7$	$5.8 \pm 0.1\%$	2.793 ± 0.027 MeV
$B^{10}(n,\alpha)Li^{7*}$	$94.2 \pm 0.1\%$	2.320 ± 0.020 MeV
$\rightarrow Li^7 + \gamma$		0.473 ± 0.020 MeV

Thus the average energy available from this reaction for ionization is 2.35 MeV. As for the energy to form an ion pair in BF_3 , the best work seems to be that of Bortner and Hurst (44), who obtain a value

of 36.0 ± 0.4 eV. This implies that, on the average, about 65,000 ion pairs are formed per neutron capture.

Not all of this ionization is detected by the electrometer unit in the ionization chamber. If the recoiling reaction products impinge upon the chamber wall, the residual energy will be expended there. Some columnar recombination of electrons and ions will occur, particularly with the low electric fields present in the chamber (the total potential difference, from the central collector to the spherical shell of 13 cm radius, is less than 300 volts). The decrease in the collected ionization current due to the wall effect is of the order of a few percent. A comparison of the expected ionization current as calculated from the observed neutron density to the ionization current actually measured indicates that as high as 25% of the ionized atoms may experience recombination. Thus an absolute calibration of the chamber response to neutrons is necessary; it is not correct to assume that the 65,000 ion pairs formed per neutron capture are collected with 100% efficiency.

That the reaction cross section is inversely proportional to the velocity of the incident neutrons has been verified out to at least 100 keV (45). If the effects of self-shielding (see Appendix D) are neglected, then the $1/v$ dependence of the cross section has the property that the counting rate of the instrument is proportional to the neutron density. The counting rate is obtained by multiplying the macroscopic

capture cross section by the chamber volume V , and by the neutron flux, and integrating over all velocities.

$$C = \int_0^{\infty} dv \Sigma_a(v) V \varphi(v) .$$

Since $\Sigma_a(v) = \frac{n\sigma_0 v_0}{v}$ and $\varphi(v) = vN(v)$,

therefore $C = n\sigma_0 v_0 V \int_0^{\infty} dv N(v) .$

($n = B^{10}$ nuclei per cm^{-3} ; $\sigma_0 =$ capture cross section at a neutron velocity of v_0 .)

As $\int_0^{\infty} dv N(v)$ is just the number of neutrons per cm^{-3} , the counting rate is proportional to the neutron density, independent of the form of $N(v)$, the differential velocity spectrum for the neutrons.

Apart from fission reactions, there are only eight cases in which thermal neutron absorption results in appreciable formation of two charged particles (46). In principle, any compound of these nuclides existing in a gaseous state could be used for detecting thermal neutrons in an ionization chamber. In practice, however, undesirable physical and chemical properties restrict the number of available compounds. With regard to the $B^{10}(n,\alpha)Li^7$ reaction, both BF_3 and $B(CH_3)_3$ have been successfully used in proportional counters (47).

TABLE III
SLOW NEUTRON REACTIONS
WHICH YIELD CHARGED PARTICLES

He ³	+ n = H ³	+ H ¹	+ 0.74 MeV	$\sigma(\text{thermal}) = 5,400$ barns
Li ⁶	+ n = He ⁴	+ H ³	+ 4.66 MeV	$\sigma(\text{thermal}) = 940$ barns
Be ⁷	+ n = Li ⁷	+ H ¹	+ 1.65 MeV	$\sigma(\text{thermal}) = 51,000$ barns
B ¹⁰	+ n = Li ⁷	+ He ⁴	+ 2.88 MeV	$\sigma(\text{thermal}) = 3,800$ barns
N ¹⁴	+ n = C ¹⁴	+ H ¹	+ 0.56 MeV	$\sigma(\text{thermal}) = 1.8$ barns
O ¹⁷	+ n = C ¹⁴	+ He ⁴	+ 1.72 MeV	$\sigma(\text{thermal}) = 0.5$ barns
S ³³	+ n = F ³³	+ H ¹	+ 0.75 MeV	$\sigma(\text{thermal}) = 0.002$ barns
Cl ³⁵	+ n = S ³⁵	+ H ¹	+ 0.6 MeV	$\sigma(\text{thermal}) = 0.3$ barns

The experimental data of this thesis were obtained by attaching to balloons ionization chambers filled with B¹⁰F₃, B¹¹F₃, and argon gases, and by recording the chamber currents as the balloons rose through the atmosphere. Transmitter units fastened to the chambers telemetered the chamber currents to a receiving station on the ground. The ionization current resulting from the B¹⁰(n,α)Li⁷ reaction was utilized to measure the density of the cosmic-ray neutrons. The B¹¹F₃ and argon chambers determined the background current in the B¹⁰F₃ chambers due to the ionizing component of cosmic radiation. Table IV gives a synopsis of the balloon flights.

TABLE IV
SYNOPSIS OF BALLOON FLIGHTS

Flight	Date	Chamber	Gas	Pres.	Measurement
1	15 Nov 61	335	Argon	8 atm	Cosmic-ray ionization
2	6 Feb 62	321	$B^{10}F_3$	1 atm	Cosmic-ray neutrons
		279	$B^{11}F_3$	1 atm	Background
3	6 Feb 62	375	$B^{10}F_3$	0.5 atm	Cosmic-ray neutrons
		347	$B^{11}F_3$	0.5 atm	Background
4	4 July 62	315	Argon	8 atm	Cosmic-ray ionization
5	5 July 62	253	$B^{10}F_3$	0.5 atm	Cosmic-ray neutrons
		366	$B^{11}F_3$	0.5 atm	Background
6	6 July 62	271	$B^{10}F_3$	0.5 atm	Cosmic-ray neutrons
		343	Argon	8 atm	Cosmic-ray ionization
7	22 Oct 62	309	$B^{10}F_3$	0.5 atm	Cosmic-ray neutrons
		257	$B^{10}F_3$	0.5 atm	Transmitter failed
8	23 Oct 62	379	$B^{10}F_3$	0.5 atm	Cosmic-ray neutrons
			$B^{10}F_3$	0.5 atm	Low altitude cosmic-ray neutrons (High sensitivity electrometer)
9	25 Oct 62	286	$B^{11}F_3$	0.5 atm	Radioactivity from bomb test debris
		404	Argon	8 atm	Radioactivity from bomb test debris

The small ionization currents present in the chambers (10^{-14} to 10^{-11} amp) limited the amount of data that could be obtained on a single flight. The results of the nine balloon flights indicate that the intensity of cosmic-rays incident at the geomagnetic latitude of 41°N did not change by more than 1% from Nov. 15, 1961 to Oct. 25, 1962. This fact is verified by the counting rates of the neutron monitor at Climax, Colorado ($\lambda_m = 48^\circ\text{N}$), which exhibited variations in the monthly averages of about $\pm 1\%$ during this period (48). This constancy of the incident primary radiation allows the data from the different flights to be collected together in the analysis. From the data obtained on the nine flights, it is possible to construct a single curve for the $\text{B}^{10}(\text{n},\alpha)\text{Li}^7$ ionization as a function of pressure altitude. The manner in which the data from the B^{10}F_3 chambers are corrected for the ionization due to the ionizing component of cosmic-rays is described in Chapter V. A calibration was performed, relating the B^{10}F_3 ionization chamber current to the density of neutrons in the vicinity of the chamber. Thus, from the flight data and the calibration results, the density of cosmic-ray neutrons in the atmosphere can be determined as a function of pressure altitude.

The construction and operation of the ionization chambers is described in Chapter IV. The construction and operation of the electrometer units for measuring the ionization chamber currents is described in Appendix B. The preparation and purification of the BF_3 is described in Appendix C.

Prior to flight, the chambers were attached to transmitters, and were normalized in a flux of γ -rays producing a known ionization in air. An explanation of the normalization procedure is given in Chapter V. Thus, in the absence of slow neutrons, the $B^{10}F_3$, $B^{11}F_3$, and argon chambers would all register the same numerical value. This value corresponded to the number of ion pairs $cm^{-3} sec^{-1}$ that would be produced by the γ -ray flux in air at a pressure of 74 cm Hg and a temperature of $24^\circ C$. This nonstandard condition for air was chosen so that the ionization values obtained on the balloon flights would be directly comparable with the earlier work of the cosmic-ray group at the California Institute of Technology (26, 49, 50).

In Chapter V and in Appendix E, the flight data are initially reduced in terms of "equivalent ion pairs." This unit, in the absence of slow neutrons, is just the quantity described in the preceding paragraph, "ion pairs $cm^{-3} sec^{-1} atm^{-1}$." In the presence of slow neutrons, the $B^{10}F_3$ chamber will indicate a higher ionization than the $B^{11}F_3$ or argon chambers, due to the $B^{10}(n,\alpha)Li^7$ reaction. This excess ionization is then related to the neutron density (neutrons cm^{-3}) by comparing the ionization current of the chamber with the counting rate of a calibrated $B^{10}F_3$ proportional counter.

The transition from "equivalent ion pairs" ionization due to the $B^{10}(n,\alpha)Li^7$ reaction to neutron density was accomplished by means of an absolute calibration. A 10 mCi Ra- α -Be neutron source

$(\alpha + \text{Be}^9 \rightarrow \text{C}^{12} + n + 5.7 \text{ MeV})$ was positioned against a concrete wall, and 40 cm of lead were placed in front. The entire assembly (front, top, and sides) was covered with 13 cm of paraffin to thermalize the neutrons. Figure 2 is a drawing of the calibration geometry. Both the ionization chamber and a B^{10}F_3 proportional counter of known cross section for the $\text{B}^{10}(n,\alpha)\text{Li}^7$ reaction were placed in front of the calibration assembly. From this calibration, a value for the neutron density N in terms of the ionization chamber current $I(n)$, expressed in "equivalent ion pairs," due to the $\text{B}^{10}(n,\alpha)\text{Li}^7$ reaction was obtained.

$$N (\text{neutrons cm}^{-3}) = 2.6 \pm 0.5 \times 10^{-9} I(n).$$

The analysis of the calibration data is undertaken in Chapter V.

An intercomparison of standards was made in the calibration facility used by Hess, et al. (14, 51).¹ The B^{10}F_3 proportional counter used as the calibration standard for this experiment (Reuter-Stokes RSN 40A Counter #C-894 filled with 96% B^{10}F_3 to a pressure of 40 cm Hg) was placed in a concrete blockhouse and irradiated with a known thermal neutron flux. The manufacturer's stated counting rate of 2.0 counts sec^{-1} per unit thermal neutron flux, when converted to a reaction cross section, agrees within 1% of the $\text{B}^{10}(n,\alpha)\text{Li}^7$ cross section value for thermal neutrons of 2.14 cm^2 obtained in the Lawrence Radiation Laboratory facility.

¹ I am indebted to H. W. Patterson and A. Smith of the Lawrence Radiation Laboratory, Berkeley, Calif., for the calibration of the BF_3 counter in their laboratory.

The transmitter units used for relaying the flight data back to the ground station broadcasted a chain of 1 watt, 100 μ sec pulses at a frequency of either 156.3 Mc or 159.3 Mc. In addition to encoding the signal from the ionization chamber electrometer, a transmitter unit also contained a device for measuring the barometric pressure (52), and on one flight a temperature sensor. A 300 volt battery and a 1.5 volt battery supplied electrical power. The batteries subtended a solid angle of less than 5% of 4π with respect to the ionization chamber. The operation of the transmitter unit is described in detail in reference 46.

The entire flight package was wrapped in red cellophane to keep the equipment warm (à la greenhouse effect) during the two hour ascent to maximum altitude, at which point the balloon would burst. The flight unit was attached to a paper parachute (53) by means of a 20 ft line of nylon cord. For flights where two instruments were carried aloft by a single balloon, the instruments were attached to a common tie point by lines of different lengths. The parachute was tied to the balloon by a 70 ft line. A long line was used to minimize the solid angle of the balloon with respect to the instruments. A launch line was attached to the neck of the balloon. The launch line enabled the flight train to be launched by two people in winds up to a few knots. One person would slowly reel out the launch line, while the second person would stand under the balloon holding the flight units. When

the units cleared the ground, the launch line was cut. Since the balloon and the flight train were aligned on a vertical axis, they would rise together and the flight units would clear the ground. See Figure 3 for a diagram of the flight train at launch. As the maximum weight of the flight train was two units of 6 lbs each and the balloon did not float at maximum altitude, no clearance was needed from the Federal Aviation Agency (54).

The balloons were manufactured by the Dewey and Almy Chemical Division of W. R. Grace and Co. (55). They are made from a rubber-like material called DAREX. The balloon film has an initial thickness of approximately 0.0035 inch and a thickness at burst of approximately 0.0001 inch. It is an extremely fragile material, and a slight surface abrasion caused by handling can impair performance seriously. The material will discolor within $\frac{1}{2}$ hour after exposure to direct sunlight, although the manufacturer states that discoloration should not affect performance. The balloons were manufactured less than 6 months prior to the launch date. Just before inflation, the balloon was carefully removed from its shipping container, and placed on a large plastic sheet. The hands and arms of the person handling the balloon were dusted with talc. A hose from the helium tank was inserted in the neck of the balloon and inflation initiated. When the balloon would just lift a set of weights equal to the weight of the flight train plus the desired net free lift, inflation was halted, the neck of the

balloon was tied off, and launch and load lines were attached. Typically, a net free lift of 1 to 2 lbs resulted in a rate of rise of 600 to 1000 ft per min.

On flights 1 through 3, Darex J11-28-2400 balloons were used. They require roughly 250 cu ft of helium to lift a flight load of 7 lbs with a net free lift of 1 lb. They have a diameter of 8 ft at inflation and a diameter of 40 ft at burst altitude. The manufacturer quotes an expected burst altitude of 115,000 ft (6 g cm^{-2}) for a payload of 7 lbs. The maximum height actually attained was 90,000 ft (16 g cm^{-2}).

On flights 4 through 9, Darex J11-42-7000 balloons were used. They require roughly 500 cu ft of helium to lift a flight load of 13 lbs with a net free lift of 1 lb. They have a diameter of 10 ft at inflation and a diameter of 60 ft at burst altitude. The manufacturer quotes an expected burst altitude of 124,000 ft (4 g cm^{-2}). The maximum height actually attained was $120,000 \pm 5,000$ ft.

Several factors entered into the determination of the balloon launch site. Since the transmitters operate in the VHF frequency band, essentially line-of-sight transmission is required between the flight train and the receiving station at the launch site. Radios operating in this frequency range are also susceptible to spark noise from automobile engines. Prudence dictates that the equipment should not be launched into heavily trafficked air lanes, nor should the equipment be expected to land in densely populated areas. The site should be

accessible on a year-round basis, and high winds are not permissible.

After consideration of all of these factors, a launch site was selected $\frac{1}{4}$ mile ENE of the giant rock located at Giant Rock Airport, Yucca Valley, California ($34^{\circ} 20'N$, $116^{\circ} 23'W$). This site (elevation: 2,880 ft) has unlimited visibility to the east and reasonably good visibility in other directions. An ungraded road dead-ends at the site, and no other roads or houses are located within half of a mile. The airport at Giant Rock is FAA certified for emergency landings of commercial airliners, and the air traffic amounts to about one light plane per day. The site is located on private property (George Van Tassel is the present owner), adjacent to the 29 Palms Marine Base. The weather is representative of that to be found in the California high desert. A typical day might encounter low winds (less than 5 knots) in the morning hours, with winds of increasing velocity and gusts up to 30 knots in the afternoon. Only on one day was a balloon launch canceled on account of winds.

IV. THE INSTRUMENT

The Neher integrating ionization chamber has been described in the literature (26, 56, 57, 58, 59). The basic elements are a spherical shell, a central electrically isolated collector, conductors at auxiliary potentials, and a quartz fiber recharging assembly. The mechanical system exclusive of the spherical shell is referred to as the "quartz electrometer unit." Figure 4 is a drawing of the quartz electrometer unit.

The quartz electrometer unit in the ionization chamber is capable of measuring a current of 10^{-13} amps with a precision of 1% by integrating the charge collected over a period of 30 minutes. The electrometer unit performs a current measurement in a period of time which is inversely proportional to the current:

$$\Delta t = \frac{\text{Calibration Constant}}{I}$$

The lower limit for current measurements is determined by leakage currents, and is probably lower than 10^{-15} amps. The upper limit is determined by the natural frequency of oscillation of the quartz fiber, and is of the order of 10^{-8} amps. The limiting factor for the sensitivity of the measurements made with an ionization chamber is the background current due to alpha particle emission from the walls of the chamber. This may run as high as 10^{-14} amps.

The electrometer action of the unit results from the capacitive coupling between the fiber and the lower end of the collector. When a differential voltage is generated between the fiber and the electrically isolated collector (due to the collection of electrons by the collector), then the resultant electrical force will displace the fiber. Due to the mechanical restoring force of the fiber, a new position of equilibrium will be attained for a certain range of fiber-to-collector differential voltages. The electrometer unit is so designed that at a preadjusted fiber-to-collector voltage, the fiber makes electrical contact and recharges the collector; the resulting current pulse is used to detect the occurrence of a recharging cycle. An analysis of the recharging mechanism and a prescription for satisfactory construction of the electrometer unit are given in Appendix B.

When operated as an ionization chamber, the fiber-to-collector differential voltage increases with time due to the collection of electrons by the collector. Thus in a constant flux of charged particles the chamber recharging pulses occur at regular intervals, with a statistical variation of the order of 1% resulting from the finite number of particles interacting in the chamber (roughly 10^4 per pulse), and a systematic variation of the order of 0.3% arising from irregularities in the amount of charge transferred to the collector during a chamber pulse.

For this experiment the electrometer unit was installed in a steel spherical shell of radius 12.8 cm and a wall thickness of 0.065 cm. The shell was given a 0.002 cm copper plating, and the outside was painted with Krylon paint. The total wall thickness was about 0.5 g cm^{-2} .

The electrometer unit was sealed into the shell, and the entire assembly was filled with a gas. For measurement of the ionization due to the charged particle and γ -ray flux of cosmic rays, argon gas at 8 atm pressure was used. For measurement of the density of cosmic ray neutrons, B^{10}F_3 gas was used in which ionization occurs due to the $\text{B}^{10}(n,\alpha)\text{Li}^7$ reaction. B^{11}F_3 gas was used to determine the background to the $\text{B}^{10}(n,\alpha)\text{Li}^7$ reaction in the B^{10}F_3 ionization chambers.

The purification of the boron trifluoride and the filling of the ionization chambers are described in Appendix C. Various tests were performed to insure proper operation of the ionization chambers. Undoubtedly a certain amount of electron-ion recombination occurs in the chamber. The density of free electrons and ions along the track of the recoiling products of the $\text{B}^{10}(n,\alpha)\text{Li}^7$ reaction is very high, and these electrons and ions can combine with each other, particularly if the track lies along the direction of the electric field between the central collector and the chamber wall. This type of recombination is referred to as columnar recombination. Volume recombination will also occur

if electrons and ions resulting from different capture reactions combine. Both columnar and volume recombination will depress the total chamber current that is collected by the electrometer unit. Neither of these recombination processes will affect the values obtained for the neutron density to first order, since the absolute calibration was performed by using a BF_3 proportional counter to sample the neutron density in the vicinity of the chamber. However, there are three second order effects of recombination that must be investigated: the temperature dependence of the ionization chamber current, the collector voltage dependence of the ionization chamber current, and nonlinearities in the chamber response to variations of the incident neutron flux (i. e., does the ionization current increase by a factor of 10 when the incident neutron flux increases by a factor of 10).

Several chambers were cycled through the temperature range from 25°C to 70°C in order to determine the temperature dependence of the ionization current. The chambers were irradiated with thermal neutrons or γ -rays, and the ionization current was recorded as a function of temperature. The temperature coefficient for the two BF_3 chambers tested was about the same for either source of ionization, and was less than 0.05% per $^\circ\text{C}$. The BF_3 chambers indicated an apparent increase in ionization current with increasing temperature. In general, the argon filled chambers showed an apparent decrease in

ionization current for increasing temperature. The temperature coefficient was less than 0.02% per °C for the better argon filled chambers.

The temperature of the flight unit was monitored on Flight No. 5. The pressure sensing element normally present in the transmitter unit (a variable resistance device: 20 M Ω to 80M Ω) was replaced by a thermistor circuit. The resistance of the thermistor circuit decreased in value with an increase in temperature. This resistance determined the pulsing rate of the transmitter. The time between transmitter pulses varied from 2.4 sec at 0°C to 0.5 sec at 50°C. The temperature sensing circuit is shown in Figure 5. The temperature of the flight unit during Flight No. 5 as a function of pressure altitude and time of day is given in Figure 6. The accuracy of the temperature measurements was probably better than $\pm 5^\circ\text{C}$. The temperature on this flight ranged from 22°C to 47°C. Over this temperature range, the calibration of the ionization chambers should change less than 1%.

The dependence of the ionization current on the collector recharging potential was investigated. Several chambers were filled with argon to a pressure of 8 atm and the collector potential varied from 100 volts to 1600 volts. Above 200 volts most of the ionization chambers exhibited a collector voltage dependence of 0.001% to 0.002% per volt. Chamber No. 375 was successively filled with argon and BF₃ to different pressures. Above 300 volts the voltage coefficients observed were 0.001% per volt for argon pressures of both 1 atm and 8 atm, 0.004%

per volt for BF_3 at a pressure of 372 mm Hg (0°C), and 0.012% per volt for BF_3 at a pressure of 682 mm Hg (0°C). In all cases an increase in the collector potential resulted in an apparent increase in the ionization current. The curves for Chamber No. 375 are shown in Figure 7. The 300 volt batteries used for the chamber collector potential are very stable and could be expected to drift only a few volts during the flight. It appears that fluctuations in the ionization chamber collector potential should account for less than a 1% error in the measured ionization currents (both for the argon chambers, and also for the BF_3 chambers filled to a pressure of 380 mm Hg (0°C)).

The presence of volume recombination of the ionization produced in the BF_3 gas was investigated. Columnar recombination decreases the percentage of ions and electrons collected from a given particle track, and therefore decreases the total number of ions and electrons collected by an amount related to the specific ionization. While columnar recombination changes only the effective calibration of the ionization chamber, the presence of volume recombination introduces nonlinear effects. Since volume recombination involves recombination of ions and free electrons produced by different particle tracks in the chamber, the loss of ionization, at least in the simple theories (60), is proportional to the square of the ionization density in the gas. Thus, volume recombination is more effective in depressing the ionization current at high levels of intensity, and tends to reduce the ratio of

maximum to minimum ionization currents observed. To determine the importance of volume recombination, the response of the chambers to several radioactive sources was measured, both individually and collectively, at various levels of ionization ranging from a fraction to several times the ionization values encountered on the balloon flights. Both γ -ray and thermal neutron sources were used. The ionization values measured for the sources used in various combinations were strictly additive. In no case did the recombination effects prove to be greater than 1%.

On the basis of semi-theoretical arguments, volume recombination effects should be small. The experimental data of J. A. Bistline (61) indicate that, for the electric fields present in the ionization chamber, electron attachment to form negative ions should occur within one cm of the location of the ionizing event. Since ion-ion recombination is much more probable than electron-ion recombination (62), any volume recombination effects must be ascribed to ion-ion recombination. The recombination rate in BF_3 at 380 mm Hg pressure can be estimated from the three-body recombination theory developed by J. J. Thomson (62). Less than 0.1% of the ions should recombine by this process.

The pressure of BF_3 to which the ionization chambers were filled was determined as a compromise between two quantities: a high counting rate and a large ratio for the $\text{B}^{10}(\text{n}, \alpha)\text{Li}^7$ ionization to that

due to the ionizing component of cosmic-rays. The ionizing component of cosmic-rays generates an ionization roughly proportional to the gas pressure in the chamber. Due to self-shielding and recombination effects, however, there is an optimum filling pressure for the ionization current from the $B^{10}(n,\alpha)Li^7$ reaction. The average path length through a spherical chamber is $\frac{4}{3} R$. For a chamber of 13 cm radius filled to a pressure of 1 atm (S.T.P.) of BF_3 , enriched in the B^{10} isotope to 96%, 73% of a thermal neutron flux will be absorbed in traversing this distance. The maximum in the cosmic-ray neutron differential energy spectrum occurs at 0.1 eV. About 50% of this flux will be absorbed in traversing the chamber. Thus, the optimum filling pressure is of the order of 1 atm of BF_3 .

Flight No. 2, consisting of one $B^{10}F_3$ and one $B^{11}F_3$ chamber, determined the ratio of $B^{10}(n,\alpha)Li^7$ ionization to cosmic-ray ionization for chambers filled with BF_3 to a pressure of 1 atm (S.T.P.). Flight No. 3, consisting of one $B^{10}F_3$ and one $B^{11}F_3$ chamber, determined the ratio of $B^{10}(n,\alpha)Li^7$ ionization to cosmic-ray ionization for chambers filled with BF_3 to a pressure of 0.5 atm. The ratio at 100 g cm^{-2} pressure altitude for the 1 atm chambers was 0.45. The ratio at 100 g cm^{-2} for the 0.5 atm chambers was 0.77. All of the subsequent flights were made with chambers filled with BF_3 to a pressure of 0.5 atm (380 mm Hg at 0°C) because of the more favorable ratio.

The balloons rose through the first 400 g cm^{-2} of the atmosphere (pressure altitude range of 760 g cm^{-2} up to 360 g cm^{-2}) in about 20 minutes (time to 25,000 ft). The low density of cosmic-ray neutrons in this pressure altitude range did not allow measurement of the $\text{B}^{10}(\text{n}, \alpha)\text{Li}^7$ ionization current with the electrometer unit described in Appendix B. The measurements in this pressure range were accomplished by the use of a high-sensitivity electrometer unit designed by H. V. Neher (63). This electrometer unit has an auxiliary potential that can be set to make the unit much more sensitive than the standard electrometers. In all other respects--construction materials, design geometry, fiber size, etc.--the high-sensitivity electrometer unit is similar to the standard electrometer units. An increase in sensitivity of a factor of 20 was obtained by adjusting the auxiliary potential to a value approximately equal to the central collector potential plus 130 volts. Unfortunately, the calibration of the high-sensitivity electrometer unit is voltage dependent because of the introduction of the additional potential. In the laboratory the chamber calibration would fluctuate by about $\pm 10\%$ over a period of a few hours. On Flight No. 8, one of the high-sensitivity electrometer units was used to measure the current in a B^{10}F_3 ionization chamber. The unit was calibrated in flight by comparing the electrometer pulsing rate above a pressure altitude of 400 g cm^{-2} with the pulsing rate of a standard B^{10}F_3 ionization chamber.

V. ANALYSIS AND COMPARISON OF THE DATA

The analysis of the balloon flight data involves the extraction of the $B^{10}(n,\alpha)Li^7$ ionization current from the total current of the $B^{10}F_3$ ionization chambers. To first order, it is only necessary to measure the ionization currents from both $B^{10}F_3$ and $B^{11}F_3$ chambers, subtract the latter from the former to obtain the $B^{10}(n,\alpha)Li^7$ ionization current, convert the $B^{10}(n,\alpha)Li^7$ ionization current into the neutron density by means of a calibration, and then determine the neutron density as a function of altitude from the pressure record obtained during the balloon flight.

There are factors that somewhat complicate the analysis procedure outlined in the foregoing paragraph. The $B^{10}F_3$ and $B^{11}F_3$ gases, as procured from the Oak Ridge National Laboratory (see Appendix C), contain an admixture of the other isotope. The $B^{10}F_3$ gas contains a $4\frac{1}{2}\%$ admixture of $B^{11}F_3$; the $B^{11}F_3$ gas contains an $11\frac{1}{2}\%$ admixture of $B^{10}F_3$. The ionization current obtained by subtracting the data of the $B^{11}F_3$ chambers must be multiplied by 1.129 to correct for the boron isotopic admixture. Self-shielding effects, that is, the attenuation of the incident neutron flux while traversing the chamber, must be taken into account. The self-shielding calculation of Appendix D requires that the neutron density data be multiplied by 1.166. Below a pressure altitude of 260 g cm^{-2} , no data were obtained

from the $B^{11}F_3$ chambers because of the low ionization currents present. The current due to the ionizing component of cosmic-rays below 260 g cm^{-2} was determined from the argon chambers.

Ionization Units and the Relative Calibration

Prior to flight, the chambers were attached to transmitters, and were normalized in a flux of γ -rays producing a known ionization in air. The chamber electrometer assembly automatically recharges after a time interval inversely proportional to the ionization induced in the chamber by the incident flux: $\Delta t = \frac{K}{I}$. The time interval between these recharging pulses, when the chamber is placed in the γ -ray flux, determines the calibration constant K . The numerical value for the ionization current in the presence of the calibration γ -ray flux is chosen to correspond to the number of ion pairs $\text{cm}^{-3} \text{ sec}^{-1}$ produced by that flux in air at 74 cm Hg and 24°C . This unit of ionization, "ion pairs $\text{cm}^{-3} \text{ sec}^{-1} \text{ atm}^{-1}$," enables a direct comparison of ionization values to be made with other balloon programs of the cosmic-ray group at the California Institute of Technology (26, 49, 50). Using this calibration procedure, the $B^{10}F_3$, $B^{11}F_3$, and argon chambers will all yield the same numerical value for the ionization current due to the ionizing component of cosmic-rays. The $B^{10}(n,\alpha)Li^7$ ionization generated in the $B^{10}F_3$ chamber, and to a lesser extent in the $B^{11}F_3$ chamber

(because of the 11% admixture of $B^{10}F_3$), increases the ionization current readings of the $B^{10}F_3$ and $B^{11}F_3$ chambers with respect to the argon chambers during the balloon flights. For this reason, the ionization currents in the $B^{10}F_3$ and $B^{11}F_3$ chambers are measured in units of "equivalent ion pairs," a quantity that reduces to "ion pairs $cm^{-3} sec^{-1} atm^{-1}$ " in the absence of a slow neutron flux. The argon chamber data can be recorded directly in terms of "ion pairs $cm^{-3} sec^{-1} atm^{-1}$."

Definitions

It is convenient to define the following quantities for the analysis of the balloon flight data.

$I(n)$ is defined as the ionization current due to the reaction $B^{10}(n, \alpha)Li^7 + 2.35 \text{ MeV}$ in a BF_3 chamber enriched in the B^{10} isotope to 96% (96% $B^{10}F_3$).

$I(c.p.)$, where c.p. = charged particles, is defined as the ionization current in the BF_3 ionization chambers due to the ionizing component of cosmic-rays. ($I(c.p.)$ is exactly the same for $B^{10}F_3$ chambers as for $B^{11}F_3$ chambers.)

$I(B^{10}F_3)$ is defined as the total current in a chamber containing $B^{10}F_3$ at an isotopic concentration of 96%.

$$I(B^{10}F_3) = I(n) + I(c.p.) .$$

$I(B^{11}F_3)$ is defined as the total current in a chamber containing $B^{11}F_3$ at an isotopic concentration of 89%. (The $B^{10}F_3$ concentration is 11%.) Therefore,

$$I(B^{11}F_3) = \frac{11\%}{96\%} I(n) + I(c.p.) .$$

$I(\text{Argon})$ is defined as the ionization current in a chamber containing argon. As will be shown from the flight data, and as is indicated on theoretical grounds, within 10%,

$$I(\text{Argon}) = I(c.p.) .$$

A measurement of the currents $I(B^{10}F_3)$ and $I(B^{11}F_3)$ permits the determination of $I(n)$ and $I(c.p.)$.

$$\begin{aligned} I(n) &= 1.129 [I(B^{10}F_3) - I(B^{11}F_3)] \\ I(c.p.) &= 1.129 I(B^{11}F_3) - 0.129 I(B^{10}F_3) . \end{aligned}$$

Absolute Calibration

The conversion of the $B^{10}(n,\alpha)Li^7$ ionization current data into a measure of the neutron density was determined by an absolute calibration. A $B^{10}F_3$ ionization chamber and a calibrated $B^{10}F_3$ proportional counter were irradiated with a thermal neutron flux as described in Chapter III. Figure 2 is a drawing of the calibration geometry. The ionization current of the $B^{10}F_3$ chamber was measured in units of "equivalent ion pairs." A subtraction was made for the current due to the ionizing component of the background radiation. The counting rate of the calibrated $B^{10}F_3$ proportional counter was measured by amplifying

the pulses to a maximum voltage of 90 volts and counting them in a Penco PA-4 Pulse Height Analyzer. Measurements were taken with the counter placed directly in front of the $B^{10}F_3$ ionization chamber, placed directly behind the $B^{10}F_3$ ionization chamber, and inserted into the center of a dummy chamber filled to the same pressure of $B^{10}F_3$ as the ionization chamber. The three counting rates were then averaged, and converted to a measurement of the neutron density by means of the known $B^{10}(n,\alpha)Li^7$ cross section for the counter.

For the $B^{10}F_3$ ionization chamber (96% $B^{10}F_3$; 380 mm Hg at 0°C) in the calibration position:

$$\begin{array}{rcl} I(B^{10}F_3) & = & 577 \text{ equivalent ion pairs} \\ I(\text{c.p.}) & = & 17 \text{ " " " "} \end{array}$$

$$I(n) = I(B^{10}F_3) - I(\text{c.p.}) = 560 \text{ equivalent ion pairs}$$

For the $B^{10}F_3$ proportional counter (Reuter-Stokes RSN 40A Counter #C-894 filled with 96% $B^{10}F_3$ to a pressure of 400 mm Hg):

Position Relative to the Ionization Chamber	Counting Rate for 1 Hour
Front	2,953 counts
Center	1,663 "
Behind	1,687 "
<hr/>	<hr/>
Average	2,101 counts

Both the manufacturer's stated counting rate in a thermal neutron flux, and the calibration at the Lawrence Radiation Laboratory (see Chapter III) yielded a $B^{10}(n,\alpha)Li^7$ reaction cross section for the proportional counter of 2.15 cm^2 for a neutron velocity of $2.2 \times 10^5 \text{ cm sec}^{-1}$. Converting the counting rate to neutron density, averaged over the ionization chamber, one obtains:

$$N = 1.23 \pm 0.25 \times 10^{-6} \text{ neutrons cm}^{-3} .$$

The $\pm 20\%$ error results from the uncertainty in the process of averaging the proportional counter rates over the volume of the ionization chamber. Thus the conversion factor for the ionization chamber becomes:

$$N(\text{neutrons cm}^{-3}) = 2.6 \pm 0.5 \times 10^{-9} I(n) .$$

Self-Shielding Calculation

The absolute calibration enables the $B^{10}(n,\alpha)Li^7$ ionization current data to be transformed into the neutron density, averaged over the chamber volume. In order to convert from the averaged neutron density in the chamber to the neutron density in the atmosphere, a correction must be estimated for the self-shielding effects of the chamber. A fraction of the neutron flux is absorbed in traversing the chamber, thus lowering the average neutron density. A correction factor for this effect was determined by calculating the $B^{10}(n,\alpha)Li^7$

reaction rate of the $B^{10}F_3$ chamber, when irradiated with slow neutrons having the energy spectrum computed by Hess. The ratio of the reaction rate, assuming an exponential absorption of the incident neutron flux, to the reaction rate in the "thin detector" approximation (no attenuation of the incident flux), determines the amount by which the presence of the $B^{10}F_3$ chamber depresses the neutron density. This calculation is carried out in Appendix D. For a chamber filled with BF_3 gas to a pressure of 380 mm Hg ($0^\circ C$) and enriched in the B^{10} isotope to a concentration of 96%, the observed neutron density must be multiplied by 1.166 to obtain the neutron density in the atmosphere, unperturbed by the instrument.

Data Reduction

Three steps are involved in the conversion of the $B^{10}F_3$ ionization chamber data into a measurement of the cosmic-ray neutron density.

- (1) Obtain the $B^{10}(n,\alpha)Li^7$ ionization current by subtraction of the chamber current due to the ionizing component of cosmic-rays.
- (2) Convert from $B^{10}(n,\alpha)Li^7$ ionization current to neutron density.
- (3) Correct for self-shielding effects.

The $B^{10}(n,\alpha)Li^7$ ionization current is equal to:

$$I(n) = I(B^{10}F_3) - I(c.p.) .$$

The $B^{10}(n,\alpha)Li^7$ ionization current can be obtained by two procedures. Either the $B^{11}F_3$ ionization chamber data or the argon chamber data can be used to subtract the current due to the ionizing component of cosmic-rays.

The $B^{11}F_3$ ionization current can be used to determine $I(c.p.)$. After correcting for isotopic admixtures in both the $B^{10}F_3$ and $B^{11}F_3$ ionization chambers,

$$I(n) = 1.129 [I(B^{10}F_3) - I(B^{11}F_3)] .$$

The argon ionization current can be used to determine $I(c.p.)$. The calibration constants of the BF_3 and argon chambers are initially normalized in a γ -ray flux. Thus both the BF_3 and argon chambers yield the same numerical value for the ionization due to γ -rays. The γ -ray flux interacts in the chamber gas by means of the Compton collision process. For photon energies of the order of 1 MeV (the energy used in the calibration), the energy loss per unit path length from a γ -ray flux will be proportional to the electron density of the medium, and will be independent of the binding energy of the electrons.

In the Bethe-Bloch formulation of the slowing down of charged particles (64, 65, 66),

$$\frac{dE}{ds} = \frac{4\pi e^4 z^2}{m_e V^2} n Z \left\{ \ln \left(\frac{Z m_e V^2}{I^*} \right) - \ln (1 - \beta^2) - \beta^2 \right\} .$$

dE/ds due to ionization and excitation of electrons in the gas, to first order, is proportional to nZ , the electron density in the medium. Only to second order does dE/ds depend upon the elemental nature of the medium, through I^* , the geometric-mean excitation and ionization potential of the medium. The geometric-mean excitation and ionization potential varies approximately as

$$I^* = kZ ,$$

where k is roughly equal to 12 eV. For charged particles of cosmic-ray energies, the variation of dE/ds between BF_3 and argon, for equal electron densities, can be neglected. Therefore, it is also true for cosmic-ray particles that the energy loss per unit path length will be proportional to the electron density of the medium, and will have only a slight dependence on the binding energy of the electrons.

Thus, on the basis of these arguments, it appears that the ratio,

$$\frac{\text{cosmic-ray ionization}}{\gamma\text{-ray ionization}} ,$$

should be independent of either the elemental nature or the pressure of the ionization chamber gas.

A. Johnston, in his Ph. D. thesis (49), has shown that on theoretical grounds the discrepancy for the cosmic-ray ionization/ γ -ray

ionization ratio between 1 atm and 8 atm of argon should be no greater than 7%. A balloon flight utilizing two ionization chambers, one filled to 1 atm of argon, the other to 8 atm of argon, actually showed that, at least above a pressure altitude of 140 g cm^{-2} , the discrepancy is less than 1%.

This constancy of the cosmic-ray ionization/ γ -ray ionization ratio permits $I(\text{Argon})$, the numerical value of the ionization as determined by the argon ionization chamber, to be equated to $I(\text{c. p.})$, the ionization in the BF_3 chamber due to the ionizing component of cosmic-rays. An analysis of the balloon flight data shows that, to within 10%, $I(\text{Argon}) = I(\text{c. p.})$. (See Table V.) Therefore,

$$I(n) = I(\text{B}^{10}\text{F}_3) - I(\text{Argon}) .$$

From a pressure altitude of 6 g cm^{-2} (115,000 ft) down to 260 g cm^{-2} (34,000 ft) the current due to the ionizing component of cosmic-rays to be subtracted from the B^{10}F_3 ionization current was determined as the average of the argon and the B^{11}F_3 ionization current. Below 260 g cm^{-2} the argon chamber data were used for the subtraction.

Individual curves were plotted for the B^{10}F_3 , B^{11}F_3 , and argon data, and a smooth curve was faired through the points. The individual points for the B^{10}F_3 and B^{11}F_3 data are shown in Figures 9 and 10. There were more data than could be displayed individually for the argon chamber current. The argon data show a 1% deviation, mostly due to

TABLE V
DATA ANALYSIS

Pressure Altitude grams cm ⁻²	$I(B^{10}F_3)$	$I(B^{11}F_3)$	$I(\text{Argon})$	$I(\text{charged particles}) =$ $1.129 I(B^{11}F_3) - 0.129 I(B^{16}F_3)$	$I(n) =$ $1.129 I(B^{10}F_3) - 1.129 I(B^{11}F_3)$	$I(n) =$ $I(B^{10}F_3) - I(\text{Argon})$	<u>Average</u> $I(n)$	Neutron Density in the Atmos- phere $N = 3.0 \times 10^{-9} I(n)$ neutrons cm ⁻³
0
5	151	134	128	132	19	23	21	63 x 10 ⁻⁹
10	174	147	136	144	30	38	34	102
15	202	158	142	152	50	60	55	165
20	226	168	154	161	65	72	68	204
25	248	176	162	167	81	86	84	252
30	265	184	170	174	91	95	93	279
35	280	191	177	180	100	103	106	318
40	294	196	182	183	111	112	112	336
50	315	203	189	188	127	126	126	378
60	332	206	195	190	142	137	140	420
70	345	208	198	190	155	147	151	453
80	350	208	198	190	160	152	156	468
90	350	206	197	188	162	153	158	474
100	348	203	193	184	164	155	160	480
120	338	195	184	176	162	154	158	474
140	321	185	172	168	153	149	151	453
160	302	175	158	159	143	144	144	432
180	280	162	145	147	133	135	134	402
200	258	148	131	134	124	127	126	378
220	236	132	119	119	117	117	117	351
240	214	117	107	104	110	107	108	324
260	193	103	96	91	102	97	100	300
280	172		85			87		261
300	155		75			80		240
320	138		67			71		213

TABLE V (continued)

Pressure Altitude grams cm ⁻²	$I(B^{10}F_3)$	$I(B^{11}F_3)$	$I(\text{Argon})$	$I(\text{charged particles}) =$ $1.129 I(B^{11}F_3) - 0.129 I(B^{10}F_3)$	$I(n) =$ $1.129 I(B^{10}F_3) - 1.129 I(B^{11}F_3)$	$I(n) =$ $I(B^{10}F_3) - I(\text{Argon})$	<u>Average</u> $I(n)$	Neutron Density in the Atmosphere $N = 3.0 \times 10^{-9} I(n)$ neutrons cm ⁻³
340	123		59			64		192×10^{-9}
360	110		51			59		177
380	97		45			52		156
400	85		40			45		135
420	76		36			40		120
440	68		32			36		108
460	61		29			32		96
480	55		26			29		87
500	50		23			27		81
520	45		21			24		72
540	40		19			21		63
560	35		17			18		54
580	31		15			16		48
600	27		13			14		42
620	23		12			11		33
640	20		11			9		27
660	17		10			7		21
680	15		9			6		18
700	14		8			6		18
720	12		7			5		15
740	11		7			4		12
760	10		6			4		12

statistics, around the curve drawn in Figure 8. The low altitude data are shown in Figure 11. In Table V the data are analyzed to determine $I(n)$ according to the two methods to correct for ionization due to the ionizing component of cosmic-rays. A comparison is also listed for the ionizing component of cosmic-rays as determined by the argon chamber, $I(\text{Argon})$, and as determined by the $B^{11}F_3$ chamber, $I(\text{c.p.})$. The average of the two methods of obtaining $I(n)$ is taken, and the neutron density is calculated by multiplying $I(n)$ by 2.56×10^{-9} for the conversion to neutrons cm^{-3} and then by 1.166 to correct for self-shielding effects.

$$N \left[\begin{array}{l} \text{neutron density} \\ \text{in the atmosphere} \end{array} \right] = 3.0 \pm 0.6 \times 10^{-9} \overline{I(n)}.$$

The curve for the neutron density is given in Figure 12. The individual points represent the $B^{10}F_3$ data after subtraction of the current due to the ionizing component of cosmic-rays.

The cosmic-ray neutron density exhibits a maximum of $4.8 \pm 1.2 \times 10^{-7}$ neutrons cm^{-3} at a pressure altitude of 100 g cm^{-2} (53,000 ft), a rapid decline above this altitude, and an exponential decrease below 250 g cm^{-2} with an absorption length of $165 \pm 20 \text{ g cm}^{-2}$.

Due to the large number of neutrons captured per data point ($\sim 10^4$), the statistical errors are of the order of $\pm 1\%$. A large systematic error of about $\pm 20\%$ is introduced by the absolute calibration. The systematic errors due to the relative calibrations in the

γ -ray flux and to calibration drifts during the flight, after subtraction of background currents, range from about $\pm 2\%$ for the measurements at the maximum ionization to about $\pm 20\%$ for the low altitude measurements. The systematic error introduced by the uncertainty in the self-shielding correction is probably less than $\pm 5\%$.

At least a factor of two improvement in the absolute calibration (from $\pm 20\%$ to at least $\pm 10\%$) could be obtained by making a comparison balloon flight with a calibrated $B^{10}F_3$ proportional counter and a $B^{10}F_3$ ionization chamber. A small proportional counter would be used so that self-shielding effects would be negligible, thus permitting the counter to measure an essentially unperturbed neutron flux. Due to the low counting rate of the small proportional counter, it would be necessary to float the balloon at an altitude of 50,000 ft (the altitude corresponding to the maximum neutron density) for a period of several hours. An absolute calibration of the proportional counter would be performed in the laboratory prior to flight. The absolute calibration would involve a determination of the counting rate of the proportional counter when placed at a point of known slow neutron density. The slow neutron density would be measured by monitoring the radioactivity of an indium foil which had been placed at the calibration position (67). The radioactivity of the indium foil would be measured by observing the emitted beta and gamma rays in coincidence. This coincidence

method eliminates the detector efficiencies from the equation relating the detector counting rates to the decay rate of the foil, thus allowing an absolute determination of the decay rate of the foil to be made.

From the observed decay rate, the size of the indium foil, and the known neutron capture cross section for In^{115} , the slow neutron density at the calibration position can be obtained.

Comparison with the Results of Other Workers

The measurements of W. Hess, et al., the N. Y. U. Cosmic-Ray Group, and L. C. L. Yuan will be compared with the work of this thesis. Because of the large geomagnetic latitude variations (10: 1) and time variations (4: 1) in the production rates of cosmic-ray neutrons, a correction procedure must be applied to the data of these workers. R. E. Lingenfelter (17), from examination of all the available cosmic-ray neutron data, has estimated the cosmic-ray neutron production as a function of pressure altitude and geomagnetic latitude for solar sunspot minimum and solar sunspot maximum. The results of this calculation, which are probably valid to within $\pm 25\%$, will be used to correct all measurements to the values expected at a geomagnetic latitude of 41°N during 1962.

Hess, et al. (4, 14) measured the neutron energy spectrum in the winter of 1956-1957 with detectors installed in a B-36 airplane, up to an altitude of 40,000 ft (200 g cm^{-2}). They assumed that the measured height dependence of the neutron source of $\exp(-x \text{ g cm}^{-2}/155)$ could be extended up to the top of the atmosphere. A multi-group diffusion analysis was then used to generate the neutron energy spectrum from 200 g cm^{-2} up to the top of the atmosphere. This assumption of an exponentially increasing source strength up to the top of the atmosphere leads to a maximum in the neutron density at about 50 g cm^{-2} .

a position that is inconsistent with all balloon measurements. Lingenfelter has shown that the exponential assumption extended to the top of the atmosphere is improper, and that a maximum in the neutron source actually occurs at a pressure altitude of 100 g cm^{-2} (53,000 ft) for geomagnetic latitudes below 55° . Since the slowing down length for the neutrons is only about 50 g cm^{-2} , a maximum in the slow neutron density is also to be expected at 100 g cm^{-2} . Thus above 200 g cm^{-2} , the C^{14} production rate calculated by Lingenfelter is a more proper comparison to the work of this thesis. The $\text{N}^{14}(n,p)\text{C}^{14}$ production cross section has a $1/v$ dependence for slow neutrons; the production rate is therefore proportional to the density of slow neutrons. Lingenfelter's C^{14} production estimates above 200 g cm^{-2} pressure altitude, normalized to Hess's experimental data, and the data of Hess, et al. below 200 g cm^{-2} form curves that can be compared with the work of this thesis. The data of Hess, et al. are transformed into neutron density measurements by multiplying their neutron flux values by the reciprocal of the velocity and then integrating over all energies. The data were then multiplied by 0.8 to correct from a geomagnetic latitude of 44° to 41° , and by 1.2 to correct for time variations. The corrected neutron density values are shown in Figure 14.

As can be seen from Figure 14, even after the neutron source corrections applied by Lingenfelter, the measured neutron densities

are still 50% higher than the values obtained in the work of this thesis. It is unlikely that a difference in the absolute calibration can be an explanation, as an intercomparison of standards between the two laboratories was made. It is possible that neutron moderation in the airplane may be responsible for the higher neutron densities observed by Hess.

The New York University Cosmic-Ray Group has undertaken a large number of balloon flights using $B^{10}F_3$ and $B^{11}F_3$ proportional counters to measure the slow neutron density (3,38,68). The N. Y. U. Group estimates that for their matched counters $177 \text{ counts min}^{-1}$ would result in a neutron counting rate of $1.01 \text{ neutrons min}^{-1}$ for a BF_3 counter with a boron component of 100% $B^{10}F_3$ at S. T. P. and with a volume of one cubic centimeter. Converting their counting rates to neutron density, one obtains:

$$N(\text{neutrons cm}^{-3}) = 4.22 \times 10^{-9} C (\text{counts min}^{-1}) .$$

For Flights No. 66 and 67 (August 1954 at $\lambda_m = 55^\circ N$), a time correction of 0.96 was made. The latitude correction was a function of pressure altitude and ranged from 0.40 at 0 g cm^{-2} to 0.81 at 680 g cm^{-2} . For Flights No. 91 and 93 (September 1958 at $\lambda_m = 41^\circ N$) a time correction of 1.22 was made. The N. Y. U. corrected neutron density values are shown in Figures 15 and 16.

There is satisfactory agreement between the N. Y. U. Group and the work of this thesis for pressure altitudes below 100 g cm^{-2} (53,000 ft), considering the $\pm 20\%$ errors assigned to the absolute calibrations. Above this altitude, the difficulties associated with assessing the proper time-and-latitude corrections introduce relative errors in the comparison.

A series of three balloon flights was carried out by L. C. L. Yuan between June of 1948 and January of 1949 (12). On each flight two identical proportional counters filled with BF_3 of 96% B^{10} were sent aloft at a geomagnetic latitude of 51°N . One counter was shielded with 0.030 inch of cadmium, and the other enclosed in tin of the same thickness. Because of the large neutron capture cross section for cadmium below 0.4 eV, the difference in the counting rate between the two counters was due only to neutrons of energies below 0.4 eV. The data were converted to neutron density by the relation:

$$N(\text{neutrons cm}^{-3}; E < 0.4 \text{ eV}) = 6.02 \times 10^{-9} C(\text{counts min}^{-1}).$$

These numbers were multiplied by 1.83 to correct the data for neutrons with energies between 0.4 eV and 10 keV. The time correction was 1.13; the geomagnetic correction varied from 0.54 at 0 g cm^{-2} to 0.82 at 680 g cm^{-2} . The corrected neutron density values are shown in Figure 17 for the January 1949 flight.

With respect to these comparisons, it should be pointed out that the instrumentation used in the work of this thesis has a total weight of 12 lbs per balloon flight, while the equipment launched by other workers weighed at least 100 lbs. The launching of payloads of this weight must necessarily be made under favorable wind conditions, and with the use of facilities usually available only under contract. While for a few flights this is only a matter of economics, if a complete geomagnetic survey (neutron density versus geomagnetic latitude) were to be undertaken during a limited period of time (to avoid time variations; this has not been done yet), then the practical matter of balloon launching becomes an important consideration. From a purely scientific standpoint, the ionization chamber measurements yield significantly smaller statistical variations due to the fact that the neutron capture rates are higher than for proportional counters. Proportional counters are limited in volume by the requirement that electron attachment to form negative ions must not occur, whereas ion-ion recombination is the only limitation to the volume of the ionization chambers. Measurements made in aircraft are capable of generating satisfactory statistics below 100 g cm^{-2} (53,000 ft), but are subject to problems associated with local neutron production and moderation.

Radioactivity from Bomb Test Debris

From Oct. 22, 1962 to Oct. 25, 1962, on Balloon Flights Nos. 7, 8, and 9, the presence of radioactivity from bomb test debris was observed in the stratosphere. All of the radioactivity appeared to be located above a pressure altitude of 100 g cm^{-2} (53,000 ft). On Flight No. 9, the maximum radioactivity occurred at 35 g cm^{-2} (75,000 ft) with a measured ionization of $376 \text{ ion pairs cm}^{-3} \text{ sec}^{-1} \text{ atm}^{-1}$ (converted into units of Roentgens: 0.73 mr hr^{-1}), a factor of two higher than the ionization due to cosmic radiation. It must be understood that the chambers measure only the ionization due to γ -rays and to charged particles capable of penetrating the wall (wall thickness: 0.5 g cm^{-2}). Thus beta rays of energies below 1 MeV were not detected. The large cosmic-ray background probably would prevent detection of the radioactivity with an ionization chamber except during the first few months, prior to the time that the bomb debris had spread uniformly throughout the stratosphere. Large thermonuclear devices were exploded by both the United States and Russia during the weeks preceding the balloon flights.

The observed ionization could not have been due to an increase in cosmic-ray intensity nor to the arrival of solar high energy particles generated by a flare. The magnetic rigidity cutoff for vertically incident particles is 5 BV at the geomagnetic latitude of the balloon

flights (41°N), and no increase in relativistic particles was observed on Mariner II Planetary Probe during Flights Nos. 7 and 8 (69).

Similar events have been observed during two other balloon flights by the Cosmic-Ray Group at the California Institute of Technology (70,71), and by other cosmic-ray workers (72,73,74).

It has been known for some time that the detonation of large thermonuclear devices injects radioactive fission products into the stratosphere, which may remain there for months or even years (75). Since the end of 1956, the Atomic Energy Commission has been monitoring the radioactive dust content of the stratosphere by means of balloon-borne filters. The filters are recovered and analyzed for gross beta activity and for six specific radioisotopes. The balloon-borne filters indicated a maximum in the Sr^{90} concentration at about 45 g cm^{-2} (70,000 ft) for equatorial latitudes, lowering to 90 g cm^{-2} (55,000 ft) in polar regions. The concentration of Sr^{90} was unobservable below the tropopause or above 15 g cm^{-2} (95,000 ft) (76).

It appears that the radioactive debris is initially injected into the stratosphere by a thermonuclear detonation, a slow settling and diffusion of the debris across the tropopause then results on a time scale of months to years, and a rapid mixing and precipitation occur out of the troposphere in the period of about a month.

The measurements of the vertical distribution of the Sr^{90} concentration are in agreement with the radioactive debris encountered on several balloon flights by the Cosmic-Ray Group at the California Institute of Technology. In the work of this thesis, the maximum radioactivity occurred at 50 g cm^{-2} (68,000 ft) on Flight No. 8 and at 35 g cm^{-2} on Flight No. 9, both at a geographic latitude of 34°N . The event observed by H. R. Anderson on Oct. 16, 1958 at Bismarck, North Dakota (geographic latitude: 47°N) displayed a maximum at 80 g cm^{-2} (58,000 ft). The event reported by H. V. Neher and H. R. Anderson that occurred at Bismarck on July 28, 1954 is difficult to interpret, but it may have been due to bomb debris originating in the spring 1954 test series (Castle). In no case was the radioactivity observed below the tropopause, or at the top of the atmosphere.

The individual points representing the data obtained on Flight No. 9 (Oct. 25, 1962) with an argon filled ionization chamber are shown in Figure 13.

VI. OTHER EXPERIMENTS

In this chapter, three problems other than the measurement of neutrons in the atmosphere are considered: (1) extrapolation of the balloon data from 6 g cm^{-2} pressure altitude up to the top of the atmosphere, (2) the measurement of slow neutrons in space using ionization chambers, and (3) the construction of a ground monitor for the nucleonic component of cosmic radiation.

Extrapolation of the Data to the Top of the Atmosphere

Haymes and Korff (77) have estimated the density of slow neutrons at the top of the atmosphere by performing a linear extrapolation of the counting rates of BF_3 proportional counters upward from an atmospheric depth of 4 g cm^{-2} . This procedure is difficult even under the best experimental conditions because the density of slow neutrons drops rapidly at these altitudes due to the outward diffusion of the neutrons. A small error in the measured neutron density or the neutron density gradient can result in an improper extrapolation. This method of extrapolation is even more difficult to apply to the ionization chamber data of this thesis, because the counting rate to background ratio is lower than for proportional counters. The ionization chambers have no bias against small ionizing events, as do the BF_3 proportional counters.

Nevertheless, using the results of neutron transport theory and a knowledge of λ_{tr} , the neutron transport length in the atmosphere (the transport length is just the scattering length corrected for the velocity of the recoiling nucleus), an estimate of the neutron density can still be made. The physical situation is akin to the soluble problem of monoenergetic neutrons diffusing from a nonabsorbing medium into an infinite empty half-space (the Milne problem) (21, 22, 46, 78). For the Milne problem, it can be shown that the density in the half-space is 0.81 times the asymptotic solution obtained from:

$$N_{\text{asym}}(x=0) = (0.71)\lambda_{tr} \frac{dN(x=0)}{dx} .$$

The factor of 0.81 results from an abrupt decrease in the number of downward scattered neutrons that occurs within the last few scattering lengths of the atmospheric boundary. Of course the slow neutrons in the atmosphere are not monoenergetic, nor can the absorption of these neutrons be totally neglected. However, these effects should not produce a large error in the asymptotic solution given above. This extrapolation procedure has been applied in neutron physics to the inverse problem, i. e., given the neutron density in the vicinity of the boundary, determine the transport length in the medium.

Thus the formula that will be used to estimate the slow neutron density at the top of the atmosphere is

$$N(x=0) = (0.575) \lambda_{tr} \left[\frac{dN}{dx} \right] ,$$

where $\left[\frac{dN}{dx} \right]$ is the averaged neutron density gradient as determined from the balloon data.

The transport length for slow neutrons in the atmosphere is $\lambda_t = 2.9 \text{ g cm}^{-2}$. Fitting the data with a straight line in the region from 5 g cm^{-2} to 20 g cm^{-2} , extrapolating to the origin, and iterating once for consistency,

$$\left[\frac{dN}{dx} \right] = 9.7 \times 10^{-9} \text{ neutrons cm}^{-3} (\text{g cm}^{-2})^{-1} .$$

Therefore,

$$N(x=0) = 16 \times 10^{-9} \text{ neutrons cm}^{-3} .$$

The accuracy of this value is limited not so much by the theory, but by the fact that neutrons of energies less than 0.66 eV are gravitationally trapped. Even at the top of the atmosphere a large fraction of the neutron density is comprised of neutrons with energies less than 0.66 eV, and gravitational trapping will increase the neutron density. Since the diffusion length for thermal neutrons is only 3 g cm^{-2} , an increase in the neutron density at the top of the atmosphere due to the return of albedo neutrons would not necessarily be observable at balloon altitudes. The magnitude of the return albedo is restricted by the removal process of neutron β -decay. A 0.1 eV neutron moving

vertically in the earth's gravitational field has roughly a 50% chance to decay before returning to the top of the atmosphere. All things considered, the value of 16×10^{-9} neutrons cm^{-3} for the density of slow neutrons at the top of the atmosphere is probably correct to within a factor of 2. A more accurate value would require a knowledge of the energy spectrum and the angular dependence of the upward moving neutrons, and a calculation would have to be made for the probability of β -decay along the various return trajectories.

Estimates of the neutron density in space have been made by several workers. The methods, dates, geomagnetic latitudes, and neutron densities corresponding to the various workers are summarized in Table VI.

The extrapolation method used for the data of this thesis was described earlier in the chapter. Hess, Canfield, and Lingenfelter (4) used a multi-group diffusion analysis, normalizing their data to experimental results obtained at a pressure altitude of 200 g cm^{-2} . Haymes and Korff (77) flew BF_3 proportional counters from a balloon to a pressure altitude of 4 g cm^{-2} and then extrapolated the data to the top of the atmosphere. (While analyzing the data of Haymes and Korff, the writer discovered an error in the flux values quoted by them in the literature. This error was subsequently verified by Haymes. The article should read, "Extrapolating to the top of the atmosphere, a value of $1.0 \pm 0.4 \times 10^{-8}$ neutrons cm^{-3} was obtained for the slow

TABLE VI
 THE DENSITY OF SLOW NEUTRONS
 AT THE TOP OF THE ATMOSPHERE

Workers	Ref.	Method	Date	λ_m	Neutrons* cm ⁻³
This Thesis		Balloon Data	1962	41°N	16x10 ⁻⁹
Hess, Canfield and Lingenfelter	4	Multi-Group Diffusion Calculation	1956	44°N	40x10 ⁻⁹
Haymes and Korff	77	Balloon Data	1959	55°N	10x10 ⁻⁹
Reidy, Haymes and Korff	79	Aerobee-150A Sounding Rocket	1960	49°N	370x10 ⁻⁹
Hess and Starnes	80	Atlas Pod	1960	40°N	57x10 ⁻⁹
Martin, Witten and Katz	81	Atlas Pod	1961	27°N	100x10 ⁻⁹
Bame, et al.	82	Atlas Pod	1961	36°N	13x10 ⁻⁹

* All workers quote absolute errors of less than + 50%.

neutron density." Reidy, Haymes, and Korff (79) instrumented an Aerobee-150A sounding rocket with 20 $B^{10}F_3$ and 24 $B^{11}F_3$ proportional counters. The rocket reached a maximum altitude of about 200 km. The fact that the instrumentation package was not separated from the rocket may account for the high neutron densities observed. Hess and Starnes (80) flew a neutron detector on an Atlas rocket to an altitude of about 1400 km. The detector was mounted on a pod on the outside of the Atlas vehicle and was detached during the flight. The detector consisted of a $B^{10}F_3$ proportional counter enclosed in a paraffin shield, and was sensitive to neutrons over an energy range of 25 keV to 4 MeV. The estimate of the neutron density in space as given in Table VI was obtained by noting the ratio of the observed counting rate to the counting rate expected from the calculation of Hess, Canfield, and Lingenfelter. Martin, Witten, and Katz (81) flew an unmoderated $B^{10}F_3$ proportional counter on an Atlas pod. Equipment associated with $B^{11}F_3$ counters in the pod malfunctioned, and a subtraction for background counts was not possible. The background counting rates observed by Haymes and Korff and by Reidy, Haymes, and Korff suggest that the densities obtained by Martin, Witten, and Katz should be multiplied by 0.5 to correct for background. Bame, Conner, Brumley, Hostetler, and Green (82) flew three moderated $Li^6I(Eu)$ scintillation detectors on an Atlas pod in 1961. The detectors measured the flux of neutrons in

the energy interval from 1 keV to 100 MeV. At a geomagnetic latitude of 36°N, they obtained a neutron flux spectrum similar in shape to that calculated by Hess, et al., but lower in absolute value by a factor of three. The results of their experiment suggest a slow neutron density of about 13×10^{-9} neutrons cm^{-3} .

The Measurement of Slow Neutrons in Space Using Ionization Chambers

The measurement of the slow neutron density in space is subject to the same difficulty as discussed in the preceding section. The ionization resulting from the charged particle background is many times the ionization resulting from the neutron capture reaction. For the B^{10}F_3 ionization chambers utilized in this thesis, the ratio of the neutron capture ionization to the charged particle ionization, extrapolating the data to the top of the atmosphere, would be

$$R = \frac{I(\text{neutrons})}{I(\text{charged particles})} = 0.045 .$$

A considerable improvement in this ratio can be attained by utilizing the $\text{He}^3(n,p)\text{H}^3 + 0.765 \text{ MeV}$ reaction. If the gas pressures of a B^{10}F_3 ionization chamber and a He^3 ionization chamber are adjusted so that both chambers have the same neutron capture cross section, then the ratio becomes

$$R(\text{He}^3) = R(\text{B}^{10}\text{F}_3) \times \left[\frac{\text{Q value for He}^3 + n}{\text{Q value for B}^{10} + n} \right]$$

$$\times \left[\frac{\text{electrons per BF}_3 \text{ molecule}}{\text{electrons per He atom}} \right]$$

$$\times \left[\frac{\text{cross section for He}^3(n,p)\text{H}^3}{\text{cross section for B}^{10}(n,\alpha)\text{Li}^7} \right]$$

$$R(\text{He}^3) = 0.31$$

This value for $R(\text{He}^3)$ is an upper limit, as some of the reaction energy will be lost if the proton intercepts the chamber wall. This wall effect is greater for He^3 because He^3 has a much lower stopping power than BF_3 , and consequently the range of the recoiling proton in the $\text{He}^3(n,p)\text{H}^3$ reaction will be greater than the range of the alpha particle in the $\text{B}^{10}(n,\alpha)\text{Li}^7$ reaction. Thus it appears that even using the $\text{He}^3(n,p)\text{H}^3$ reaction, counting rates to background ratios for ionization chambers are lower than those attainable with proportional counters (which are at least equal to unity) for the measurement of slow neutrons in space.

The Construction of a Ground Monitor for the Nucleonic Component of Cosmic Radiation

Simpson, Fonger, and Treiman (83) have developed an experimental method for extending the study of primary cosmic radiation intensity variations versus time to the low energy portion of the primary

particle spectrum by measuring the nucleonic component intensity within the atmosphere. The detector system is a pile structure of lead and paraffin within which the rate of local neutron production is measured by $B^{10}F_3$ proportional counters.

The disintegration product neutrons and slow neutrons in the atmosphere are produced predominantly by the nucleonic component, since, for example, neutron yields from γ -n, π -star-n, μ -star-n, and similar processes are small, but the nucleon-induced disintegrations have large cross sections and yield on the average, more than one neutron per disintegration. It has been determined that at $\lambda = 52^\circ$ the local neutron production from showers, π and μ mesons, and γ -produced stars is less than 3% of the total neutron production. Thus, the counting rate of the detector will be only a function of the nucleonic component, and will be insensitive to changes in the mass distribution of the atmosphere due to temperature variations. If the entire neutron local production in a pile were related to the primary radiations only by secondary nucleons, there would be no observable temperature effect for the nucleonic component, since nucleons have long mean lives. The small meson links which are present contribute a temperature dependence of less than -0.006% per $^\circ C$ at $\lambda = 50^\circ$. Of course a correction for variations in the total mass of air above the detector system must be made. This is about -1% per mm Hg.

By using a local condensed moderating material such as paraffin or carbon surrounding the detector, the detector avoids the atmosphere as a moderator and thus reduces or eliminates the difficulties which arise from changes in air moderator characteristics in the region of clouds, during precipitation, etc., and eliminates detector response to changes in neutron production near the detector owing to movement of heavy materials, snowfall, personnel, and neutron emitting radioactive sources.

The average number of neutrons emitted by a low energy nuclear disintegration is called the multiplicity. The ratio of neutron multiplicity from lead to carbon is 8:1. Thus it is clear that by using materials of large atomic number mixed with a local neutron moderator, the atmosphere and the environment of the detector are excluded as both the neutron source and moderating medium, while, on the other hand, the neutron yield has been increased.

A detector system of this type is referred to as a neutron monitor pile. Such a detector system has more sensitivity to the low energy portion of the cosmic-ray spectrum than previously designed monitors as evidenced by the greater latitude variation (at sea level, a factor of 1.8 from 0° to 50° for the neutron monitor pile as compared with 1.1 for a shielded ionization chamber).

A neutron monitor pile can be constructed using the ionization chambers described in this thesis. A neutron monitor pile similar in

philosophy to that designed by Simpson, Fonger, and Treiman was assembled. An ionization chamber was surrounded by 5 cm of paraffin, and the top and two sides were covered with 1,000 lbs of lead bricks. The equipment was transported to the top of Onyx Peak, San Bernardino National Forest, California (34°46'N, 116°50'W; elevation: 9,114 ft), and assembled there. The pile was operated for several hours with a $B^{10}F_3$ ionization chamber, and with an argon ionization chamber. (The barometric pressure was 765 g cm^{-2} on Nov. 3, 1962.) The ionization currents which were measured are given in Table VII.

It was shown in Chapter V that $I(n)$, the ionization current due to the capture of neutrons, can be obtained by subtracting the argon chamber data from the $B^{10}F_3$ chamber data. For the unshielded chambers, $I(n) = I(B^{10}F_3) - I(\text{Argon}) = 21.7$ ion pairs equivalent. After the chamber was surrounded with paraffin, $I(n) = 38.3$ ion pairs equivalent. The assembly of the pile was completed by adding the lead, then $I(n) = 71.3$ ion pairs equivalent. Thus the neutron counting rates increased in the ratio of unshielded : paraffin : pile = 1 : 1.8 : 3.3 . In this context it should be noted that the value for $I(n)$ obtained on the balloon flights at this pressure altitude was $I(n) = 4$ ion pairs equivalent. Thus the moderating effect of the ground increases the slow neutron density by a factor of 5 at this altitude.

TABLE VII

IONIZATION CHAMBER MEASUREMENTS ON ONYX PEAK

Ionization Chamber Gas	Configuration	Date	Ionization in ion pairs equiv.
B ¹⁰ F ₃	Neutron Monitor Pile	Nov. 3, 1962	77.7
Argon	Neutron Monitor Pile	Nov. 3, 1962	6.4
B ¹⁰ F ₃	Paraffin Only	Nov. 3, 1962	47.7
Argon	Unshielded	Nov. 3, 1962	10.0
B ¹⁰ F ₃	Unshielded	Oct. 4, 1962	31.1
B ¹¹ F ₃	Unshielded	Oct. 4, 1962	12.8
Argon	Unshielded	Oct. 4, 1962	9.4

For the study of time variations in cosmic radiation, the precision of the data of such a monitor is limited mainly by variations in the amount of charge transferred to the collector during an electrometer recharging cycle. These variations appear to be of the order of 0.3%. A pile of this design would be most useful for monitoring the low energy portion of primary cosmic radiation at remote locations at high elevations, where electrical power is not available.

VII. CONCLUSIONS

The construction of an ionization chamber, using the Neher quartz electrometer system, for the detection of slow neutrons is reasonably straightforward. Even when care is taken to insure cleanliness of the chamber, and the gas is purified, it is possible that some charge recombination occurs within the chamber gas. Nevertheless, this does not introduce large temperature effects, nor does it degrade the voltage dependence to the point where the precision of the measurements is affected.

Recombination problems and self-shielding effects limit the pressure of $B^{10}F_3$ to which the chambers may be filled. The number of data points obtained on a single balloon flight with chambers using the standard electrometer system does not give sufficient altitude resolution. Improvements in the calibration stabilization of the high sensitivity electrometer units would enable the entire neutron density profile to be obtained on a single flight. The precision of the low altitude measurements (below 20,000 ft), which require the high sensitivity electrometer unit, would be improved also. At least a factor of two improvement in the absolute calibration (from $\pm 20\%$ to at least $\pm 10\%$) could be obtained by making a comparison balloon flight with a calibrated $B^{10}F_3$ proportional counter and a $B^{10}F_3$ ionization chamber.

Such a calibration would inherently correct for self-shielding effects in the ionization chamber.

It was fortunate that the intensity of cosmic radiation did not change at the geomagnetic latitude of the balloon flights during 1962, for it allowed all of the data to be plotted together, thereby gaining in altitude resolution. The small spread of the data as evidenced in Figures 9 and 10 attests to the precision of the measurements.

Comparison of the values obtained for the neutron density from $I(n) = I(B^{10}F_3) - I(\text{Argon})$ and from $I(n) = 1.129 [I(B^{10}F_3) - I(B^{11}F_3)]$ indicate that it is not necessary to fly $B^{11}F_3$ chambers. Both the neutron data and the cosmic-ray ionization data can be obtained from analysis of $B^{10}F_3$ chamber and argon chamber measurements. The large volume of the ionization chambers (9 liters) resulted in a significant reduction of statistical errors relative to earlier balloon flights. The small size of the flight units (3 kilograms) avoided the problems associated with local neutron production and moderation which are present in airplane measurements.

The counting rate to background ratio at the maximum balloon altitude was too poor to enable a simple extrapolation of the data to be made to the top of the atmosphere. By the use of neutron transport theory, however, an estimate of the density of slow neutrons above the atmosphere was made. Other workers that have attempted to

determine this quantity have obtained such a divergence of values that the actual number is still in question.

The agreement with the cosmic-ray neutron measurements of the New York University Cosmic-Ray Group is excellent, considering the difficulty of making proper time-and-geomagnetic latitude corrections, plus the $\pm 20\%$ error assigned to the absolute calibration for the work of this thesis. The discrepancy with the work of Hess, et al. (4) (the measurements of this thesis are lower by more than a factor of two at altitudes above 150 g cm^{-2}) undoubtedly results from their assumption that the neutron production rate increases exponentially up to the top of the atmosphere. The corrections of Lingenfelter (17), when applied to the data of Hess, et al., give an altitude dependence that agrees with the measurements of this thesis, but their absolute values are still about 50% higher. Neutron moderation in their airplane may be responsible for the higher densities that they observe.

While free neutrons are produced in the atmosphere by a number of processes, by far the majority of them are products of the nuclei of air disrupted by cosmic-ray interactions. The experimental work of this thesis enabled the density of these cosmic-ray neutrons to be determined throughout the atmosphere. The observed altitude dependence is in agreement with the notions of production by cosmic-ray nuclear interactions, followed by a period of slowing-down and diffusion, and

then terminating in $N^{14}(n,p)C^{14}$ capture, or, at the top of the atmosphere, upward diffusion into space.

References

1. H. V. Neher and S. Prakash,
"Metal System for Chemical Reactions and for Studying
Properties of Gases and Liquids,"
Rev. Sci. Instr. 28, 267-270 (1957).
2. H. A. C. Neuberg, R. K. Soberman, M. J. Swetnick, and
S. A. Korff,
"High-Altitude Cosmic-Ray Neutron Density at the
Geomagnetic Pole,"
Phys. Rev. 97, 1276-1279 (1955).
3. R. K. Soberman,
"High-Altitude Cosmic-Ray Neutron Intensity Variations,"
Phys. Rev. 102, 1399-1409 (1956).
4. W. N. Hess, E. H. Canfield, and R. E. Lingenfelter,
"Cosmic-Ray Neutron Demography,"
J. Geophys. Research 66, 665-677 (1961).
5. J. Chadwick,
"Possible Existence of a Neutron,"
Nature 129, 312 (1932).
6. J. Chadwick,
"The Existence of a Neutron,"
Proc. Roy. Soc. A-136, 692-708 (1932).
7. G. L. Locher,
"Neutrons from Cosmic-Ray Stösse,"
Phys. Rev. 44, 779-781 (1933).
8. L. M. Rumbaugh and G. L. Locher,
"Neutrons and Other Heavy Particles in Cosmic Radiation
of the Stratosphere,"
Phys. Rev. 49, 855 (1936).
9. E. Fünfer,
"Detection of Slow Neutrons in the Atmosphere,"
Naturwissenschaften 25, 235 (1937).

10. S. A. Korff,
"Evidence for Neutrons in the Cosmic Radiation,"
Phys. Rev. 56, 210 (1939).
11. H. A. Bethe, S. A. Korff, and G. Placzek,
"On the Interpretation of Neutron Measurements in Cosmic
Radiation,"
Phys. Rev. 57, 573-587 (1940).
12. L. C. L. Yuan,
"Distribution of Slow Neutrons in Free Atmosphere up to
100,000 Feet," Phys. Rev. 81, 175-184 (1951).
13. R. K. Soberman,
"High-Altitude Cosmic-Ray Neutron Intensity Variations,"
Phys. Rev. 102, 1399-1409 (1956).
14. W. N. Hess, M. W. Patterson, R. Wallace, and E. L. Chupp,
"Cosmic-Ray Neutron Energy Spectrum,"
Phys. Rev. 116, 445-457 (1959).
15. S. F. Singer,
" 'Radiation Belt' and Trapped Cosmic-Ray Albedo,"
Phys. Rev. Letters 1, 171-173 (1958).
16. P. J. Kellogg,
"Possible Explanation of the Radiation Observed by Van
Allen at High Altitudes in Satellites,"
Nuovo Cimento 11, 48-66 (1959).
17. R. E. Lingenfelter,
"Carbon 14 Production Rate by Cosmic Rays,"
Reviews of Geophysics, to be published in 1963.
18. S. Flügge, "On the Excitation of Neutrons by Cosmic Rays
and Their Distribution in the Atmosphere,"
Cosmic Radiation, (Dover Publications, New York,
1946), pp. 144-158, ed. by W. Heisenberg.
19. E. Bagge and K. Fincke,
"The Intensity Distribution of Cosmic-Ray Neutrons in
the Atmosphere,"
Annalen der Physik 6, 321-337 (1950).
20. E. Freese and P. Meyer, "Neutrons in the Atmosphere,"
Kosmische Strahlung, (Springer-Verlag, Berlin, 1953),
pp. 225-237, ed. by W. Heisenberg.

21. B. Davison,
Neutron Transport Theory,
(Oxford University Press, London, 1958).
22. S. Glasstone and M. C. Edlund,
The Elements of Nuclear Reactor Theory,
(D. Van Nostrand Co., Inc., Princeton, 1952).
23. O. C. Kistner and B. M. Rustad,
"Ratio of the Gamow-Teller and Fermi Coupling Constants
Determined from β Values,"
Phys. Rev. 114, 1329-1332 (1959).
24. D. J. Hughes and R. B. Schwartz,
Neutron Cross Sections,
(Brookhaven National Laboratory, Upton, N.Y., 1958).
25. R. E. Lingenfelter, (private communication).
26. H. R. Anderson, Primary Cosmic Radiation in 1958,
(Thesis, California Institute of Technology, 1961, unpublished).
27. C. J. Waddington, "The Composition of the Primary Cosmic
Radiation," Prog. in Nuclear Physics, (Pergamon Press,
New York, 1960), Vol. 8, pp. 1-45.
28. J. A. Simpson, "The Production of Tritons and C^{14} in the
Terrestrial Atmosphere by Solar Protons," J. Geophys.
Research 65, 1615-1616 (1960).
29. H. H. Malitson and W. R. Weber, "A Summary of Cosmic Ray
Events," Solar Proton Manual, (Goddard Space Flight Center,
Greenbelt, Md., 1962), X-611-62-122, pp. 1-17.
30. W. C. G. Ortel, "Neutron Production by Cosmic Rays,"
Phys. Rev. 93, 561-567 (1954).
31. J. A. Simpson, "Neutrons Produced in the Atmosphere by the
Cosmic Radiation," Phys. Rev. 83, 1175-1188 (1951).
32. H. W. Bertini and L. Dresner, "Compilation of Reactions
Calculated for Particles with Energies from about 50 to
350 MeV," Neutron Physics Division Space Radiation
Shielding Research Annual Progress Report for Period
Ending August 31, 1962 (Oak Ridge National Laboratory,
Oak Ridge, Tenn.), ORNL-CF-62-10-29, pp. 58-91.

33. G. P. Millburn, W. Birnbaum, W. E. Crandall, and L. Schechter, "Nuclear Radii from Inelastic Cross-Section Measurements," *Phys. Rev.* 95, 1268-1278 (1954).
34. J. J. Quenby and W. R. Weber, "Cosmic Ray Cut-Off Rigidities and the Earth's Magnetic Field," *Phil. Mag.* 4, 90-113 (1959).
35. J. R. Winckler, P. D. Bhavsar, and L. Peterson, "The Time Variations of Solar Cosmic Rays during July 1959 at Minneapolis," *J. Geophys. Research* 66, 995-1022 (1961).
36. P. Meyer and R. Vogt, "Primary Cosmic-Rays and Solar Protons II," *Phys. Rev.* (to be published), 1963.
37. R. Vogt, "Primary Cosmic-Ray and Solar Protons," *Phys. Rev.* 125, 366-377 (1962).
38. R. C. Haymes, "High Altitude Neutron Intensity Diurnal Variations," *Phys. Rev.* 116, 1231-1237 (1959).
39. H. G. Thode, J. Macnamara, F. P. Lossing, and C. B. Collins, "Natural Variations in the Isotopic Content of Boron and Its Chemical Atomic Weight," *J. Am. Chem. Soc.* 70, 3008-3011 (1948).
40. V. Shiuttse, "An Investigation of the Isotopic Constitution of Boron," *J. Exptl. Theoret. Phys. (U.S.S.R.)* 29, 486 (1955); *Trans. JETP* 2, 402-405 (1956).
41. F. Ajzenberg-Selove and T. Lauritsen, "Energy Levels of Light Nuclei. VI," *Nuclear Phys.* 11, 1-340 (1959).
42. G. C. Hanna, "The Disintegration of Boron by Slow Neutrons," *Phys. Rev.* 80, 530-534 (1950).
43. B. Petree, C. H. Johnson, and D. W. Miller, "Disintegration of Boron by Fast Neutrons," *Phys. Rev.* 83, 1148-1153 (1951).
44. T. E. Bortner and G. S. Hurst, "Ionization of Pure Gases and Mixtures of Gases by 5-MeV Alpha Particles," *Phys. Rev.* 93, 1236-1241 (1954).
45. H. Bichsel and T. W. Bonner, "Reactions $\text{Li}^7(\alpha, n)\text{B}^{10}$, $\text{Li}^7(\alpha, \alpha')\text{Li}^{7*}$, and $\text{B}^{10}(n, \alpha)\text{Li}^7$," *Phys. Rev.* 108, 1025-1027 (1957).

46. A. M. Weinberg and E. P. Wigner, The Physical Theory of Neutron Chain Reactors, (Univ. of Chicago Press, Chicago, 1958).
47. U. H. Hauser, "Neutron Detection with $B(CH_3)_3$ and Investigation of the $B^{10}(n,\alpha)Li^7$ Reaction," Z. Naturforsch. 7a, 781-785 (1952).
48. J. A. Simpson.
49. A. R. Johnston, The Absolute Cosmic-Ray Ionization in the Atmosphere at Balloon Altitudes, (Thesis, California Institute of Technology, 1956, unpublished).
50. H. V. Neher, "The Primary Cosmic Radiation," Ann. Rev. Nuclear Sci. 8, 217-242 (1958).
51. H. W. Patterson and R. Wallace, A Method of Calibrating Slow-Neutron Detectors (Lawrence Radiation Laboratory, Berkeley, 1958), UCRL-8359.
52. H. V. Neher, "A Barometric Element for Radio-Sondes," Rev. Sci. Instr. 24, 97-98 (1953).
53. C. G. Stott and Co., Inc., 1310 New York Avenue, Northwest, Washington 5, D. C.
54. Office of Naval Research, private communication.
55. W. R. Grace and Company, Dewey and Army Chemical Division, 62 Whittemore Ave., Cambridge 40, Mass.
56. H. V. Neher, "An Automatic Ionization Chamber," Rev. Sci. Instr. 24, 99-102 (1953).
57. H. V. Neher, V. Z. Peterson, and E. A. Stern, "Fluctuations and Latitude Effect of Cosmic Rays at High Altitudes and Latitudes," Phys. Rev. 90, 655-674 (1953).
58. H. V. Neher and A. Johnston, "Techniques Useful in Evacuating and Pressurizing Metal Chambers," Rev. Sci. Instr. 25, 517-518 (1954).
59. H. V. Neher and A. Johnston, "Modification to the Automatic Ionization Chamber," Rev. Sci. Instr. 27, 173-174 (1956).

60. L. B. Loeb, Basic Processes of Gaseous Electronics, (University of California Press, Berkeley, 1960).
61. J. A. Bistline, "Some Properties of BF_3 in Ionization Chambers," Rev. Sci. Instr. 19, 842-846 (1948).
62. H. S. W. Massey and E. H. S. Burhop, Electronic and Ionic Impact Phenomena, (Oxford University Press, London, 1958).
63. H. V. Neher, "Variable Sensitivity Automatic Ionization Chamber," Rev. Sci. Instr. 32, 48-49 (1961).
64. H. A. Bethe and J. Ashkin, "Passage of Radiations through Matter," Experimental Nuclear Physics (John Wiley, New York, 1953), Vol. I, pp. 166-357.
65. R. D. Evans, The Atomic Nucleus, (McGraw-Hill, New York, 1955).
66. W. H. Barkas, "The Range-Energy Relation in Emulsions," Nuovo Cimento 8, 201-214 (1958).
67. W. D. Allen, Neutron Detection, (Philosophical Library Inc., New York, 1960), pp. 145-155.
68. H. A. C. Neuberg, R. K. Soberman, M. J. Swetnick, and S. A. Korff, "High Altitude Cosmic Ray Neutron Density at the Geomagnetic Pole," Phys. Rev. 97, 1276-1279 (1955).
69. H. R. Anderson, private communication.
70. H. R. Anderson, "Sudden Increase of Cosmic-Ray Intensity," Phys. Rev. 116, 461-462 (1959).
71. H. V. Neher and H. R. Anderson, "Two Unusual Events at High Altitudes," Proc. of the Moscow Cosmic Ray Conference (Moscow, 1960), English ed., Vol. 4, pp. 101-103.
72. K. A. Anderson, "Solar Flare X-Ray Burst on Sept. 28, 1961," J. Geophys. Research 67, 4103-4117 (1962).
73. J. R. Winckler, "Balloon Study of High-Altitude Radiations during the International Geophysical Year," J. Geophys. Research 65, 1331-1359 (1960).

74. H. T. Mantis and J. R. Winckler, "Balloon Observation of Artificial Radioactivity at the Base of the Stratosphere," *J. Geophys. Research* 65, 3515-3519 (1960).
75. W. F. Libby, "Radioactive Strontium Fallout," *Proc. Natl. Acad. Sci. U. S.* 42, 365-390 (1956).
76. L. Machta and R. J. List, "Analysis of Stratospheric Strontium⁹⁰ Measurements," *J. Geophys. Research* 64, 1267-1276 (1959).
77. R. C. Haymes and S. A. Korff, "Slow-Neutron Intensity at High Altitudes," *Phys. Rev.* 120, 1460-1462 (1960).
78. R. F. Christy, "Point Source Problems and Albedo," *Lecture Series on Nuclear Physics*, (U. S. Govt. Printing Office, Washington, 1947), pp. 117-121.
79. W. P. Reidy, R. C. Haymes, and S. A. Korff, "A Measurement of Slow Cosmic-Ray Neutrons up to 200 Kilometers," *J. Geophys. Research* 67, 459-465 (1962).
80. W. N. Hess and A. J. Starnes, "Measurement of the Neutron Flux in Space," *Phys. Rev. Letters* 5, 48-50 (1960).
81. J. P. Martin, L. Witten, and L. Katz, "Cosmic-Ray Albedo Neutron Flux Measurement Above the Atmosphere," (to be published in 1963).
82. S. J. Bame, J. P. Conner, F. B. Brumley, R. L. Hostetler, and A. C. Green, "Neutron Flux and Energy Spectrum Above the Atmosphere," *J. Geophys. Research* 68, 1221-1228 (1963).
83. J. A. Simpson, W. Fonger, and S. B. Treiman, "Cosmic Radiation Intensity-Time Variations and Their Origin. I. Neutron Intensity Variation Method and Meteorological Factors," *Phys. Rev.* 90, 934-950 (1953).
84. J. Strong, Procedures in Experimental Physics, (Prentice-Hall New York, 1938), pp. 188-216.
85. P. L. Kirk and R. Craig, "Reproducible Construction of Quartz Fiber Devices," *Rev. Sci. Instr.* 19, 777-784 (1948).

86. P. L. Kirk and F. L. Schaffer, "Construction and Special Uses of Quartz Helix Balances," *Rev. Sci. Instr.* 19, 785-790 (1948).
87. F. M. Ernsberger and C. M. Drew, "Improvements in Design and Construction of Quartz Helix Balances," *Rev. Sci. Instr.* 24, 117-121 (1953).
88. H. V. Neher, private communication.
89. H. S. Booth and D. R. Martin, Boron Trifluoride and Its Derivatives, (John Wiley, New York, 1949).
90. I. L. Fowler and P. R. Tunncliffe, "Boron Trifluoride Proportional Counters," *Rev. Sci. Instr.* 21, 734-740 (1950).
91. V. C. Tongiorgi, S. Hayakawa, and M. Widgoff, "High Pressure BF_3 Proportional Counters," *Rev. Sci. Instr.* 22, 899-904 (1951).
92. R. B. Mendell, Plateau Slopes and Pulse Characteristics of Large, High-Pressure BF_3 Counters, New York University AFOSR-TN-59-738, July 1959.
93. W. D. Allen, op. cit., pp. 155-159.
94. R. V. Meghreblian and D. K. Holmes, Reactor Analysis, (McGraw-Hill, New York, 1960), p. 246.
95. D. J. Hughes, Neutron Cross Sections, (Pergamon Press, New York, 1957), p. 25.

APPENDIX A. SYMBOLS, UNITS, AND NOMENCLATURE

Most of the symbols used in this thesis are defined along with the equations in which they appear. A few symbols are used repetitively, and are defined only for their initial appearance. The definitions of these symbols are repeated here.

N = neutron density (neutrons cm^{-3}).

ϕ = neutron flux (neutrons $\text{cm}^{-2} \text{sec}^{-1}$).

S = neutron source function expressed in neutrons $\text{cm}^{-3} \text{sec}^{-1}$ or neutrons $\text{cm}^{-2} \text{sec}^{-1}$, depending upon the context.

n = density of medium expressed in nuclei cm^{-3} , or;

n = used as identification symbol for "neutron,"
e.g., $\phi(n)$, the neutron flux.

σ = reaction cross section per target nuclei.

Σ = macroscopic cross section of a medium for some specified reaction. $\Sigma = n\sigma$.

E = energy.

v = velocity.

V = volume of a detector (cm^3).

I = ionization current measured by an ionization chamber.

Neutron flux is expressed in neutrons sec^{-1} that intercept a sphere of unit cross section area. $\phi = Nv$.

Pressure altitude is expressed in grams cm^{-2} mass of air overhead. The conversion from pressure altitude in grams cm^{-2} to standard altitude in feet is given in Figure 1.

$I(\text{B}^{10}\text{F}_3)$, $I(\text{B}^{11}\text{F}_3)$, and $I(\text{Argon})$ are the ionization currents measured by chambers filled with the indicated gas. The ionization currents are expressed in "equivalent ion pairs," a unit that reduces to "ion pairs $\text{cm}^{-3} \text{sec}^{-1} \text{atm}^{-1}$ of air" in the absence of a neutron flux.

$I(n)$ is the ionization current due to the reaction $\text{B}^{10}(n, \alpha)\text{Li}^7 + 2.35 \text{ MeV}$ in a B^{10}F_3 chamber enriched in the B^{10} isotope to 96%.

$I(\text{c.p.})$ is the ionization current due to the ionizing component of cosmic-rays.

APPENDIX B. THE ELECTROMETER UNIT

The Neher integrating ionization chamber has been described in the literature (26, 56-59). See Chapter IV for a description of the ionization chamber and for an outline of the operation of the quartz electrometer unit. Figure 4 is a drawing of the quartz electrometer unit. If a significant level of impurities is present in the chamber gas, or if the electrometer unit is improperly constructed, the total number of pulses attainable from the ionization chamber will be severely restricted. This section presents an analysis of the recharging mechanism and provides a prescription for satisfactory construction of the electrometer unit.

Analysis of the Recharging Mechanism

Given the fiber restoring force $F_f(z)$ and the electrostatic attractive force of the fiber to the collector $F_e(z, \Delta V)$, where z represents the fiber displacement from an unstressed position and ΔV represents the fiber-to-collector differential voltage, then a position of stable equilibrium will be found for

$$F_f(z) = F_e(z, \Delta V) . \quad \text{Condition (1)}$$

provided

$$\frac{\partial F_f(z)}{\partial z} > \frac{\partial F_e(z, \Delta V)}{\partial z} . \quad \text{Condition (2)}$$

The fiber restoring force will vary roughly as some power law of the displacement z . However, as the fiber approaches the collector, the electrostatic forces will increase without limit. Thus, by proper spacing of the fiber-to-collector distance, condition (2) will be violated for a particular ΔV , instability will result, and the fiber will accelerate toward the collector.

The motion of the fiber subsequent to impact upon the collector is rather involved, and depends not only upon the particular fiber-collector geometry, but also on the associated electrical circuit. "Dynamic" forces due to the motion of the fiber, the coefficient of restitution for fiber impact, the fiber-to-collector adhesion, the various capacitances of the electrometer system, the electrical resistance of the fiber, and the rate of recharging are factors which determine how long the fiber remains in contact with the collector and the duration of time for maintenance of electrical continuity from the fiber to the collector. After discharge of the current pulse to the collector, the fiber-to-collector differential voltage is nullified and the fiber returns to its unstressed position.

When the electrometer unit and the associated grounded shell are operated as an ionization chamber, ΔV increases with time due to the collection of electrons by the collector. Thus in a time independent flux of charged particles, the chamber recharging pulses occur at regular intervals, with a statistical variation resulting from

the finite number of particles interacting in a chamber, and a systematic variation due to irregularities in the amount of charge transferred to the collector during a chamber pulse.

The waveform of the recharging pulse from the ionization chamber and the associated electrical circuit can be interpreted in terms of the schematic shown in Figure 18.

The collector to spherical shell capacitance, C_c , is estimated to be about 3 pf, as determined from

$$C_c = \frac{Q_o}{\Delta V_o} ,$$

where ΔV_o is the fiber-to-collector potential necessary to initiate the recharging cycle, and Q_o is the amount of charge per pulse. ΔV_o can be measured directly; Q_o can be calculated by placing the chamber at a point of known ionization.

The quartz fiber resistance is determined by the thickness of aquadag deposited on the fiber. Values from 0.2 M Ω to 2 M Ω perform in a satisfactory manner.

Because of the small dimensions involved, the fiber-to-collector capacitance is small with respect to the collector-to-spherical shell capacitance ($C_f \ll C_c$).

The distributed capacitance of the electrometer system and the distributed capacitance of the recharging circuit are estimated by measuring the pulse height on an oscilloscope. The observed pulse

height, $\Delta V'_o$, is related to ΔV_o by

$$\Delta V'_o = \Delta V_o \frac{C_c}{C_c + C_e + C_r + C_i}$$

Also, by observing the decay time of the pulse, an independent value is obtained:

$$\tau_d \approx R_r (C_e + C_r + C_i).$$

Values of $C_e + C_r \approx 20$ pf are in agreement with either method.

The recharging circuit resistor, R_r , is determined by requirements on the pulse length. For $R_r = 1$ M, the decay time of the pulse is observed to be about 30 μ sec.

The blocking capacitor of the recharging circuit serves to isolate the amplifier input from the recharging battery. Its value is chosen to be large with respect to other capacitances ($C_b = 0.001$ μ f).

R_i and C_i represent the input impedance of the associated amplifier and are:

$$R_i = 1 \text{ M}\Omega, \quad C_i = 10 \text{ pf} \quad \text{for a flight unit;}$$

$$R_i = 10 \text{ M}\Omega, \quad C_i = 10 \text{ pf} \quad \text{for an oscilloscope.}$$

As soon as continuity is established between the fiber and the collector, a current results which transfers charge from C_e , C_r , and C_i to the collector capacitance, C_c . Thus the rise time of the electrometer pulse is determined primarily by the fiber resistance

and the collector capacitance. Rise times measure 0.2 to 2 μ sec for fiber resistances of 0.1 to 1 M Ω . It is somewhat difficult to ascertain the fiber resistance at the point of contact, since the resistance varies considerably over small distances. The characteristic rise time ought to be of the order of $\tau_r = R_f C_c = 0.3$ to 3 μ sec, which agrees with the observed times.

As soon as the voltages across C_c and $C_e + C_r + C_i$ have equalized, the pulse attains its maximum value. All the capacitances then charge together until the fiber-to-collector continuity is lost. Because $C_f \ll C_c \ll C_e + C_r + C_i$; it is not possible to determine the exact time when continuity ceases from examination of the oscilloscope display.

The presence of the blocking capacitor C_b does not affect the shape of the recharging pulse. While C_b does introduce a normal mode with a long characteristic time,

$$\tau_b = C_b (R_r + R_i) = 2 \times 10^{-3} \text{ sec.},$$

the amplitude of this mode is not excited by the pulsing operation.

The time when the fiber-to-collector conduction stops is related to the fiber motion away from the collector. Interpretation of this event is involved, because there are present several effects difficult to estimate. The manner of impact of the fiber onto the collector is certainly important, as well as the adhesion of the fiber to the

collector. Unless the impact occurs somewhere near the radius of gyration of the fiber about the attached end, then lateral motions and fiber rebound are likely to occur, resulting in intermittent continuity. Adhesion sets a lower limit for the fiber restoring force, and also restricts the materials that may be brought into contact: e. g., a gold-to-gold contact is unsatisfactory. The presence of impurities in the chamber gas may also increase the adhesive effects.

As long as the time scale of the recharging operation is short with respect to motions of the fiber, then the potential to which the collector is finally charged should be repeatable. The fundamental frequency of vibration of a quartz fiber 10 microns in diameter and 0.9 cm in length, fastened to a support at one end, is about 100 cycles per second. This is in correspondence with the maximum pulsing rates observed which are of the order of 50 pulses per second. Thus motions of the fiber occur on a time scale of milliseconds, a duration long with respect to the recharging time.

Apparently the collector never does reach battery potential. If the input capacitance of the amplifier is raised by a factor of 10, the pulsing rate of a chamber may change a few percent. The decreased size of the pulse permits the collector to be charged to a higher potential, thus increasing the time between chamber pulses. This implies that some chambers maintain fiber-to-collector conduction for periods as short as 50 μ sec. The presence of this effect requires

that the ionization chamber be calibrated with the particular transmitter to be used on a flight.

In a constant flux of charged particles, the recharging pulses are observed to occur at regular intervals, with a variation of 1% which can be attributed to the finite number of particles interacting in the chamber (approximately 10^4 per pulse). Averaging over a number of pulses will improve the statistics, but only up to a systematic variation of the order of 0.3%. The systematic variations are probably due to alterations of the fiber null position, irregularities in the fiber instability point for commencement of the recharging cycle, and variations in the final potential to which the collector is charged--all of which result in a varying amount of charge being transferred to the collector.

Secular variations for the individual ionization chambers appear to be quite small. Five chambers which have been used as standards on summer trips to Thule, Greenland since 1959 and consequently have been subjected to rather severe treatment exhibit variations from their mean value of less than 1%. A much larger value would probably be indicative of a chamber leak or malfunctioning of the electrometer unit.

The pulsing rate of the ionization chamber has some dependence upon the battery potential of the recharging circuit. This is due to electrostatic effects in the electrometer system and to recombination

of ions in the chamber gas. As originally designed, the ionization chamber displayed a voltage dependence of 0.7% per volt. After the fiber region was enclosed with a conducting shield held at battery potential, the voltage dependence decreased by over a factor of a hundred (59). This improvement results from the elimination of electrostatically induced stresses on the fiber due to fiber-to-electrometer ground capacitance. These stresses alter the fiber null position and change ΔV_0 , the fiber-to-collector voltage required for initiation of the recharging cycle. Ionization chambers filled with argon to a pressure of eight atmospheres have voltage coefficients varying between 0.001% to 0.005% per volt.

The temperature dependence is quite small. For ionization chambers filled with 8 atm of argon, the temperature sensitivity is less than 0.03% per °C for the better units. The dependence on temperature is due to recombination in the chamber gas, changes in the fiber elastic constant, and to nonuniform coating of the fiber.

Because of the small diameter of the recharging fiber, the effects of gravity and of chamber accelerations are important. Treating the fiber as a cantilever beam of uniform cross sectional area, the change in the fiber-to-collector spacing when the chamber is inverted can be estimated. For a 10 micron quartz fiber, 0.9 cm in length, the displacement of a point on the fiber 0.5 cm from the attached end is 0.002 cm when the chamber is inverted. For a fiber-to-collector

spacing of 0.013 cm, this corresponds to a percentage change in spacing of 15%. The observed change in the pulsing rate of an ionization chamber is of this order, ranging from 10% to 20%. This sensitivity to the direction of gravity dictates the geometry of the electrometer system as shown in Figure 4. The unit is designed to displace the fiber in a vertical direction with respect to gravity. Thus the calibration of the chamber has a $(10\% \cos \theta)$ dependence on the angle of tilt, which for angles smaller than 20 degrees will have less than a 1% effect.

In summary, there are many forces that act on the recharging fiber--electrostatic, dynamic, adhesive, gravitational--and each of them places certain stipulations on the design and construction of the electrometer unit.

Prescription for Satisfactory Construction of the Electrometer Unit

The materials for construction of the electrometer unit and techniques for mounting in the chamber have been discussed in the literature (26, 56-59). This section is primarily concerned with mounting and preparation of the quartz fiber for recharging the collector.

The quartz system is best constructed using a binocular microscope, micromanipulators, small torches, and other equipment as described by H. V. Neher in Chapter V:

"The Use of Fused Silica" of Procedures in Experimental Physics (84).

The basic quartz framework of the unit is most efficiently assembled in a jig with provision for linear motion of the fiber support arm in order to adjust the fiber-to-collector spacing.

Except for insulating sections about 0.5 cm long, all of the exposed quartz is coated with graphite to eliminate spurious electrostatic fields resulting from charge deposited on nonconducting surfaces. The recharging fiber is also coated with graphite because graphite-to-graphite contacts seem to have lower adhesion than most metal-to-metal contacts. The graphite is deposited out of solution by painting the surface with diluted "aquadag," a suspension of colloidal graphite in water. ("Aquadag," colloidal graphite in water--22% solids, can be obtained from the Acheson Colloids Company, Port Huron, Michigan.) The diluted solution of aquadag is prepared as follows:

- 1) Stir 10 ml of "Aquadag" in 50 ml of distilled water.
- 2) Shake well, and let the solution stand for 24 hours so that the graphite not in suspension will settle out.
- 3) Pour off the top 75% for use.

The recharging fibers are constructed from fused quartz, 5 to 10 microns in diameter. Several methods of producing quartz fibers of this size are known (85, 86, 87). The method of drawing quartz fibers out of the molten tip of a quartz rod and winding them on a revolving

drum appears to be the most satisfactory. Using such an apparatus, H. V. Neher has drawn fibers as small as 3 microns (88). The 10 micron fibers used in this experiment were made on such a machine. Immediately after production, the fibers are cut into 20 cm lengths and stored in a desiccator. Small gummed labels are attached to both ends of the fibers to facilitate handling.

The following procedure was found to be satisfactory for mounting the 10 micron fiber on the support arm of the electrometer unit. Attach a small gummed label about 4 cm from the lower tab of a suspended length of fiber. First cut the attached tab in half, then cut the short length of fiber in half. This results in two 2 cm lengths of fiber, both secured to tabs.

Now heat the end of the fiber support arm and with another quartz rod pull it out to form a small tip. Then mount the tab, with attached fiber, in a holder of a micromanipulator and adjust the manipulator until the fiber lies over the tip of the support arm in a direction roughly corresponding to its final attachment position. Then, using a small hydrogen-oxygen flame, heat the support arm in the vicinity of the fiber, being careful not to direct the flame onto the fiber. When the tip of the support arm becomes molten, the surface tension of the molten quartz will draw the fiber in. Advance the manipulator so no tension is present in the fiber, and then flex the fiber with a steel needle to test the attachment. Back the manipulator off until the fiber

is straight, but still under no tension, and then heat the fiber in a very small pure natural gas flame. This will straighten out the fiber and adjust its position. Finally, cut the fiber to the desired length. Figure 19 gives the dimensions of the fiber and of the attachment geometry for the electrometer units used in this experiment.

Preparation of the collector contact region consists of painting on the aquadag, baking with a hot wire heater, and buffing with a cotton swab to remove any irregular deposits. The graphite will take on a polished finish with enough reflection to mirror the fiber when it is brought into contact.

The coating of the fiber is the most difficult operation in the assembly of the electrometer unit. The manner in which it is done determines the stability and lifetime of the unit. Fiber sizes ranging down to 10 microns in diameter can be coated using a small artist's brush. For smaller fibers, and for a more uniform distribution of the aquadag coating, the method described here is recommended.

The applicator for the aquadag is made from a 1 mm quartz rod. One end of the rod is necked down by pulling it out in a flame. The forces of surface tension will cause a drop to adhere to this end when the rod is dipped in the aquadag. A #36 Pt wire mounted in a conducting holder and supported by a manipulator is used for measuring the resistance of the applied aquadag coating. Better electrical contact

is maintained with the fiber if the Pt wire is also coated with aquadag. A hot wire heater, held directly under the fiber serves to enhance the deposition of aquadag onto the fiber. The heater also bakes the fiber coating to insure that the fiber does not change position when the assembled chamber is evacuated and degassed in an oven. By applying the hot wire directly to the quartz fiber, irregular deposits of aquadag can be removed, without apparent damage to the fiber. The arrangement of equipment for the coating process is shown in Figure 19.

The deposition of the aquadag onto the fiber is most effectively accomplished by holding the applicator in the worker's hands. Trembling of the fingers can be minimized by cupping the hands together, and by bracing the heel of one hand against a rigid support. The entire operation should be viewed through a binocular microscope. The aquadag is evaporated onto the fiber by slowly working the aquadag drop down the length of the fiber, starting at the attached end. By means of the micromanipulator, bring the Pt wire into contact with the conducting coating to measure the resistance, and to locate non-conducting regions. Continue to apply aquadag until the resistance of the fiber is $0.2 M\Omega$ to $2 M\Omega$ in the region that makes contact with the collector. A thicker coating of aquadag should be applied to the region where the fiber makes contact with the collector. This thicker coating will increase the total number of pulses attainable from the unit.

After the fiber has been coated, the quartz system should be mounted in a jig, and final adjustment made for the desired fiber-to-collector spacing. Finally, the entire quartz system, exclusive of insulating sections, should be coated with aquadag to eliminate spurious electrostatic fields.

Proper fiber coating techniques will result in pulsing lifetimes in excess of 10^4 pulses in an inert atmosphere. Using a wider fiber-to-collector spacing, H. R. Anderson has obtained pulsing lifetimes in excess of 10^6 pulses (69).

APPENDIX C. PREPARATION AND PURIFICATION OF BF_3 .

The boron trifluoride was obtained from Union Carbide Nuclear Company, Oak Ridge National Laboratory, Radioisotopes Sales Dept., P. O. Box P, Oak Ridge, Tennessee. The natural abundance of B^{10} in boron is 19%. Oak Ridge National Laboratory supplies two isotopic ratios of B^{10} to B^{11} in the BF_3 . In one, the B^{10} concentration is enriched to 96% (4% B^{11}); in the other, the B^{10} concentration is depleted to 11% (89% B^{11}). The BF_3 is chemically combined with CaF_2 to form a $\text{BF}_3 \cdot \text{CaF}_2$ complex. The complex is a white powder and may be exposed to air. Approximately 6.5 grams of $\text{BF}_3 \cdot \text{CaF}_2$ are needed to obtain 1 liter of BF_3 at S. T. P. The BF_3 is easily released by heating to temperatures above 250°C . BF_3 is an extremely useful compound, both industrially and in the laboratory. A large amount of literature exists concerning its chemical and physical properties (89).

Boron trifluoride is a colorless gas which hydrolyzes in ordinary air, producing a copious white smoke. It has a melting point of -127°C and a boiling point of -101°C . It is thermally stable and is not changed by the passage of a spark. It combines readily with water, forming a strongly acidic solution, and it will react with organic compounds. It begins to react with silica at 350°C , and the reaction is relatively rapid at 450°C .

The reactivity of boron trifluoride with water and organic materials precludes the use of stopcock grease and rubber O-rings, stoppers, and gaskets. The reactivity of BF_3 with silica at high temperatures eliminates glass as a construction material for the container in which the thermal decomposition of $\text{BF}_3 \cdot \text{CaF}_2$ takes place. Thus the properties of BF_3 require that the preparation, purification, and storage of the gas take place in a metal system. Several similar procedures have been developed by various workers for processing the boron trifluoride prior to filling the instruments (61, 90-92). The method presented here is essentially an adaptation of these procedures.

The system used for the work of this thesis was constructed principally out of copper. The techniques of assembly of such a copper processing system have been described by H. V. Neher and S. Prakash in the literature (1). The number of valves in the system was kept to a minimum by employing the pinching and de-pinching techniques for copper tubing as described by H. V. Neher and A. R. Johnston (58). A rubber seating gasket and a rubber O-ring in the main valve to the pump station were removed, and were replaced by ones composed of teflon (teflon is a fully-fluorinated hydrocarbon). Other valves in the system were of an all-metal construction. Figure 20 depicts the processing system. The pump station consisted of a thermocouple-type vacuum gauge, an ionization-type vacuum gauge, a liquid nitrogen cold trap, a mercury diffusion pump, a three-way stopcock, and a

forepump. The main portion of the processing system consisted of a 1 inch diameter manifold, to which were attached by copper tubing four cylinders: a cylinder for the thermal decomposition of $\text{BF}_3 \cdot \text{CaF}_2$ (Cyl. A), a CaF_2 settling tank, and two cylinders for vacuum distillation of the BF_3 (Cyl. B and Cyl. C). Also attached to the manifold were two pressure gauges (vacuum to 1 atm and vacuum to 3 atm), a filling line to the ionization chambers, a thermocouple-type vacuum gauge, two storage tanks for B^{10}F_3 and B^{11}F_3 , an argon tank, and a sub-system for disposing of waste gases.

The boron trifluoride was evolved from 200 gram lots of $\text{BF}_3 \cdot \text{CaF}_2$. This quantity of $\text{BF}_3 \cdot \text{CaF}_2$ should produce 30 liters of BF_3 at S. T. P. (The volume of an ionization chamber was 9 liters.) The $\text{BF}_3 \cdot \text{CaF}_2$ powder was placed in a copper cylinder, which was then brazed into the system. During the brazing process, the cylinder was immersed in a pan of water to prevent the $\text{BF}_3 \cdot \text{CaF}_2$ from rising above 100°C . Using only the forepump, the cylinder was evacuated very slowly to prevent scattering of the $\text{BF}_3 \cdot \text{CaF}_2$ powder. This was accomplished by opening the pump station valve only a fraction of a turn. After the cylinder was evacuated, the pump station valve was turned to the fully open position and the $\text{BF}_3 \cdot \text{CaF}_2$ powder was outgassed for 24 hours. At the end of this period, the pressure was down to a few microns of mercury as determined by the thermocouple-type vacuum

gauge (these gauges monitor the pressure from 1 to 1000 microns of mercury).

The mercury diffusion pump was turned on, and the temperature of the cold trap was lowered to -196°C by the use of liquid nitrogen. An electric oven was placed around the cylinder and the temperature raised to 80°C . The temperature was regulated by a Fenwal Thermostat and was monitored by a Weston Industrial Thermometer. The pressure rose to about 50 microns, stabilized, and then slowly decreased. After 8 hours of outgassing at 80°C , the temperature was raised to 110°C . An additional 8 hours of outgassing followed, and the pressure decreased to a few microns. Then the temperature was raised to 350°C to initiate the thermal decomposition of the $\text{BF}_3 \cdot \text{CaF}_2$. When the system pressure reached 50 microns, the pump station valve was closed, one of the BF_3 storage tanks (500 ml stainless steel cylinder; maximum pressure: 1800 p. s. i.) was opened to the system, and the temperature of the storage tank was lowered to -196°C . As the BF_3 evolved from the complex, it condensed and solidified in the storage tank. The BF_3 continued to evolve for a period of 4 hours. At this time the oven was turned off, the $\text{BF}_3 \cdot \text{CaF}_2$ cylinder and the CaF_2 settling tank were isolated from the system by the pinching technique, the storage tank valve was closed, the pump station valve was opened, and the entire system was outgassed with a torch.

The storage tank valve was opened and the condensed BF_3 was pumped on. When the indicated pressure dropped to 1×10^{-4} mm Hg, the storage tank valve was closed. The temperature of the storage tank was raised to room temperature and then lowered to -78°C (the temperature of a dry ice and acetone bath). The pump station valve was closed and the temperature of Cyl. B was lowered to -196°C . The BF_3 storage tank valve was slowly opened to allow the BF_3 to enter the system and condense in Cyl. B. The storage tank valve was opened at such a rate that 2 atm pressure was maintained in the system. An abrupt decrease in pressure indicated that the transfer of most of the BF_3 was complete, and the storage tank valve was closed.

The remainder of the purification process consisted of a vacuum distillation procedure. The condensed BF_3 was pumped on in one of the two cylinders (either Cyl. B or Cyl. C) until an indicated pressure of 1×10^{-4} mm Hg was obtained. Then the BF_3 was transferred to the other cylinder to allow any occluded gases to escape. The transfer of the BF_3 was done at a system pressure of 2 atm in a length of time of about 10 minutes. It was found that transfer of the gas at low pressures (about 1 mm Hg) took a very long time, and that any attempt to speed up the transfer by heating the cylinder generally resulted in a sudden increase in the system pressure that was difficult to control. After the transfer and vacuum distillation procedure had been carried out several times, the system pressure immediately after transfer but

prior to reopening the pump station valve was less than 10 microns.

Prior to the BF_3 processing, the ionization chambers to be filled were heated in an electric oven to 300°C , and were evacuated and outgassed until an indicated pressure of 1×10^{-5} mm Hg was obtained. When the vacuum distillation procedure had been completed, the pump station valve was closed. Then the condensed BF_3 was allowed to warm. The first portion of the released gas was discarded. Then the filling line to the ionization chambers was opened slightly. The rate of release of the BF_3 was adjusted so that the system pressure did not rise more than a factor of two above the final filling pressure for the chambers. The BF_3 pressure in the chambers was closely monitored on an accurate pressure gauge (0-760 mm Hg; accuracy: $\pm 0.5\%$) during the filling procedure. When the desired pressure was obtained, the filling line was closed by the pinching technique. The ionization chambers and pressure gauge were allowed to sit for five minutes to achieve pressure and thermal equilibrium. Then the pressure and temperature of the ionization chambers were recorded. The remaining condensed BF_3 in the system was transferred to the storage tank.

Any gases to be discarded were condensed in the cylinder of the waste gas subsystem. These gases were allowed to slowly bubble through n-butyl ether in an Erlenmeyer flask, and then the subsystem

was flushed with argon. All of the BF_3 present in the waste gas would dissolve in the n-butyl ether, which could easily be disposed of by pouring down a sink.

APPENDIX D. IONIZATION CHAMBER SELF-SHIELDING
CALCULATION.

As a result of the $1/v$ energy dependent character of the $B^{10}(n,\alpha)Li^7$ reaction used to detect neutrons, the ionization chambers used in this experiment measure the density of slow neutrons ($E < 10$ keV). However, the measurement process perturbs the neutron flux (by absorbing the neutrons in the $B^{10}(n,\alpha)Li^7$ reaction), and a correction to the observed neutron density must be made for this perturbation. Two effects have to be considered. The presence of the chamber gas (as an absorber) depresses the neutron flux in the vicinity, thereby decreasing the flux incident on the chamber. The neutron absorbing property of the chamber gas also attenuates the incident neutron flux as it traverses the chamber.

For the depression of the neutron flux incident on the chamber, it can be shown that

$$\frac{\Delta\phi}{\phi} \sim 0.3 \frac{R}{\lambda_s} \alpha ,$$

where R is the radius of the chamber, λ_s is the neutron scattering length in air, and α is the probability that an incident neutron will be absorbed (93). The radius of the chamber is 13 cm; λ_s has its minimum value of 22 meters at sea level; the maximum value for α is unity.

Thus, $\frac{\Delta\phi}{\phi} < 2 \times 10^{-3}$.

Therefore, the flux depression in the vicinity of the chamber may be neglected. It is a correction which is mainly applicable to absorbers located in condensed media.

The attenuation of the neutron flux as it traverses the chamber is significant, and a calculation must be made to determine the correction to the observed neutron density. This effect is referred to as "self-shielding" (94), "self-absorption," or "self-protection" (95).

Let the "self-shielding factor" for the ionization chamber be defined as

$$f = \frac{W}{W'} \quad ,$$

where W = neutron capture rate of the ionization chamber

W' = neutron capture rate of the ionization chamber under the assumption that no attenuation of the incident flux occurs (thin detector approximation).

$$\text{Now } W = \int_0^{\infty} dE w(E) = \int_0^{\infty} dE \Sigma(E) \phi(E)$$

$$\text{and } W' = \int_0^{\infty} dE w'(E) = \int_0^{\infty} dE \Sigma'(E) \phi(E) \quad ,$$

where $\phi(E)$ is the neutron differential energy flux expressed in units of neutrons $\text{cm}^{-2} \text{sec}^{-1} \text{eV}^{-1}$,

$\Sigma(E)$ is the total cross section of the chamber expressed in units of cm^2 ,

and $\Sigma'(E)$ is the total cross section of the chamber in the limit of the thin detector approximation expressed in units of cm^2 .

The ionization chamber is filled with BF_3 gas to a pressure of 380 mm Hg at 0°C . The gas is enriched in the B^{10} isotope to a concentration of 96%. The chamber is a sphere of radius 13 cm.

The cross section for the $\text{B}^{10}(n, \alpha)\text{Li}^7$ is

$$\sigma(E) = \frac{\sigma_0 \sqrt{E_0}}{\sqrt{E}}$$

where $\sigma_0 = 3813$ barns and $E_0 = 0.0253$ eV (24).

The value for the self-shielding factor will depend upon the shape of the energy spectrum of the incident neutron flux. The energy spectrum to be applied to the calculation of the self-shielding factor is that obtained by Hess, Canfield, and Lingenfelter (4) in a multi-group diffusion computation using an experimentally determined neutron source spectrum (14).

The maximum in the neutron flux occurs at an energy of 0.1 eV. Normalizing the results of the multi-group diffusion computation to a value of

$$\phi_0(E = 0.1 \text{ eV}) = 1,$$

the following functions fit the data (at least out to 100 keV. Since 99% of the counts are due to the capture of neutrons with energies less than 10 keV, no error will be introduced by assuming the same power law dependence out to infinity.):

$$\begin{aligned}\phi_0(E) &= 27.2 E \exp(-10 E) & E < 0.2 \text{ eV} \\ \phi_0(E) &= 0.173 E^{-0.90} & E > 0.2 \text{ eV}\end{aligned}$$

W_0' can be calculated in a straightforward manner. In the thin detector approximation, $\Sigma'(E)$ is just equal to $\sigma(E)$ times the number of B^{10} nuclei present in the chamber,

$$\Sigma'(E) = (0.5)(0.96) L_0 V_0 \frac{\sigma_0 \sqrt{E_0}}{\sqrt{E}}$$

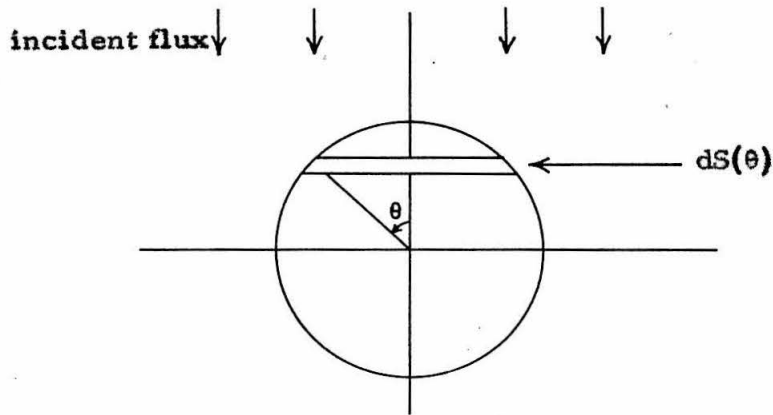
where $L_0 = 2.687 \times 10^{19}$ (Loschmidt's number)

and $V_0 = 9,203 \text{ cm}^3$. (Volume)

Integrating $\Sigma'(E)\phi_0(E)$ numerically from 0 to 0.2 eV and analytically from 0.2 eV to ∞ ,

$$W_0' = \int_0^{\infty} dE \Sigma'(E)\phi_0(E) = 99.1 \text{ neutrons cap't sec}^{-1}.$$

W_0 must be obtained by integrating over the different path lengths through the chamber. Since the chamber is spherical, the total cross section will be independent of the direction of incidence. The total cross section as a function of energy can be calculated by considering the absorption of a uniform monoenergetic beam of neutrons incident upon the detector.



The fraction of the flux entering $dS(\theta)$ which is absorbed is

$$1 - \exp\left[-\frac{2r_o \cos \theta}{\lambda}\right]$$

where $\lambda = \frac{1}{n_o \sigma} = \text{mean absorption length}$

$[n_o = \text{number of B}^{10} \text{ nuclei cm}^{-3} = (0.5)(0.96)L_o].$

Integrating over the sphere, the total cross section becomes:

$$\Sigma(\lambda) = \int_0^{\pi} \frac{\pi}{2} d\theta r_o \cos \theta 2\pi r_o \sin \theta \left[1 - \exp\left(-\frac{2r_o \cos \theta}{\lambda}\right)\right].$$

Performing the integration,

$$\Sigma(\lambda) = \pi r_o^2 \left\{ 1 - 2\left(\frac{\lambda}{2r_o}\right)^2 \left[1 - e^{-\frac{2r_o}{\lambda}} \left(1 + \frac{2r_o}{\lambda}\right)\right] \right\}.$$

Now $\lambda = \frac{1}{n_o \sigma} = \frac{\sqrt{E}}{n_o \sigma_o \sqrt{E_o}}.$

Define $C_o = \frac{1}{2r_o n_o \sigma_o \sqrt{E_o}} = 4.92.$

Then,

$$\Sigma(E) = \pi r_0^2 \left\{ 1 + 2 C_0 \sqrt{E} \exp(-1/C_0 \sqrt{E}) - 2 C_0^2 E + 2 C_0^2 E \exp(-1/C_0 \sqrt{E}) \right\} .$$

$W_0(E)$ will be obtained by integrating $\Sigma(E)\phi_0(E)$ numerically from 0 to 0.2 eV, and by integrating $\Sigma(E)\phi_0(E)$ analytically from 0.2 eV to ∞ .

For the region from 0.2 eV to ∞ , $\Sigma(E)$ can be placed in a form amenable to analytical integration by expanding $\Sigma(E)$ in powers of $(1/C_0 \sqrt{E})$ and neglecting terms of sufficiently high order.

For integration from 0.2 eV to ∞ ,

$$\Sigma(E) = \pi r_0^2 \left\{ \frac{2}{3} \left(\frac{1}{C_0 \sqrt{E}} \right) - \frac{1}{3} \left(\frac{1}{C_0 \sqrt{E}} \right)^2 + \frac{1}{15} \left(\frac{1}{C_0 \sqrt{E}} \right)^3 - \frac{1}{72} \left(\frac{1}{C_0 \sqrt{E}} \right)^4 + \frac{1}{420} \left(\frac{1}{C_0 \sqrt{E}} \right)^5 - \dots \right\} .$$

The first term for $\Sigma(E)$ in this expansion is just the total cross section in the thin detector approximation. The other terms are the corrections for the attenuation of the flux in passing through the chamber, ordered in increasing powers of $(1/C_0 \sqrt{E})$.

Performing the integration over all energies,

$$W_0 = \int_0^{\infty} dE \Sigma(E)\phi_0(E) = 85.0 \text{ neutrons cap't sec}^{-1} .$$

Now that values for W_0' and W_0 have been calculated, f_0 can be obtained (the subscript "0" indicates that the energy spectrum of Hess et al. was used).

$$f_0 = \frac{W_0}{W_0'} = \frac{85.0}{99.1} = 0.857 .$$

The observed neutron density must be multiplied by

$$1/f_0 = 1.166 ,$$

to obtain the neutron density in the atmosphere, unperturbed by the measuring instrument. The value of $f_0 = 0.857$ indicates that the density of neutrons, averaged over the volume of the chamber, is depressed by 14%.

Near the top of the atmosphere the energy spectrum of the neutrons will change, due to the outward diffusion past the atmospheric boundary of a certain fraction of the neutrons. This will modify the ratio of W_0 to W_0' , and will therefore change f_0 . However, the multi-group diffusion calculations of Hess, Canfield, and Lingenfelter indicate that the maximum in the energy spectrum for the flux of neutrons at the top of the atmosphere still occurs at 0.1 eV, and the decrease in intensity falls off at higher energies with roughly the same power law dependence. Thus the value for f_0 that has been obtained here should be valid throughout the entire atmosphere, and is applied as a correction factor to the data analysis of Chapter V.

A similar calculation was performed for a chamber filled to twice the concentration of $B^{10}F_3$, corresponding to a BF_3 pressure of 1 atm at 0°C, enriched to 96% in the B^{10} isotope. A value for f_0 of 0.76 was obtained.

APPENDIX E.

BALLOON FLIGHT DATA

FLIGHT NO. 1

Giant Rock Airport
 Yucca Valley, California
 November 15, 1961

Ionization Current: I (Argon) in ion pairs $\text{cm}^{-3} \text{sec}^{-1}$ per atm of air
 Pressure Altitude: P (Mass of air overhead) in grams cm^{-2}

Ionization Chamber No. 335 (8 atm. of argon)
 Transmitter No. 60
 Barometer No. 69

<u>P</u>	<u>I (Argon)</u>
17	150.2
19	148.8
21	152.8
24	157.8
27	163.5
30	169.8
34	172.8
38	177.2
43	181.7
48	187.4
54	188.9
60	195.7
66	199.5
73	198.8
81	198.8
92	194.7
105	189.5
118	184.6
129	176.2
142	168.0
154	160.6
169	149.5
186	140.5
209	125.1
232	112.4
245	103.8
263	94.2
280	83.2
305	71.5
338	59.5
380	45.4
421	35.9

FLIGHT NO. 2

Giant Rock Airport
 Yucca Valley, California
 February 6, 1962

Pressure Altitude: P (Mass of air overhead) in grams cm^{-2}
 Ionization Current: I(B^{10}F_3) in equivalent ion pairs

Ionization Chamber No. 321 (B^{10}F_3 at 682 mm Hg)
 Transmitter No. 54
 Barometer No. 79

P	I (B^{10}F_3)
30	210.8
32	220.2
35	231.9
38	233.5
42	242.5
45	252.2
50	258.8
55	262.7
61	275.2
66	276.3
72	281.9
78	281.9
85	285.4
93	285.4
102	287.8
109	275.2
119	275.2
136	262.7
153	245.9
168	239.1
183	225.9
201	210.2
224	180.6
272	142.4
332	109.7

FLIGHT NO. 2 (cont'd)

Pressure Altitude: P (Mass of air overhead) in grams cm^{-2}

Ionization Current: I (B^{11}F_3) in equivalent ion pairs

Ionization Chamber No. 279 (B^{11}F_3 at 684 mm Hg)

Transmitter No. 41

P	I (B^{11}F_3)
30	175.6
34	180.1
39	188.6
46	196.4
56	203.3
66	204.1
78	206.6
93	204.9
110	200.4
130	186.8
155	172.6
186	152.0
235	117.9
385	52.1

FLIGHT NO. 3

Giant Rock Airport
 Yucca Valley, California
 February 6, 1962

Pressure Altitude: P (Mass of air overhead) in grams cm⁻²
 Ionization Current: I (B¹⁰F₃) in equivalent ion pairs

Ionization Chamber No. 375 (B¹⁰F₃ at 372 mm Hg)

Transmitter No. 42

Barometer No. 80

P	I(B ¹⁰ F ₃)
31	267.8
31	272.5
32	274.7
34	279.3
36	284.0
41	294.8
48	310.1
55	321.5
64	333.1
77	347.4
92	348.6
112	342.1
131	329.8
155	310.1
186	274.7
225	232.1
303	155.2

FLIGHT NO. 3 (cont'd)

Pressure Altitude: P (Mass of air overhead) in grams cm^{-2}

Ionization Current: I (B^{11}F_3) in equivalent ion pairs

Ionization Chamber No. 347 (B^{11}F_3 at 368 mm Hg)

Transmitter No. 36

P	I (B^{11}F_3)
31	187.0
33	187.8
36	189.0
40	194.7
47	196.8
56	205.6
68	209.1
82	296.6
98	204.7
123	195.2
150	179.8
190	150.2
253	108.1

FLIGHT NO. 4

Giant Rock Airport
Yucca Valley, California
July 4, 1962

Pressure Altitude: P (Mass of air overhead) in grams cm^{-2}
Ionization Current: I (Argon) in ion pairs $\text{cm}^{-3} \text{sec}^{-1}$ per atm of air

Ionization Chamber No. 315 (8 atm of argon)
Transmitter No. 73
Barometer No. 82

<u>P</u>	<u>I (Argon)</u>	<u>P</u>	<u>I (Argon)</u>
6	126.8	62	193.4
6	126.5	64	197.9
6	127.3	67	193.4
6	129.8	70	197.4
6	129.5	73	196.0
7	131.4	77	199.1
7	139.3	80	196.8
8	125.0	83	199.9
9	130.6	87	197.2
10	136.0	92	194.3
10	137.4	96	196.2
11	135.6	102	191.4
12	140.3	105	193.2
13	141.5	111	191.9
15	143.2	116	188.2
16	144.3	122	184.2
18	151.2	128	181.4
20	154.0	135	173.2
22	157.3	143	171.4
24	162.9	151	167.2
26	167.2	159	160.9
29	169.8	169	151.6
32	176.2	179	147.2
34	178.4	190	137.2
38	179.3	203	130.5
41	181.9	219	119.6
45	186.3	238	107.4
50	188.4	264	94.9
54	191.2	295	78.1
56	192.7	340	59.8
59	192.7	414	39.8
		639	12.1

FLIGHT NO. 5

Giant Rock Airport
 Yucca Valley, California
 July 5, 1962

Pressure Altitude: P (Mass of air overhead) in grams cm^{-2}
 Ionization Current: I (B^{10}F_3) in equivalent ion pairs

Ionization Chamber No. 253 (B^{10}F_3 at 380 mm Hg)
 Transmitter No. 53
 Barometer No. 96

P	I (B^{10}F_3)
6	154.2
7	162.2
10	174.4
12	183.8
16	208.4
20	223.2
25	248.9
32	268.1
38	287.0
46	307.7
55	327.5
66	342.2
78	347.1
94	349.0
114	337.4
142	317.0
178	283.7
268	180.3

FLIGHT NO. 5 (cont'd)

Pressure Altitude: P (Mass of air overhead) in grams cm^{-2}
 Ionization Current: I (B^{11}F_3) in equivalent ion pairs

Ionization Chamber No. 366 (B^{11}F_3 at 380 mm Hg)

Transmitter No. 57

Temperature monitored

P	I (B^{11}F_3)
6	140.9
9	145.2
13	152.2
20	163.7
28	178.4
47	196.2
80	204.5
120	191.5
187	169.6

FLIGHT NO. 6

Giant Rock Airport
Yucca Valley, California
July 6, 1962

Pressure Altitude: P (Mass of air overhead) in grams cm^{-2}
Ionization Current: I (B^{10}F_3) in equivalent ion pairs

Ionization Chamber No. 271 (B^{10}F_3 at 380 mm Hg)
Transmitter No. 40
Barometer No. 101

P	I (B^{10}F_3)
7	160.2
9	175.1
13	189.1
17	213.0
22	239.0
29	255.0
35	282.3
45	307.8
55	329.2
68	347.3
85	351.6
112	343.7
147	313.6
200	260.2
287	169.1

FLIGHT NO. 6 (cont'd)

Pressure Altitude: P (Mass of air overhead) in grams cm^{-2}
 Ionization Current: I (Argon) in ion pairs $\text{cm}^{-3} \text{sec}^{-1}$ per atm of air

Ionization Chamber No. 343 (8 atm of argon)

Transmitter No. 56

<u>P</u>	<u>I (Argon)</u>	<u>P</u>	<u>I (Argon)</u>
4	131.9	53	194.0
5	127.8	61	193.2
6	130.0	65	195.8
6	131.1	70	198.3
7	132.2	75	200.4
8	134.3	79	196.6
9	134.9	83	198.3
10	136.8	88	195.0
11	141.8	94	196.2
12	137.0	100	192.4
13	143.6	107	185.8
15	140.4	113	185.8
16	152.0	119	179.0
17	148.6	128	175.8
19	153.0	137	173.4
21	158.9	147	162.9
24	160.4	157	155.8
26	164.5	170	152.9
29	179.2	190	137.3
31	172.0	213	121.0
34	175.5	231	111.1
37	181.3	254	97.4
41	183.5	278	83.2
45	188.5	318	67.0
48	190.2	370	48.0
		465	27.6

FLIGHT NO. 7

Giant Rock Airport
Yucca Valley, California
October 22, 1962

Pressure Altitude: P (Mass of air overhead) in grams cm^{-2}
Ionization Current: I (B^{10}F_3) in equivalent ion pairs

Ionization Chamber No. 309 (B^{10}F_3 at 380 mm Hg)
Transmitter No. 141
Barometer No. 102

P	I (B^{10}F_3)
56	360.6
66	356.6
77	356.4
91	352.6
111	345.3
133	324.4
161	301.0
198	257.5
254	200.3
369	106.8

Ionization Chamber No. 257 (B^{10}F_3 at 380 mm Hg)
High Sensitivity Electrometer Unit
Transmitter No. 52

P	I (B^{10}F_3)
---	---------------------------------

No data. Transmitter failed.

FLIGHT NO. 8

Giant Rock Airport
 Yucca Valley, California
 October 23, 1962

Pressure Altitude: P (Mass of air overhead) in grams cm^{-2}
 Ionization Current: I (B^{10}F_3) in equivalent ion pairs

Ionization Chamber No. 379 (B^{10}F_3 at 380 mm Hg)
 Transmitter No. 142
 Barometer No. 105

P	I (B^{10}F_3)
6	171.7
7	181.0
9	188.4
10	194.3
13	209.5
15	226.1
18	245.9
21	263.0
25	285.5
30	315.1
34	358.2
38	424.2
44	439.7
49	456.2
56	397.3
64	375.2
76	361.1
90	350.3
107	342.8
127	323.8
147	302.6
182	275.6
224	226.4
278	170.7
372	101.9

FLIGHT NO. 8 (cont'd)

Ionization Chamber No. 318 ($B^{10}F_3$ at 380 mm Hg)

High Sensitivity Electrometer Unit

Transmitter No. 49

Pressure Altitude: P (Mass of air overhead) in grams cm^{-2} Time between ionization chamber pulses: Δt in min

Ionization Chamber Calibration: K in min equivalent ion pairs

Ionization Current: I ($B^{10}F_3$) in equivalent ion pairs

P	Δt	K	I ($B^{10}F_3$)
760	8.150	86.8	10
657	4.791	86.8	18
606	3.174	86.8	27
568	2.571	86.8	34
538	2.178	86.8	40
516	1.841	86.8	47
495	1.646	86.8	53
480	1.460	86.8	59
461	1.438	86.8	60
448	1.276	86.8	68
434	1.248	86.8	70
419	1.108	86.8	78
413	1.092	86.8	79

P	Δt	Calculated I ($B^{10}F_3$)	K = I Δt
403	1.038	90	93.4
349	0.930	93	86.5
386	0.962	96	92.4
378	0.826	100	82.6
372	0.843	102	86.0
364	0.782	106	82.9
358	0.762	109	83.1
351	0.740	113	83.6
346	0.685	116	79.5
341	0.702	120	84.2
336	0.711	123	87.4
331	0.701	127	89.0
326	0.687	130	89.3
318	0.611	136	83.1
313	0.657	141	92.6
308	0.635	145	92.1
303	0.587	149	87.5
298	0.549	153	84.0
293	0.575	158	90.8
289	0.562	161	90.5
285	0.546	164	89.5
280	0.545	169	92.1

FLIGHT NO. 8 (cont'd)

Ionization Chamber No. 318 ($B^{10}F_3$ at 380 mm Hg)
 High Sensitivity Electrometer Unit
 Transmitter No. 49

P	Δt	Calculated ($B^{10}F_3$)	$K = I \Delta t$
271	0.507	178	90.2
251	0.459	197	90.4
234	0.416	215	89.4
215	0.400	236	94.4
193	0.367	261	95.8
175	0.338	281	95.0
159	0.324	297	96.2
143	0.320	313	100.2
129	0.312	326	101.7
117	0.310	336	104.2
103	0.313	345	108.0
91	0.318	349	111.0
81	0.320	357	114.2
72	0.325	365	118.6
63	0.332	376	124.8
56	0.315	397	125.0
50	0.284	450	127.8
47	0.274	450	123.3
42	0.281	436	122.5
38	0.292	415	121.2
35	0.330	374	123.4
31	0.348	325	113.1
28	0.360	305	109.8
25	0.372	288	107.1
22	0.385	274	105.5
20	0.374	258	96.5
18	0.383	246	94.2
15	0.379	228	86.4
15	0.380	225	85.5
14	0.376	216	81.3
13	0.382	214	81.7
11	0.359	201	72.2
9	0.353	191	67.4
9	0.346	188	65.0
8	0.339	184	62.4
8	0.332	177	58.8
7	0.308	177	54.5
6	0.290	175	50.8

FLIGHT NO. 9

Giant Rock Airport
 Yucca Valley, California
 October 25, 1962

Pressure Altitude: P (Mass of air overhead) in grams cm^{-2}
 Ionization Current: I (B^{11}F_3) in equivalent ion pairs

Ionization Chamber No. 286 (B^{11}F_3 at 380 mm Hg)
 Transmitter No. 143
 Barometer No. 108

P	I (B^{11}F_3)
7	164.2
10	162.1
12	171.6
15	188.2
19	211.7
22	248.9
28	319.6
33	444.1
39	389.2
48	298.3
64	246.6
96	213.9
168	172.7

FLIGHT NO. 9 (cont'd)

Pressure Altitude: P (Mass of air overhead) in grams cm⁻²Ionization Current: I (Argon) in ion pairs cm⁻³sec⁻¹ per atm of air

Ionization Chamber No. 404 (8 atm of argon)

Transmitter No. 145

P	I(Argon)	P	I(Argon)	P	I(Argon)	P	I(Argon)
7	151.1	14	173.9	25	275.4	40	376.4
7	153.5	14	174.7	25	271.2	40	373.0
7	145.9	14	181.0	26	296.4	40	362.1
7	149.3	14	177.9	26	298.6	41	362.1
8	147.7	15	183.7	27	310.5	41	359.0
8	153.5	15	176.9	27	317.6	42	328.6
8	152.8	15	190.5	27	310.5	43	334.8
8	145.4	16	187.6	28	314.4	43	331.2
8	151.8	16	177.7	28	327.7	44	331.2
8	152.2	16	189.0	28	333.0	44	328.6
9	153.9	16	195.0	29	339.3	45	320.9
9	154.1	17	193.4	29	354.8	46	318.5
9	157.2	17	195.0	29	357.9	46	300.7
9	157.6	17	192.6	30	363.2	47	310.5
9	154.7	17	199.7	30	371.8	48	302.9
9	152.8	17	192.6	30	368.5	48	299.3
9	156.6	18	202.6	31	370.7	49	296.4
10	156.4	18	198.7	31	389.3	50	308.2
10	154.1	18	201.6	31	388.1	50	285.5
10	159.0	18	223.0	32	403.2	51	294.3
10	155.0	19	196.2	32	412.6	52	293.6
10	160.5	19	208.0	32	416.8	53	274.2
10	166.5	19	212.7	33	443.6	54	273.0
11	159.0	19	214.9	33	450.0	55	272.4
11	158.8	19	214.9	33	454.9	56	267.7
11	156.8	20	231.7	34	481.4	57	248.8
11	163.0	20	223.4	34	477.7	58	260.9
11	163.6	20	221.0	34	515.4	60	247.9
11	165.6	20	227.5	34	521.8	61	245.9
12	161.7	21	230.0	35	552.0	62	241.6
12	165.2	21	229.2	35	533.0	64	235.7
12	168.8	21	239.8	35	537.7	66	232.6
12	164.9	21	237.0	35	500.8	67	228.3
12	168.7	22	238.4	36	477.7	69	214.1
13	171.3	22	238.4	36	489.0	71	208.4
13	163.8	22	246.4	36	494.8	73	219.8
13	171.8	22	252.4	37	460.0	75	211.2
13	178.4	23	254.0	37	426.8	77	217.5
13	169.2	23	262.6	38	419.6	79	225.8
14	176.4	23	259.3	38	412.6	81	218.7
14	189.9	24	264.2	39	403.2	83	202.9
14	177.7	24	268.2	39	390.6	85	231.3

FLIGHT NO. 9 (cont'd)

Ionization Chamber No. 404 (8 atm of argon)

Transmitter No. 145

<u>P</u>	<u>I (Argon)</u>
88	200.6
90	223.8
93	195.3
95	192.0
98	194.7
103	198.4
105	196.5
108	187.3
112	189.9
116	180.5
119	185.1
123	173.9
128	170.6
133	183.2
137	177.7
142	168.5
146	165.6
152	185.1
157	159.0
163	153.1
170	151.0
178	139.2
184	146.6
192	132.7
198	148.7
207	139.6
217	116.4
228	114.5
240	103.2
257	94.5
273	96.6
290	79.7
314	70.5
345	55.4
381	46.7
434	33.5
550	17.6

FIGURES

Fig. 1: ARDC Model Atmosphere (1959).

The mass of air overhead in grams cm^{-2} is plotted as a function of altitude. The curve corresponds to the 1959 ARDC Model Atmosphere as tabulated in the Handbook of Geophysics, Edited by the U. S. Air Force Cambridge Research Center, (The MacMillan Company, New York, 1960).

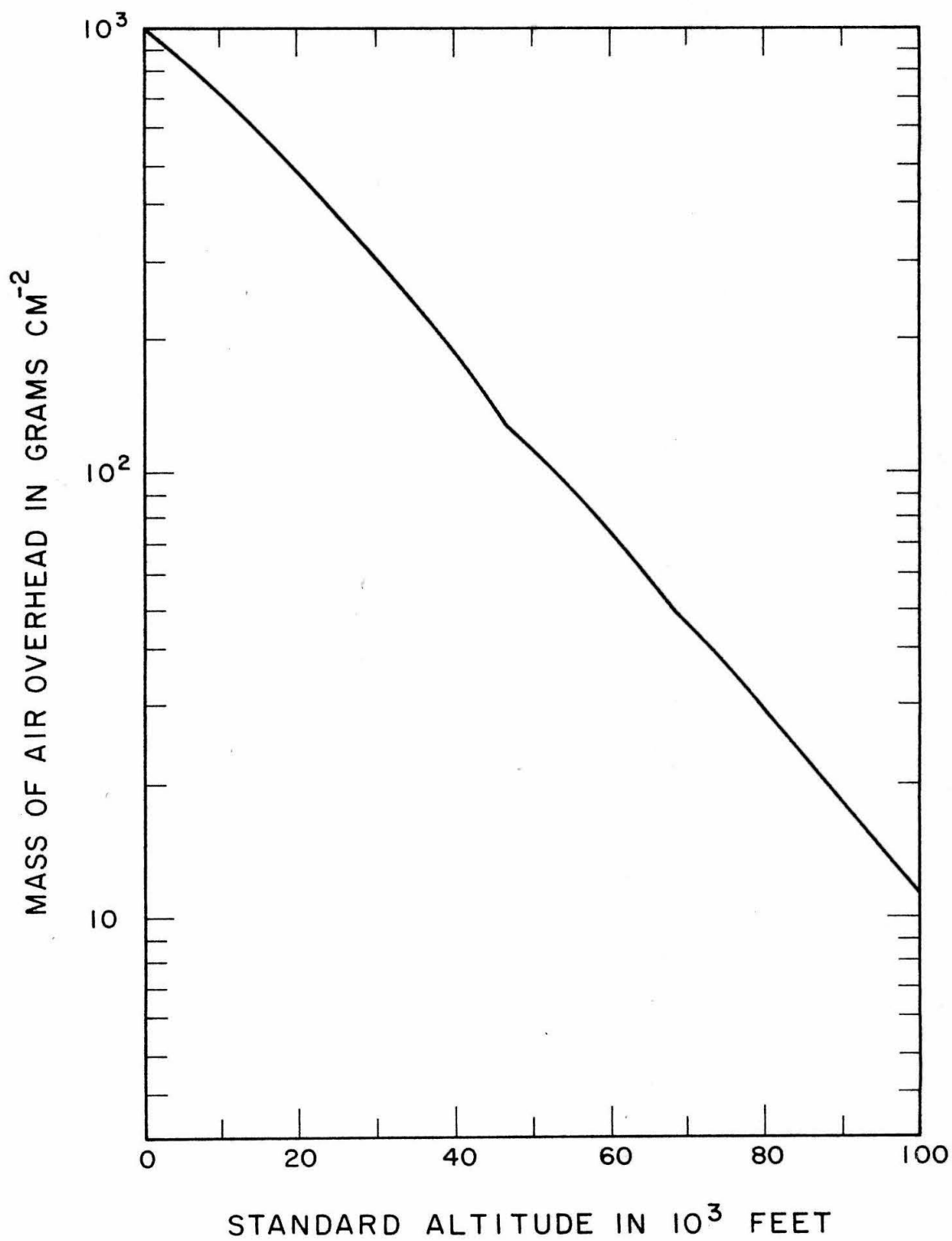


Fig. 1

Fig. 2: Calibration Geometry for the Absolute Calibration of the $B^{10}F_3$ Ionization Chambers.

The $B^{10}(n,\alpha)Li^7$ ionization current of the $B^{10}F_3$ ionization chambers was calibrated in terms of the slow neutron density in the chamber. The slow neutron density was measured by a $B^{10}F_3$ proportional counter of known cross section for the $B^{10}(n,\alpha)Li^7$ reaction.

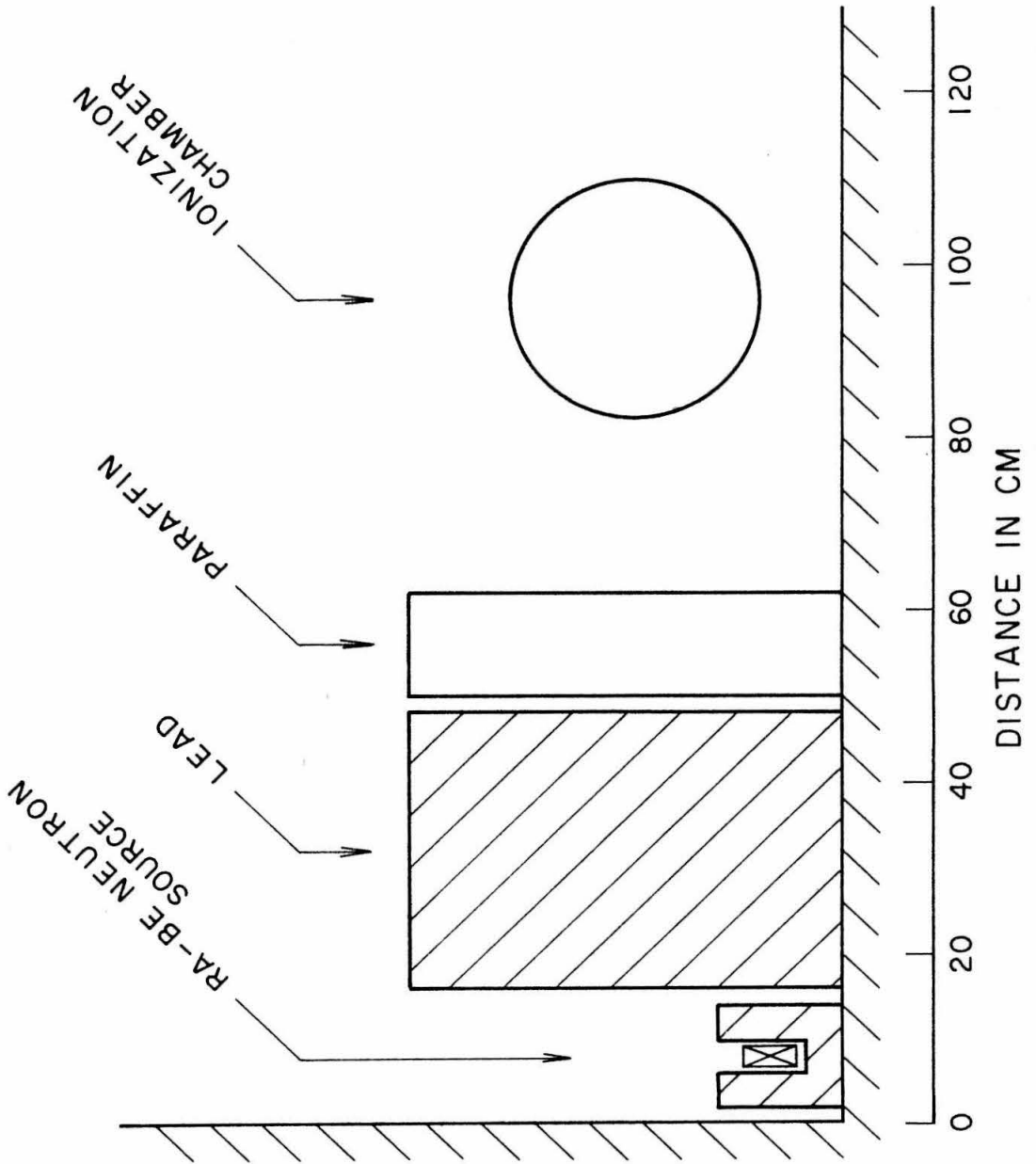


Fig. 2

Fig. 3 : Balloon Flight Train at Launch.

The flight units (instrument plus transmitter) and the parachute are attached to the balloon by means of a 70 ft load line. The additional line from the balloon is used to stabilize the flight train just prior to launch.

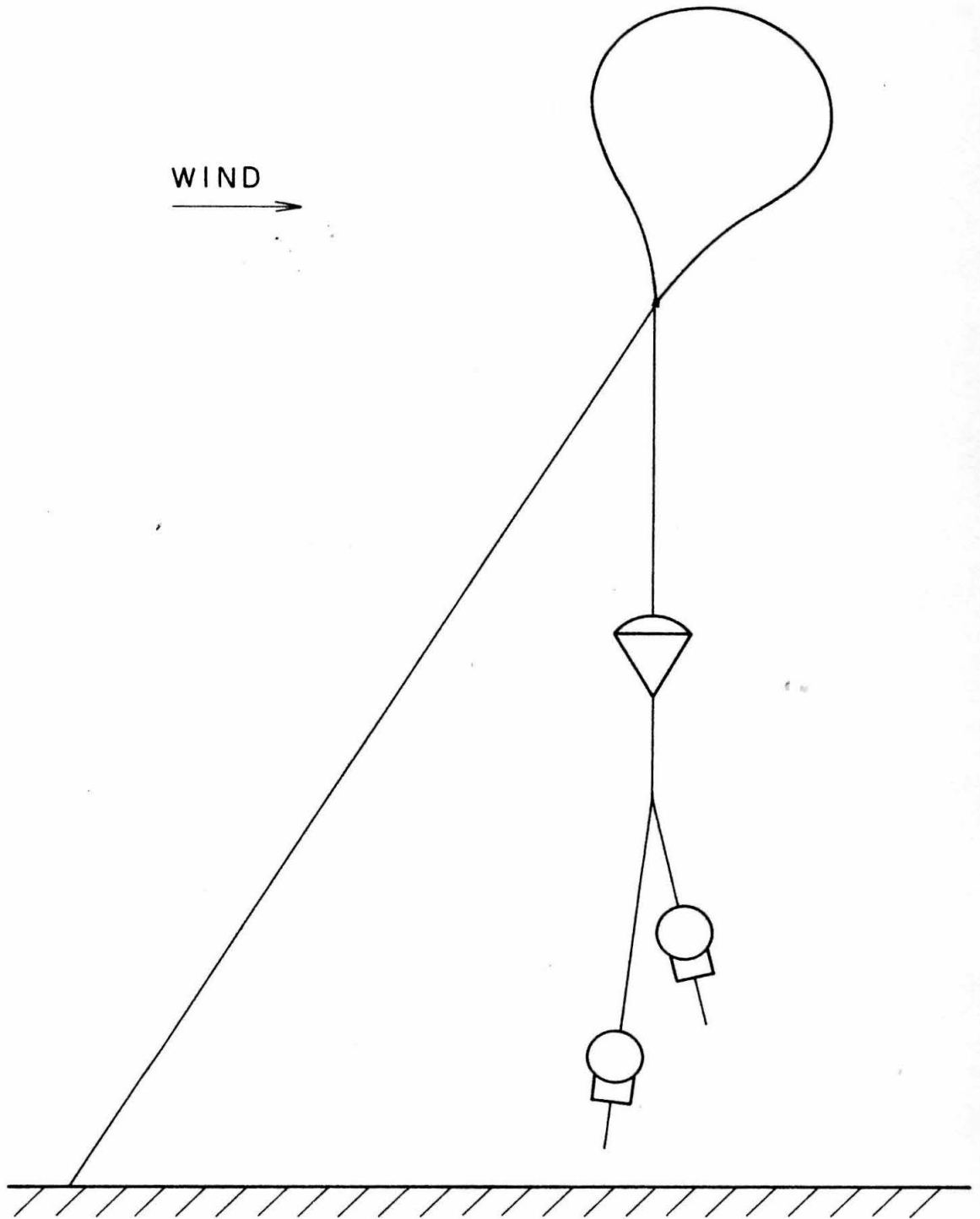


Fig. 3

Fig. 4: Quartz Fiber Electrometer Unit of the Neher Design.

An aquadag coated quartz fiber periodically recharges the central collector. The time interval between the recharging pulses is a measure of the ionization current in the chamber.

146

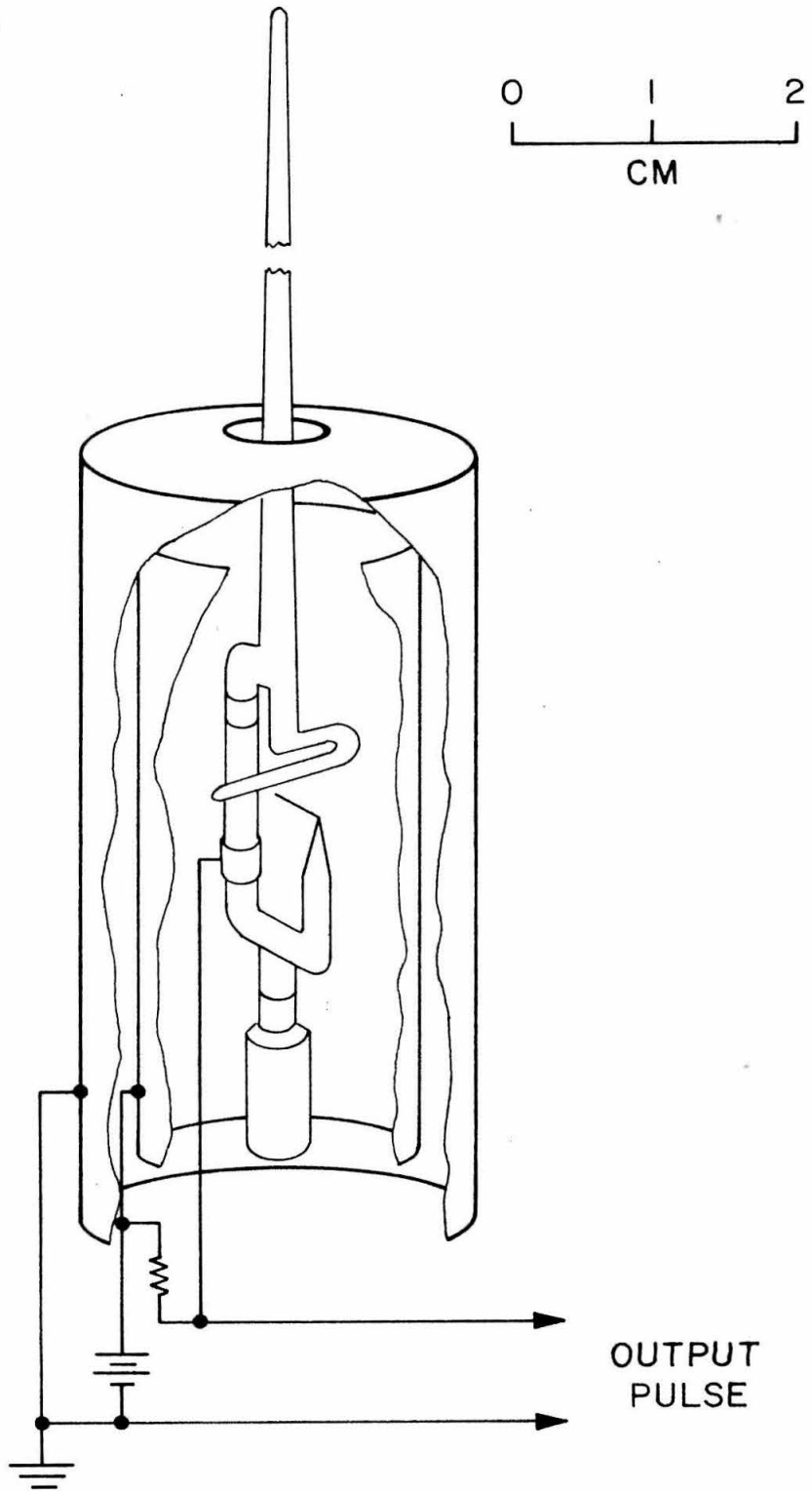


Fig. 4

Fig. 5: The Temperature Monitoring Circuit Used on
Flight No. 5.

The pressure sensing element normally present in the transmitter unit (a variable resistance device: 20 MΩ to 80 MΩ) was replaced by a thermistor circuit. The thermistors (10 MΩ VECO 71A5) are manufactured by Victory Engineering Corp., Springfield Ave., Springfield, N. J.

Fig. 6 : The Instrument Temperature on Flight No. 5.

The temperature of the flight unit during Flight No. 5 is given as a function of pressure altitude and time of day.

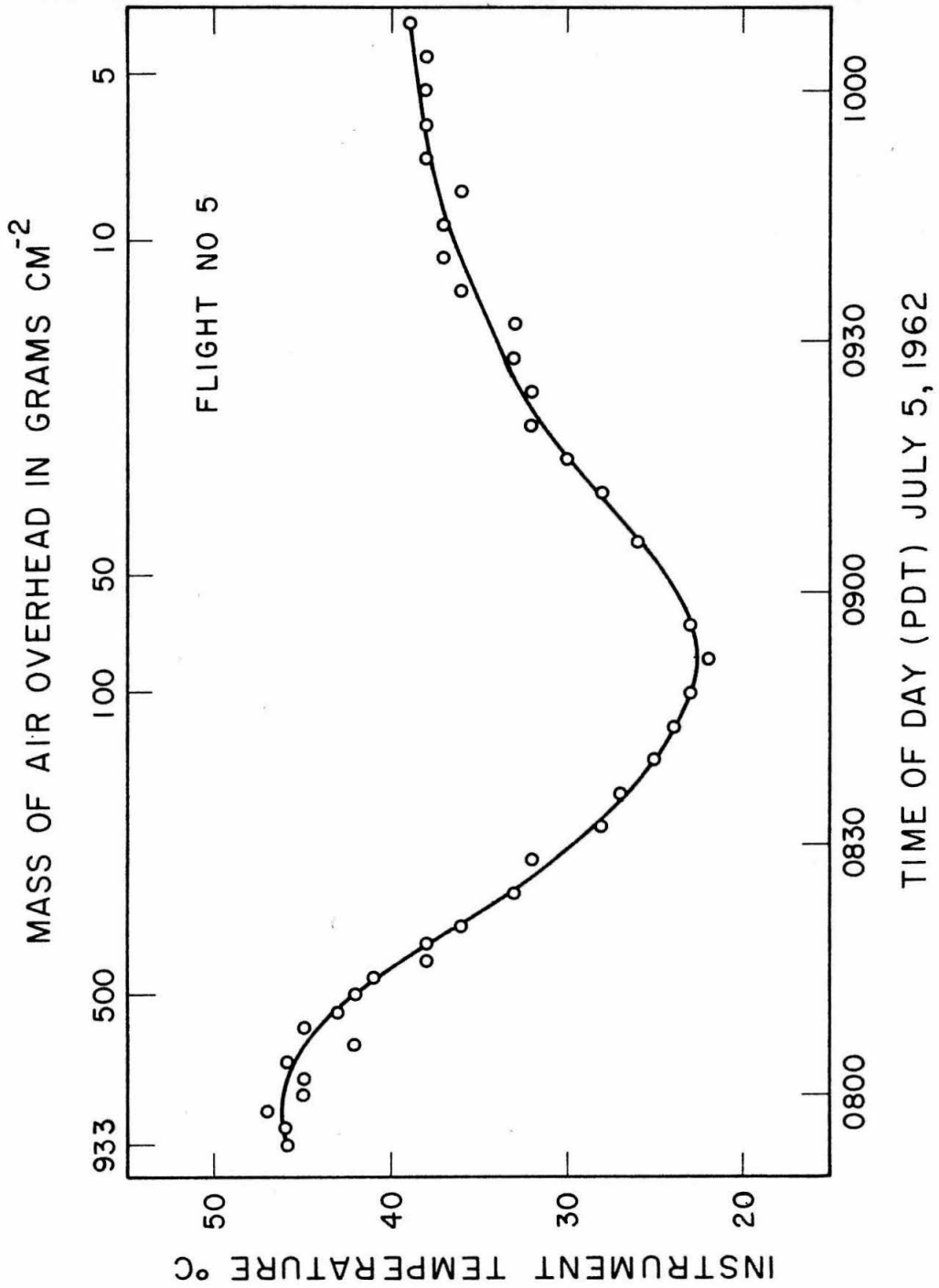
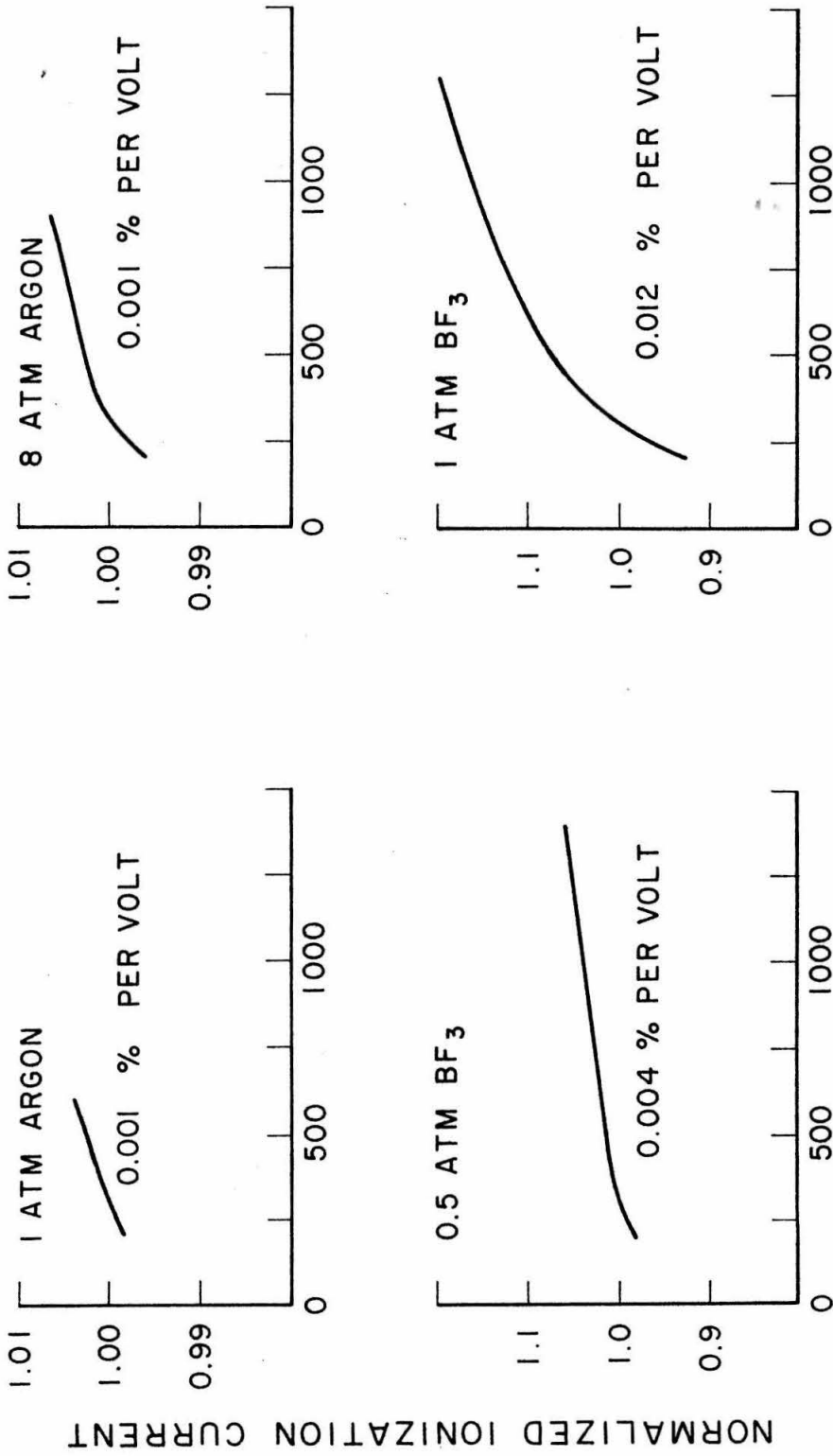


Fig. 6

Fig. 7 : Ionization Current Versus Collector Voltage for
Chamber No. 375

The ionization current of Chamber No. 375 is normalized
to unity at a collector potential of 300 volts.



CHAMBER NO. 375 COLLECTOR VOLTAGE

Fig. 7

Fig. 8: Ionization in the Atmosphere Due to the Ionizing Component of Cosmic-Rays.

The ionization in the atmosphere due to the ionizing component of cosmic-rays was measured with ionization chambers filled with argon to a pressure of 8 atm. From a pressure altitude of 5 g cm^{-2} to 640 g cm^{-2} , the data were obtained on Flights Nos. 1, 4, and 9. From a pressure altitude of 640 g cm^{-2} to 760 g cm^{-2} , the data were obtained by R. A. Millikan, H. V. Neher, and S. K. Haynes [Phys. Rev. 50, 994-998 (1936)]. The statistical errors of the data are of the order of 1%. The curve represents a smooth fit to the data.

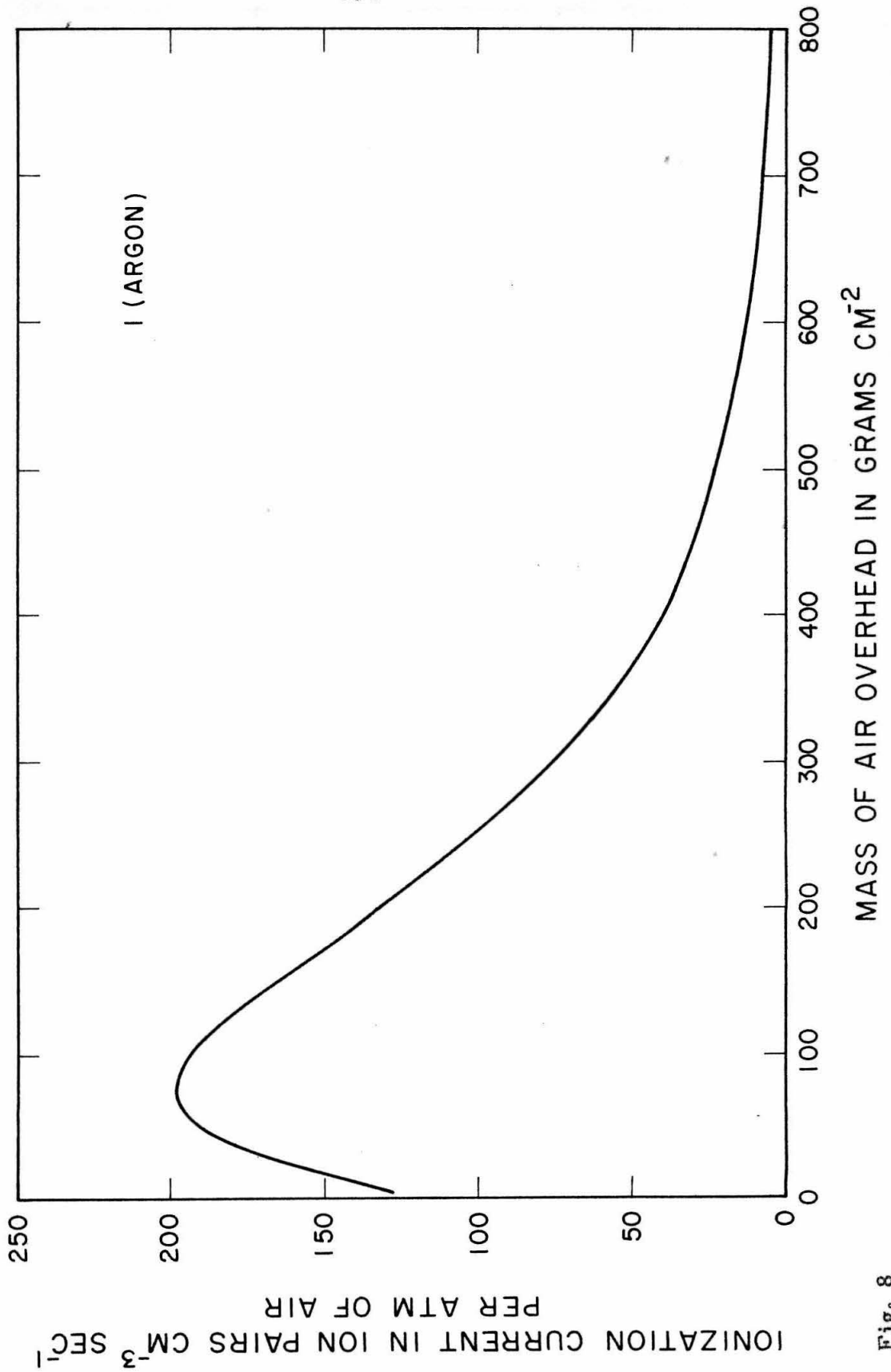


Fig. 8

Fig. 9: Ionization Current of the $B^{10}F_3$ Ionization Chambers as a Function of Pressure Altitude.

$I(B^{10}F_3)$ is defined as the total current in an ionization chamber containing BF_3 enriched in the B^{10} isotope to 96%. The current is measured in units of "equivalent ion pairs," as defined in Chapter V. The data were obtained on Flights Nos. 3, 5, 6, 7, and 8. The curve represents a smooth fit to the data.

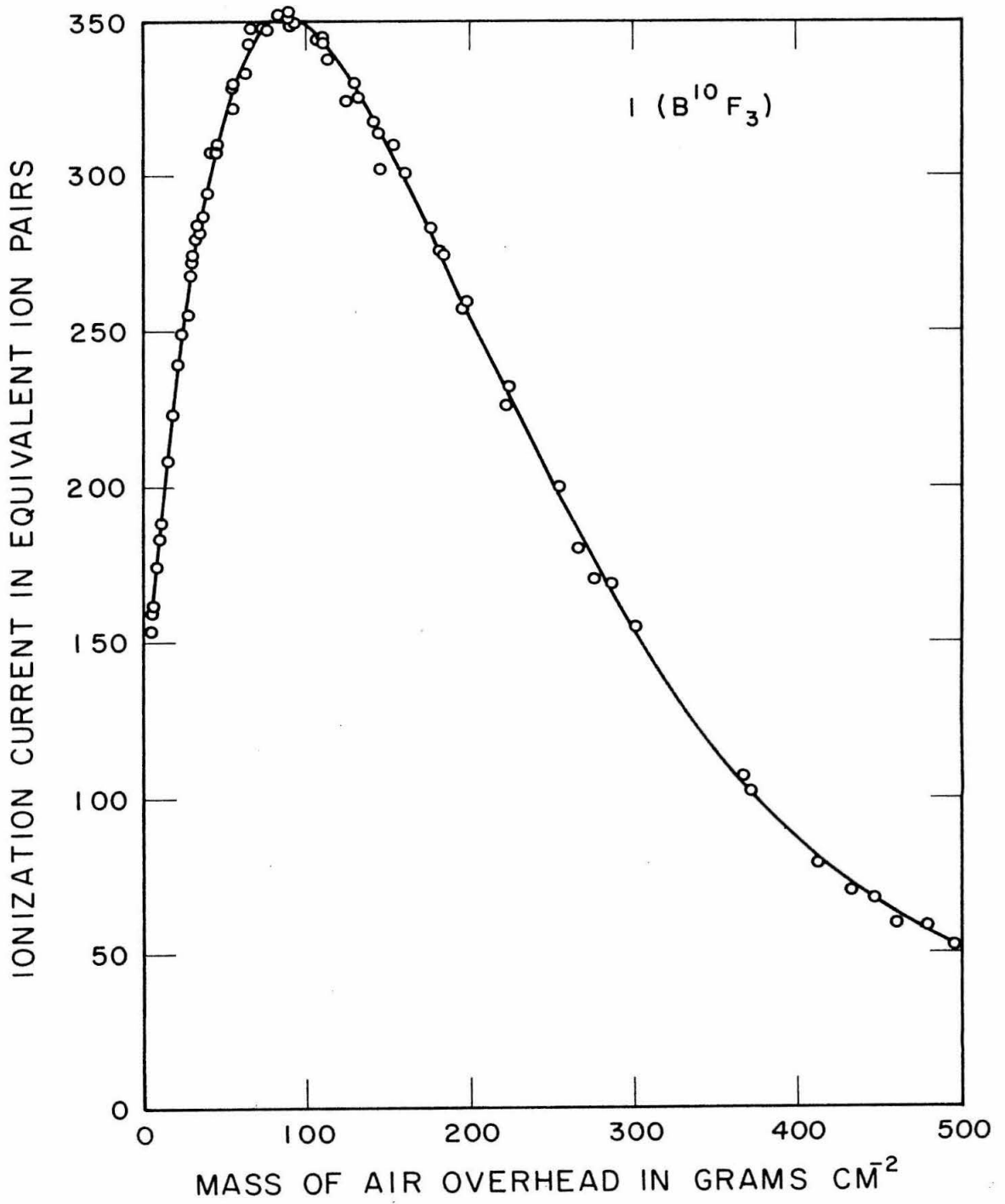


Fig. 9

Fig. 10: Ionization Current of the $B^{11}F_3$ Ionization Chambers as a Function of Pressure Altitude.

$I(B^{11}F_3)$ is defined as the total current in an ionization chamber containing BF_3 enriched in the B^{11} isotope to 89%. (The $B^{10}F_3$ concentration is 11%.) The current is measured in units of "equivalent ion pairs," as defined in Chapter V. The data were obtained on Flights Nos. 3, 5, and 9. The curve represents a smooth fit to the data.

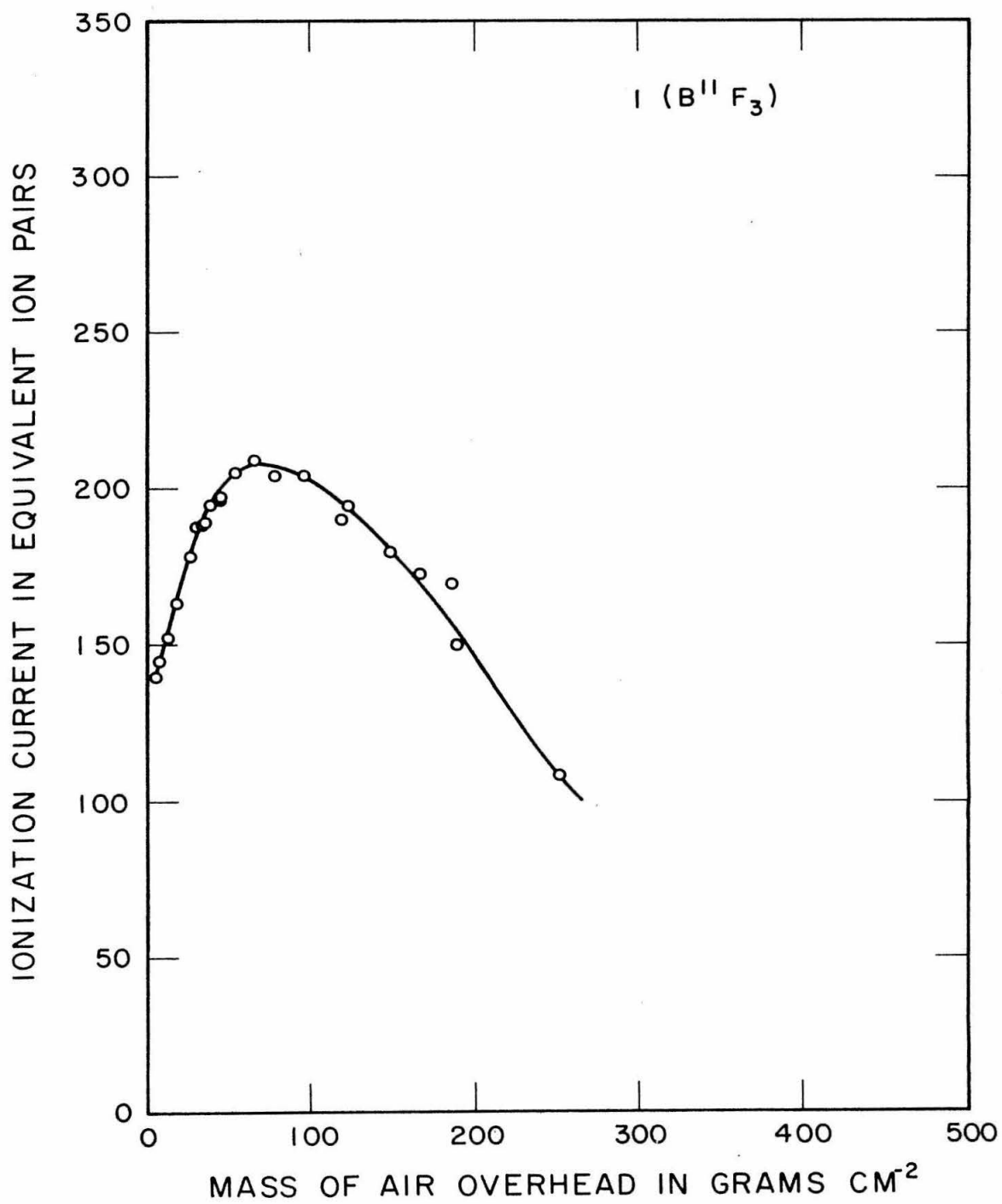


Fig. 10

Fig. 11: Ionization Current at Low Altitude.

The individual data points are displayed for the $B^{10}F_3$ ionization chambers and the argon chambers in the pressure altitude range of 300 g cm^{-2} to 800 g cm^{-2} . The data for $I(B^{10}F_3)$ are indicated by "o." For pressures greater than 400 g cm^{-2} , the data for $I(B^{10}F_3)$ were obtained with a high sensitivity electrometer unit on Flight No. 8. The data marked "Δ" were obtained with argon chambers on Flights Nos. 1, 4, and 9. The data marked "∇" were obtained by R. A. Millikan, H. V. Neher, and S. K. Haynes [Phys. Rev. 50, 994-998 (1936)]. The curves represent a smooth fit to the data.

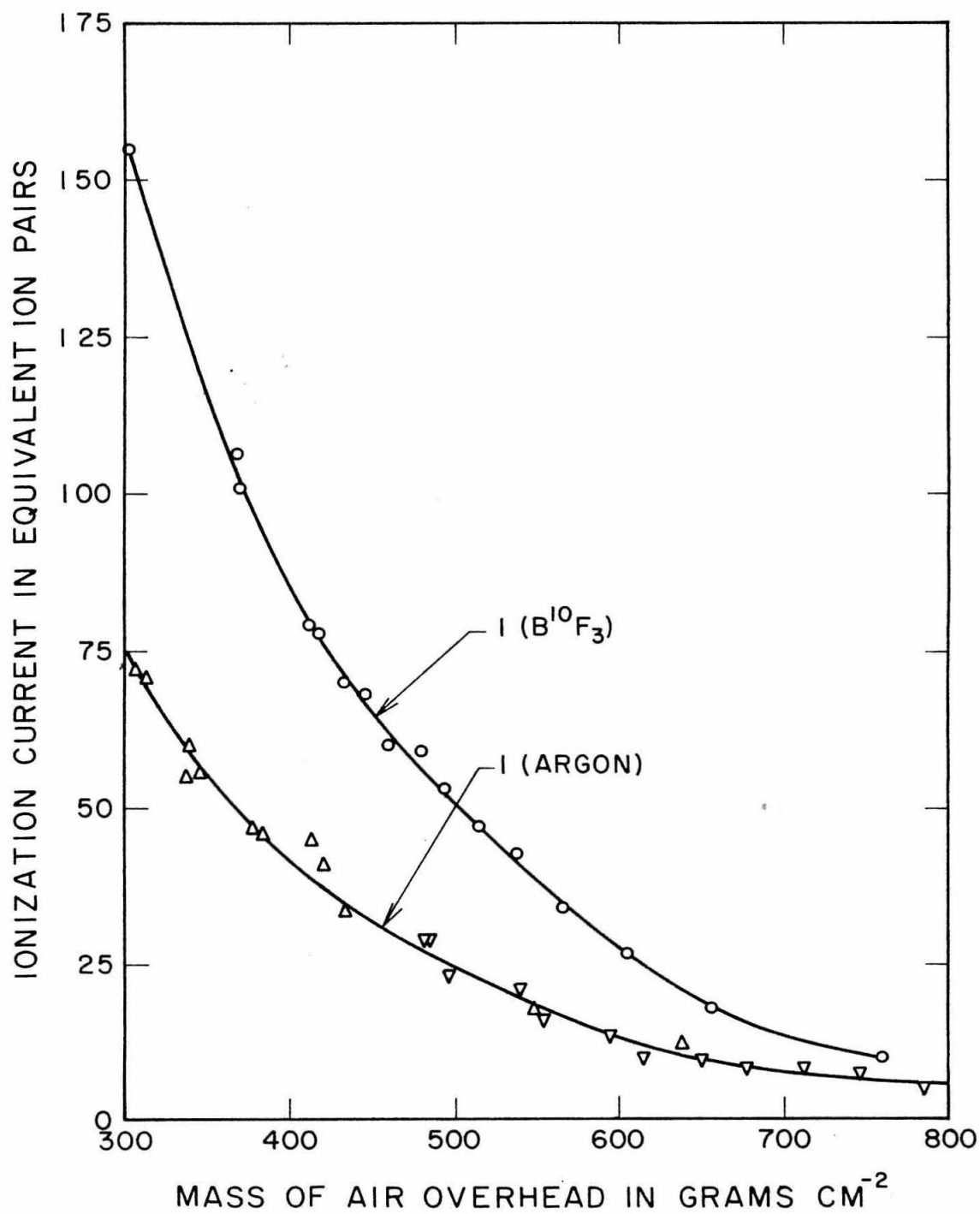


Fig. 11

Fig. 12: The Cosmic-Ray Neutron Density in the Atmosphere.

The density of cosmic-ray neutrons is given as a function of pressure altitude in the range from 6 g cm^{-2} to 760 g cm^{-2} . The individual points represent the B^{10}F_3 ionization chamber data, corrected for background ionization and transformed into neutron density values as described in Chapter V. The relative errors due to statistics and calibration drifts are about $\pm 2\%$ at a pressure altitude of 100 g cm^{-2} and about $\pm 20\%$ at a pressure altitude of 700 g cm^{-2} . The error in the absolute values is estimated to be about $\pm 25\%$. The curve represents a smooth fit to the data.

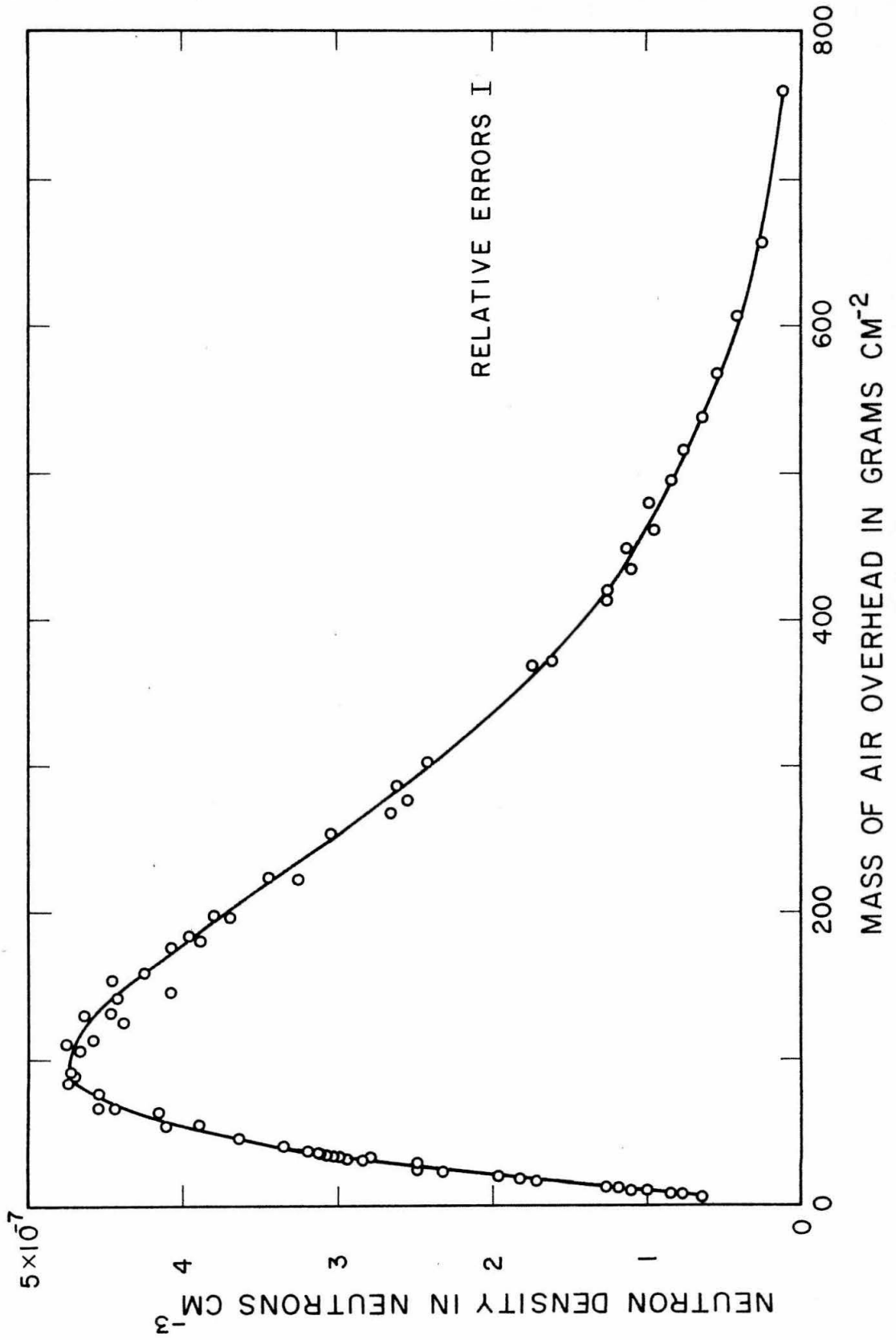


Fig. 12

Fig. 13: Ionization in the Atmosphere on Oct. 25, 1962
Due to Bomb Test Debris.

The individual points represent the data obtained on Flight No. 9 (Oct. 25, 1962) with an ionization chamber filled with argon. The solid curve represents the ionization due to the ionizing component of cosmic-rays as determined on Flights Nos. 1 and 4. The rapid increase in ionization above a pressure altitude of 100 g cm^{-2} (53,000 ft) was also observed on Flights Nos. 7 and 8 earlier in the same week. This increase in ionization is due to radioactive materials injected into the stratosphere by the detonation of thermonuclear devices during the preceding months.

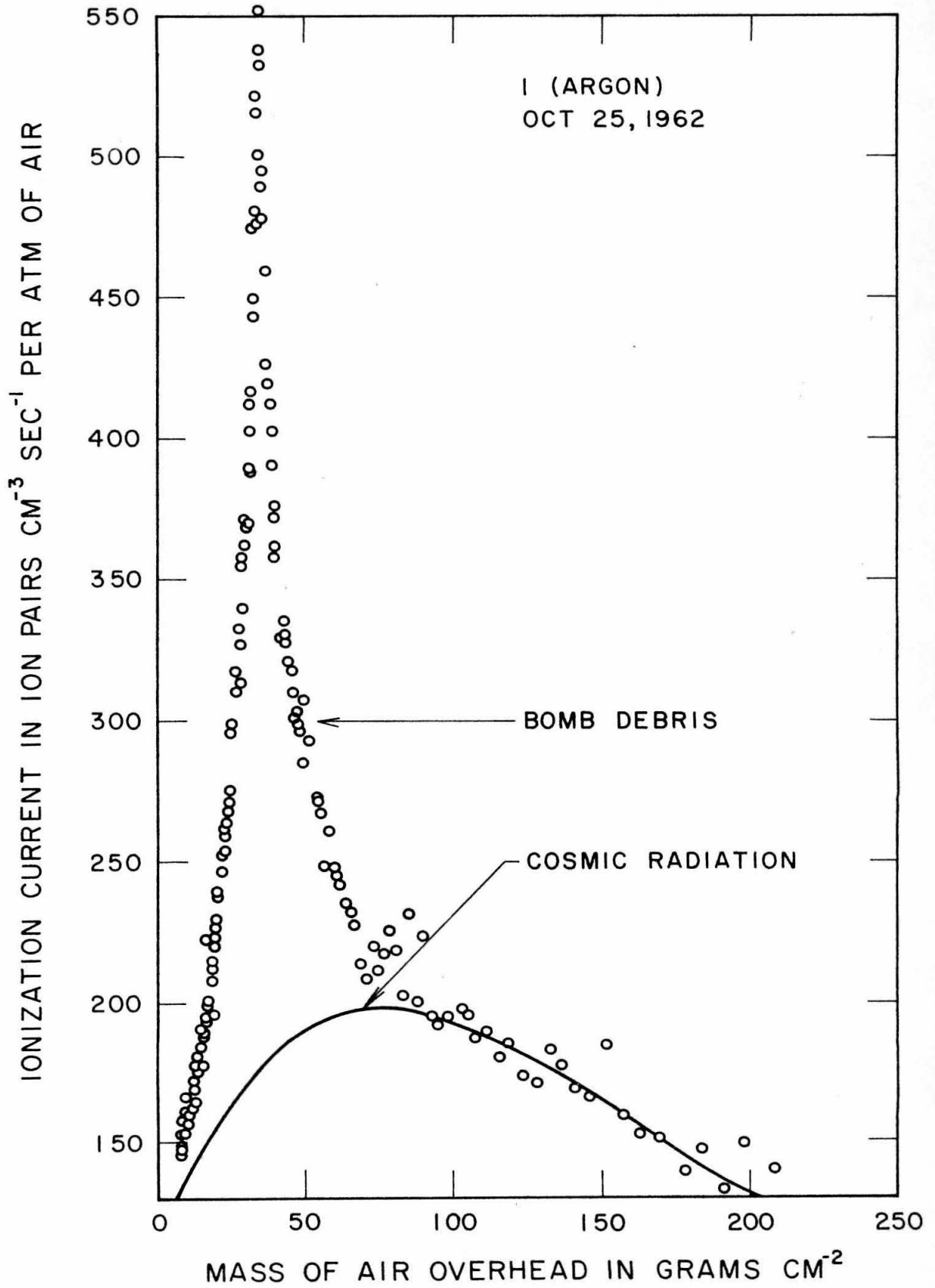


Fig. 13

Fig. 14: Cosmic-Ray Neutron Density in the Atmosphere as Determined by Hess, et al., and by Lingenfelter.

Hess, et al. (4, 14) measured the neutron energy spectrum in the winter of 1956-1957 with detectors installed in a B-36 airplane, up to a pressure altitude of 200 g cm^{-2} . They assumed that the measured height dependence of the neutron source of $\exp(-x \text{ g cm}^{-2}/155)$ could be extended up to the top of the atmosphere. A multi-group diffusion analysis was then used to generate the neutron energy spectrum from 200 g cm^{-2} up to the top of the atmosphere. Lingenfelter (17) has shown that the exponential assumption extended to the top of the atmosphere is improper, and that a maximum in the neutron source actually occurs at a pressure altitude of 100 g cm^{-2} for geomagnetic latitudes below 55° .

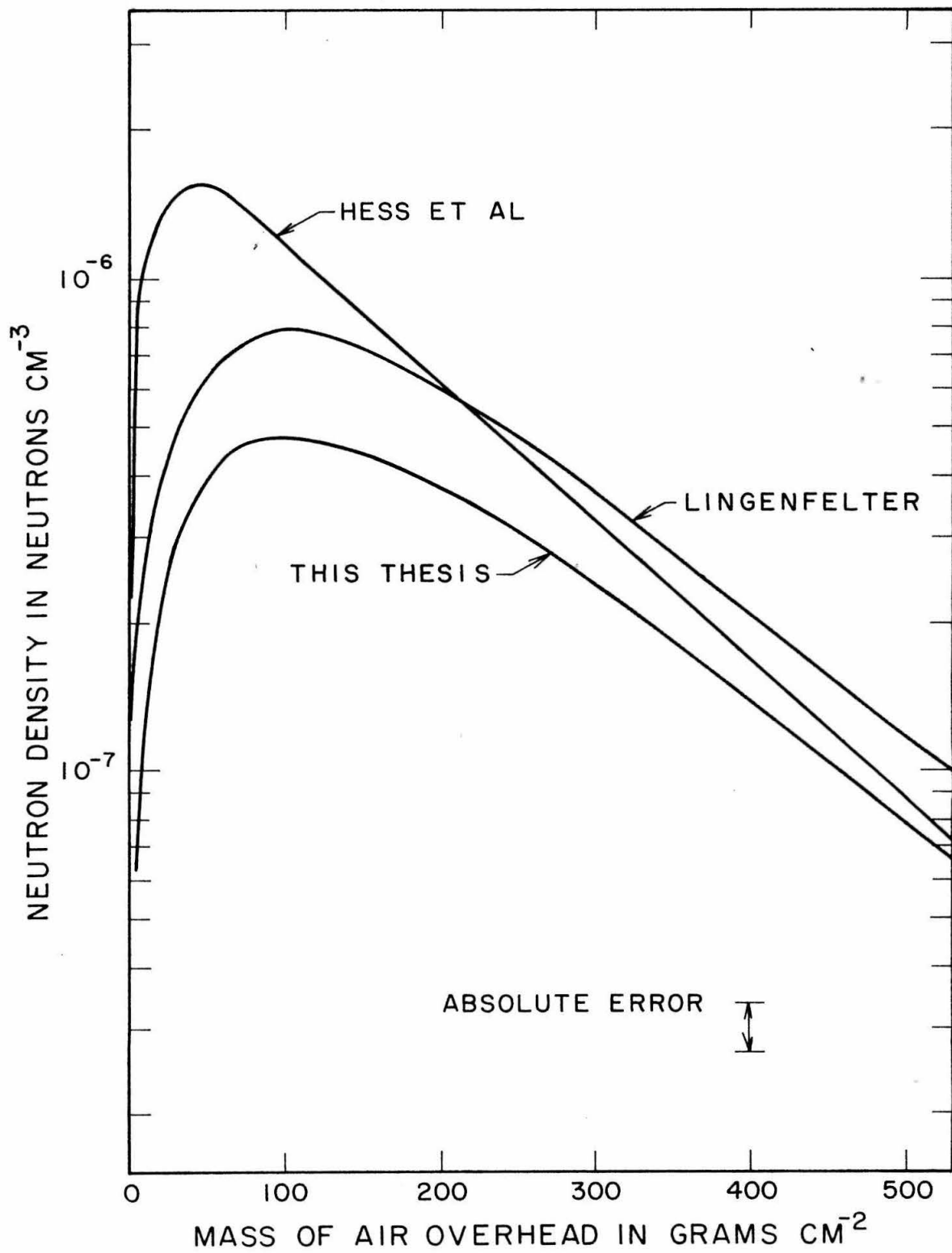


Fig. 14

Fig. 15: Cosmic-Ray Neutron Density in the Atmosphere
as Determined by the New York University
Cosmic-Ray Group (Soberman).

The data presented here represent Flights Nos. 66 and 67 (August 1954 at $\lambda_m = 55^\circ\text{N}$) of the New York University Cosmic-Ray Group (Soberman; Ref. 3). A time correction of 0.96 was applied to the data. The latitude correction was a function of pressure altitude and ranged from 0.40 at 0 g cm^{-2} to 0.81 at 680 g cm^{-2} .

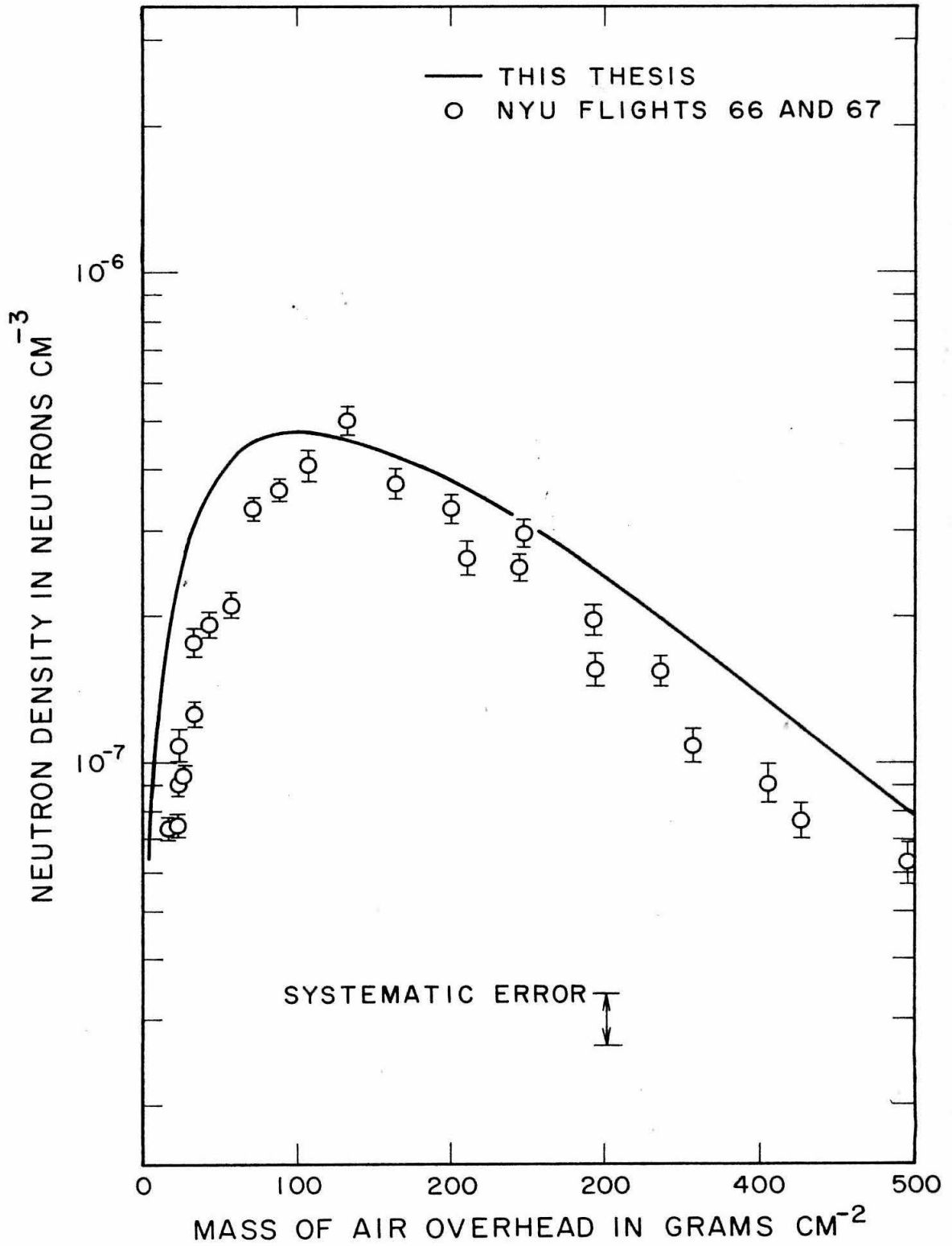


Fig. 15

Fig. 16: Cosmic-Ray Neutron Density in the Atmosphere
as Determined by the New York University
Cosmic-Ray Group (Haymes).

The data presented here represents Flights Nos. 91
and 93 (September 1958 at $\lambda_m = 41^\circ\text{N}$) of the New York Uni-
versity Cosmic-Ray Group (Haymes; Ref. 38). A time
correction of 1.22 was applied to the data.

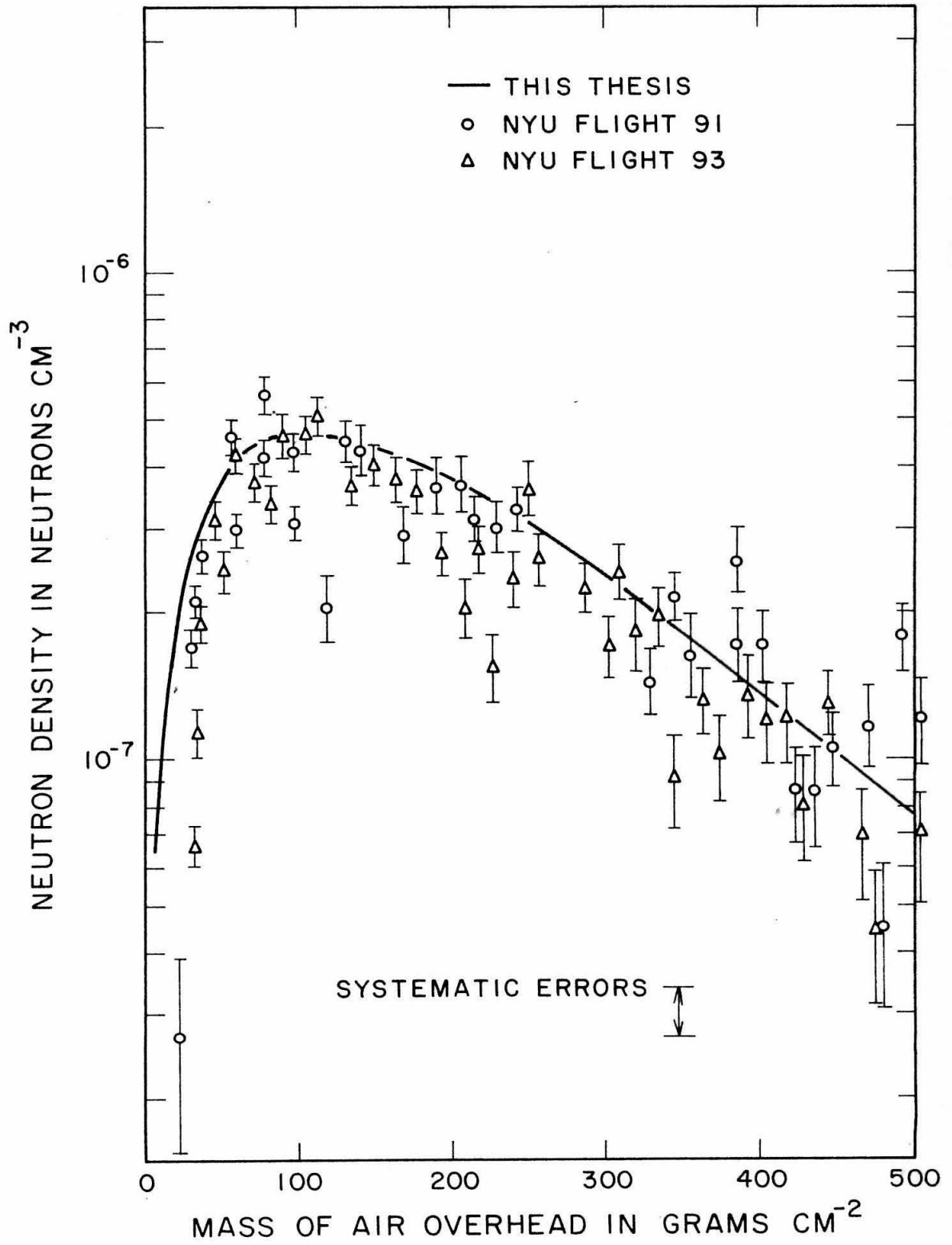


Fig. 16

Fig. 17 : The Density of Cosmic-Ray Neutrons in the
Atmosphere as Determined by L. C. L. Yuan.

The data presented here represent the January 1949 flight of L. C. L. Yuan (12). Two identical proportional counters filled with BF_3 enriched to 96% in the B^{10} isotope were sent aloft at a geomagnetic latitude of 51°N . One counter was shielded with 0.030 inch of cadmium, and the other enclosed in tin of the same thickness. The values of L. C. L. Yuan were multiplied by 1.83 to correct for the cadmium absorption. The time correction was 1.13; the geomagnetic correction varied from 0.54 at 0 g cm^{-2} to 0.82 at 680 g cm^{-2} .

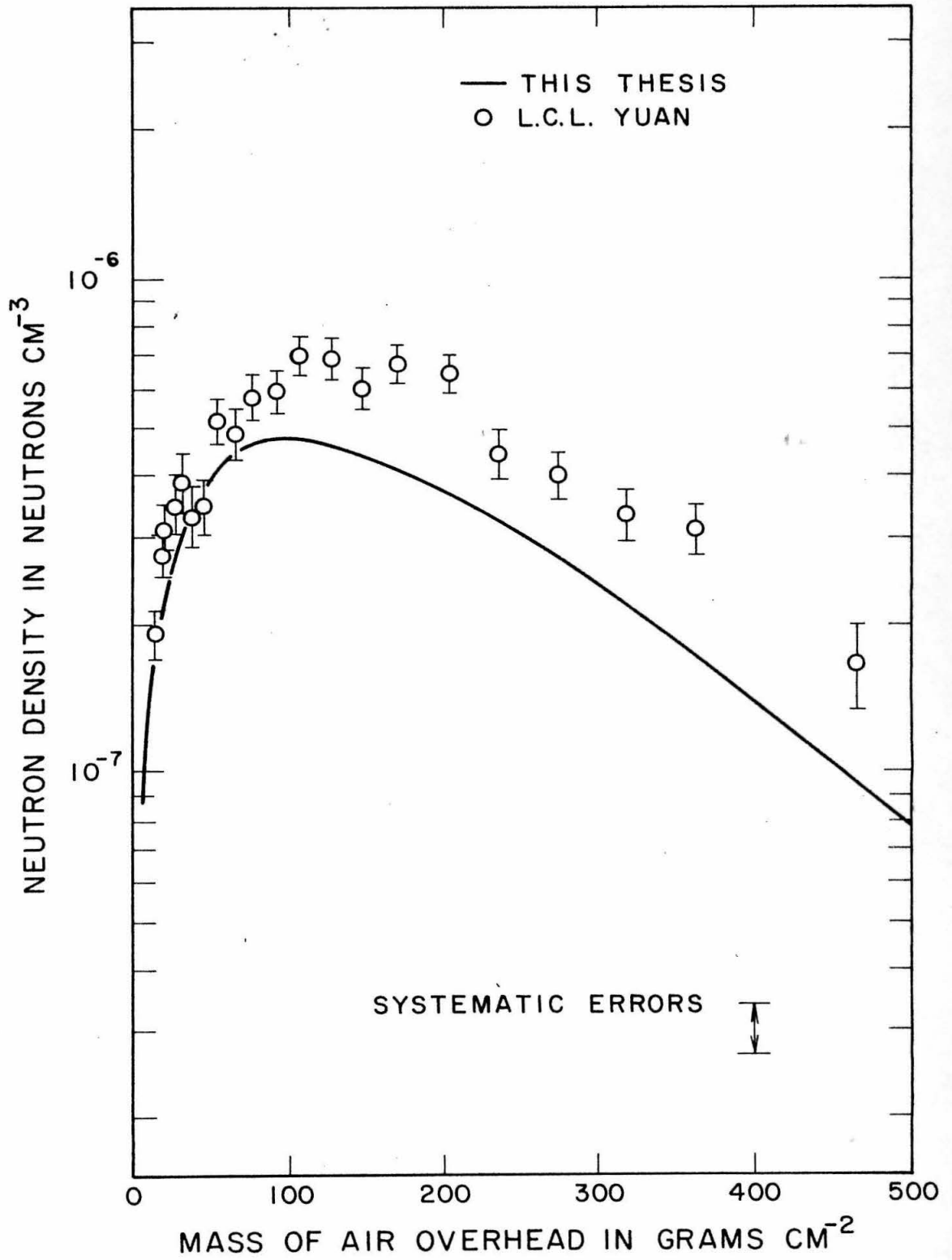


Fig. 17

Fig. 18: Schematic of the Ionization Chamber and Associated Electrical Circuits.

Component	Function	Typical Value
C_b	Blocking Capacitor of the Recharging Circuit	0.001 μ f
C_c	Collector to Spherical Shell Capacitance	3 pf
C_e	Distributed Capacitance of the Electrometer Unit	10 pf
C_f	Fiber to Collector Capacitance of the Electrometer Unit	$\ll C_c$
C_i	Input Capacitance of the Amplifier	10 pf
C_r	Distributed Capacitance of the Recharging Circuit	10 pf
R_f	Resistance of the Recharging Fiber	0.2-2 M Ω
R_i	Input Resistance of the Amplifier	1 M Ω
R_r	Resistor of the Recharging Circuit	1 M Ω

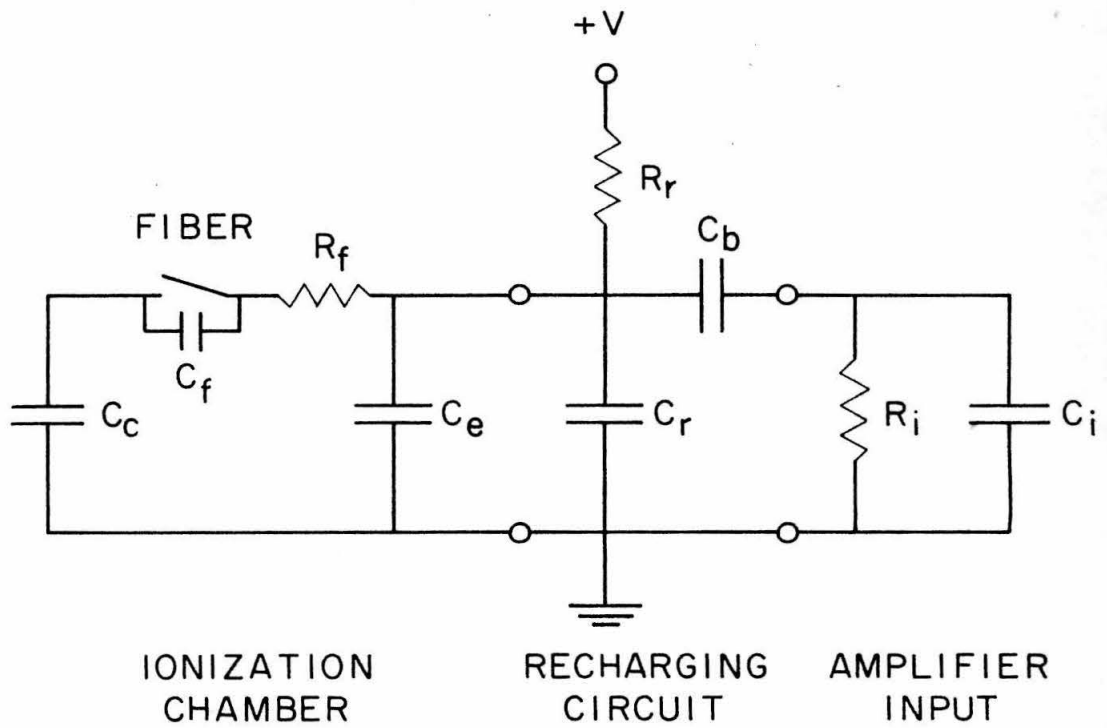


Fig. 18

Fig. 19: Fiber Geometry for the Electrometer Unit of
the Neher Design.

The upper drawing shows the attachment geometry
of the fiber. The lower drawing shows the arrangement of
equipment for the aquadag coating process of the quartz
fiber.

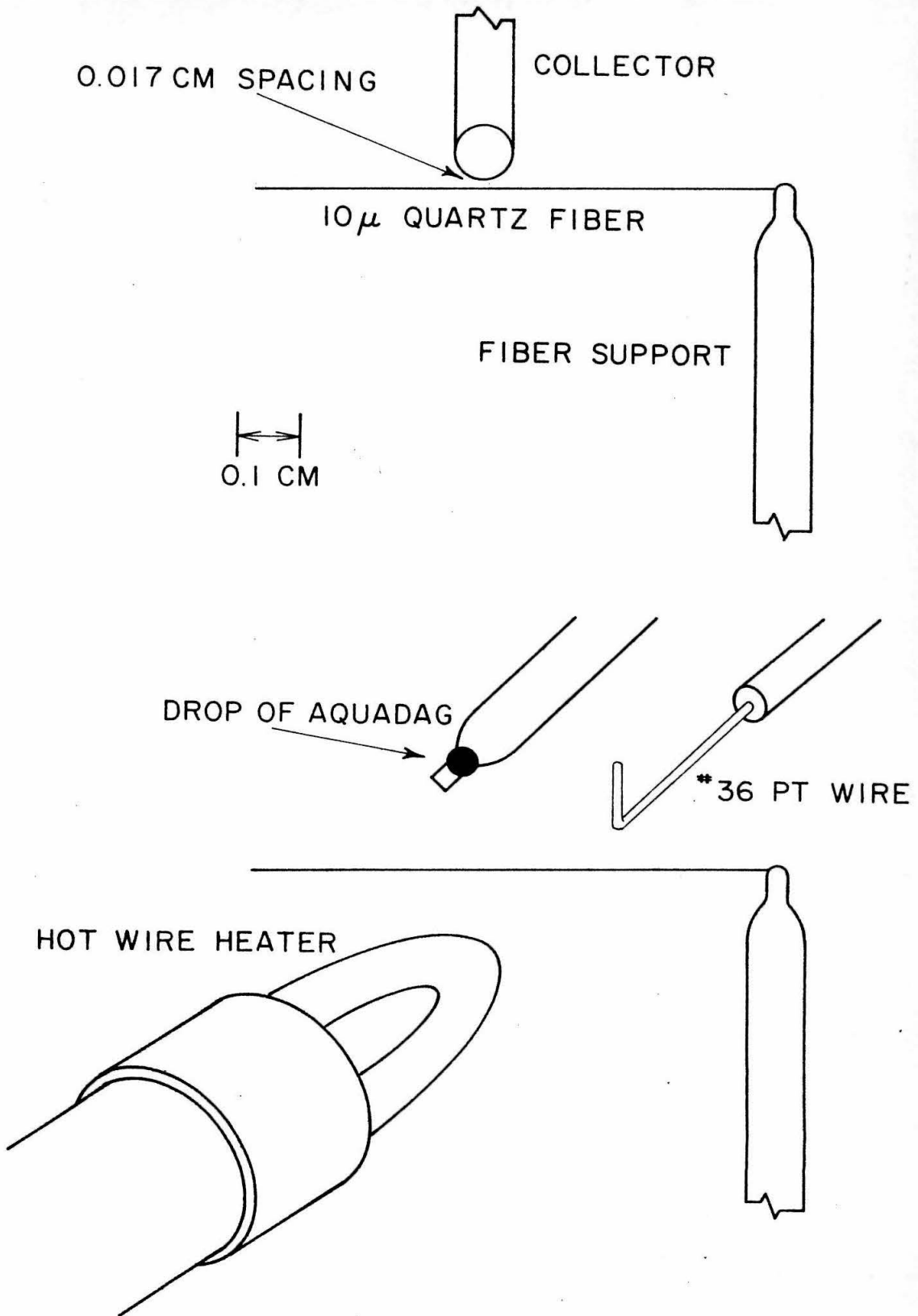


Fig. 19

Fig. 20: Boron Trifluoride Processing and Purification System.

The processing of the $\text{BF}_3 \cdot \text{CaF}_2$ complex takes place in Cyl. A ($\text{BF}_3 \cdot \text{CaF}_2 \rightarrow \text{BF}_3 \uparrow + \text{CaF}_2$). The purification of the BF_3 by vacuum distillation takes place in Cyl. B and Cyl. C.

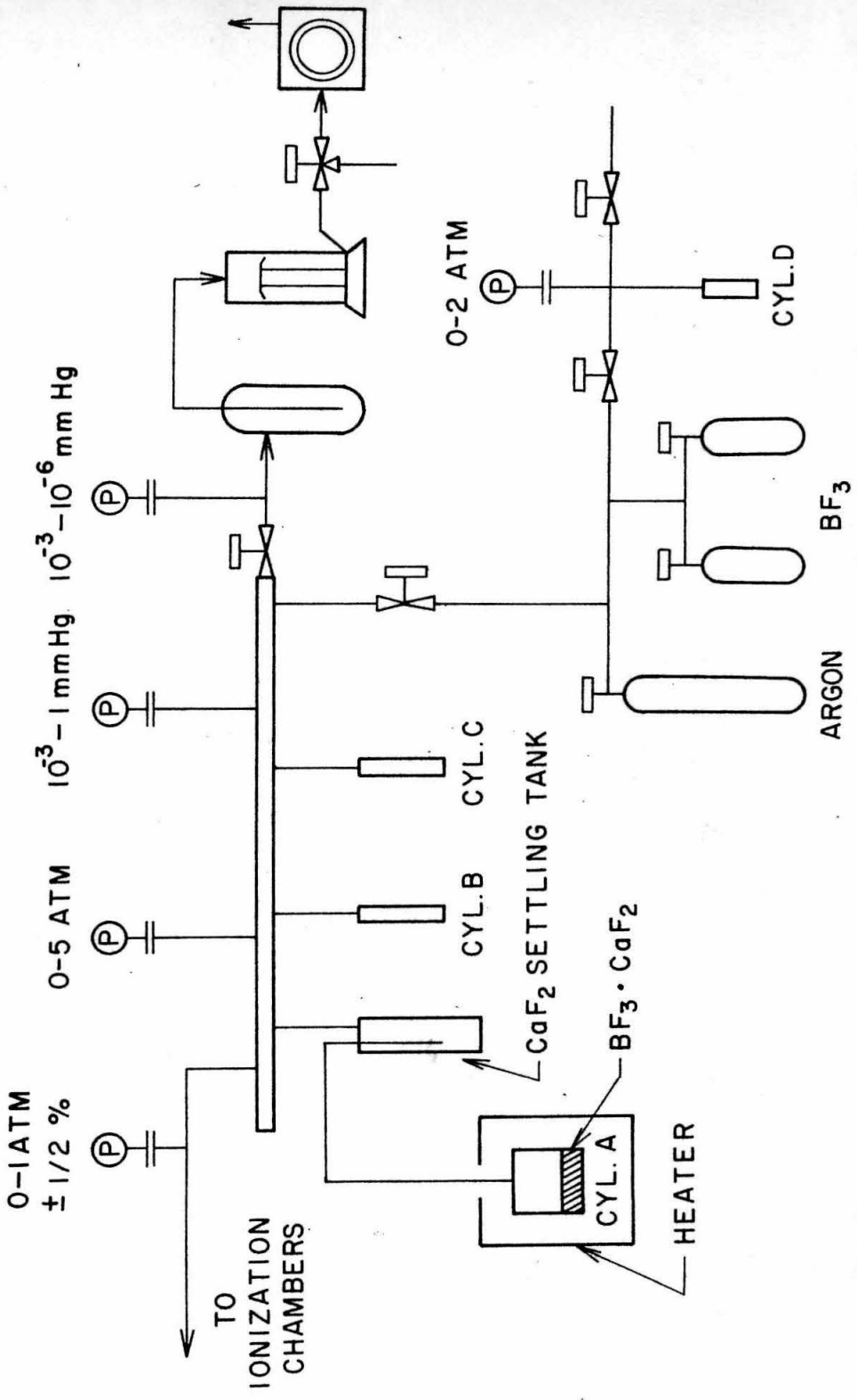


Fig. 20